



iCLEAN – Loitering Attack UCAV



Project Team Members:

(Left to Right)

Lellouche Nathaniel, Etlis Moshe, Rozenheck Oshri, Hagbi Meiran,
Zazon Matan, Dashevski Yanina, Karniel Ya'ara,
Weinberger Menahem, Levy Daniel, Ram-On Mor

Supervisor: Artzi Dror

ABSTRACT

The following report presents the entire work process that had been done during the year of 2011-2012, as part of a student project of the Aerospace faculty at the Technion Institute of Technology.

The "iCLEAN" project.

"iCLEAN" is a suicide Unmanned Combat Air Vehicle (UCAV) with loitering and reconnaissance capabilities, designed to perform missions beyond

line-of-sight in a range of 400 [NM] and for a long period of time, suggesting a long endurance of just about 5[hr].

Carrying a 20+ warhead and equipped with an EO/IR (Electro-Optical and Infra-Red) sensor, the "iCLEAN" provides an advantage to the forces on the ground and constitute a big threat on the enemy during combat.

During the work process a UCAV configuration survey was conducted, two configurations were chosen for the preliminary design.

One of those configurations had been chosen due to several comparisons and requirements arose during the process.

A detailed design and a wind tunnel model test were conducted on the chosen configuration in order to ensure that the theoretical calculations and design are valid.

TABLE OF CONTENTS

Abstract	2
Table of Contents	3
1. Introduction	13
2. Customer Specifications	14
3. Mission Profile	15
4. Market Survey	16
4.1. Market Survey – Configurations	16
4.1.1. HARPY.....	17
4.1.2. HAROP	19
4.1.3. HARPY, HAROP and Required UAV Comparison.....	21
4.2. Market Survey - Sub Systems.....	22
4.2.1. Sensors	22
4.2.2. Engines	24
4.2.3. Launcher Technology Selection.....	25
5. Preliminary Design	27
5.1. Initial Sizing.....	27
5.1.1. Initial Weight Estimation	27
5.1.2. Initial Wing Geometry Evaluation	30
5.1.3. Power-to-Weight Ratio and Wing Loading.....	42
5.1.4. Revised Weight Estimation	46
5.1.5. Initial and Revised Evaluation Comparison.....	50
5.1.6. Revised Geometry Evaluation.....	51
5.2. Configurations Review	52
5.2.1. Configuration A.....	53
5.2.2. Configuration B	57
5.2.3. Configurations Comparison	62
5.2.4. Final Combined Configuration.....	66
5.3. Radar Cross Section- RCS	67
5.3.1. RCS Calculated	67
6. PDR Remarks	69
7. Detailed Design	70
7.1. Propeller Selection.....	70
7.2. Airfoil Selection.....	76
7.3. Rocket Booster	79
7.3.1. Booster Design and Sizing.....	79

7.3.2. Moment vs. Time For Different Booster Angles	79
7.4. Plane Geometry Improvements	82
7.5. Aerodynamic	84
7.5.1. Lift Coefficient	84
7.5.2. Drag Coefficient	91
7.6. Performance Calculations	92
7.6.1. Thrust Calculations	92
7.6.2. Velocity Calculations	93
7.6.3. Climb & Turn Calculations	94
7.6.4. Range and Endurance	96
8. Wing Detailed Design	98
8.1. Wing Structure - Introduction	98
8.2. Wing Structure – Design	101
8.3. Calculations of The Thickness of The Web	104
8.4. Calculation of The Hinges Area	105
8.5. Calculation of The Skin Thickness	107
8.6. Wing Root Joints	110
8.7. Pivot Modeling	115
8.8. Pivot Stress Calculatiobs and Analysis	117
8.8.1. Stress Calculations	117
8.8.2. Analysis	119
9. Wing's Folding Mechanism	122
9.1. Description of The Displayed Solution	123
9.2. Calculations	124
9.3. Mechanism Components	126
9.3.1. The Calculation of Bearing and Hinge Diameters	126
9.3.2. Choosing of The Main Spring	128
9.3.3. Connecting Rods Between The Spring and The Wings	131
9.3.4. Movement Limiters Design	131
10. Final Configuration	133
10.1. Internal Layout of The Components	135
10.2. Weights Table	136
10.3. Aerodynamic Calculations	137
10.3.1. Center of Gravity	137
10.3.2. Aerodynamic Center	139
10.3.3. Stability Margin	143
10.3.4. Calculations Results	144

11. Wind Tunnel Model Design	148
11.1. Technion's Wind Tunnel Specifications	148
11.2. Model Sizing	149
11.2.1. The Full Assembly of The Model	151
11.2.2. Balance Rod's Adapter Design	152
11.2.3. Printing The Model – The Result of The Process	154
12. Wind Tunnel Test	155
12.1. Experiment Plan	155
12.2. Wind Tunnel's Results	158
12.2.1. Opened Configuration	158
12.2.2. Semi-Closed Configuration (45° Open)	163
13. GNC - Guidance, Navigation and Control System	165
13.1. GNC Systems	165
13.1.1. Background	166
13.1.2. Coordinate Systems	167
13.1.3. Parameterization	170
13.1.4. Transformation	171
13.1.5. Equation of Motions	172
13.1.6. Control System	177
13.1.7. Guidance	186
Summary	187
Bibliography	188
Appendix	189

LIST OF FIGURES

Figure 1 - Mission Profile	15
Figure 2 - IAI HARPY	18
Figure 3 - IAI HAROP	20
Figure 4 - Wing Geometry	31
Figure 5 - Wing Aerodynamic Chord.....	31
Figure 6 - Effect of Aspect Ratio on Lift.....	32
Figure 7 - Effect of Sweep on Desired Aspect Ratio	33
Figure 8 - Tail Geometry.....	36
Figure 9 - Aft Tail Positioning.....	39
Figure 10 - Initial Tail Sizing	40
Figure 11 - Configuration A, Isometric	52
Figure 12 - Configuration B, Isometric	52
Figure 13 - Final Configuration A	53
Figure 14 - Lockheed Martin's Minion.....	53
Figure 15 - Initial Configuration A, Opened.....	54
Figure 16 - Initial Configuration A, Closed.....	54
Figure 17 - Final Configuration , Opened and Closed	55
Figure 18 - Internal Layout of Configuration A.....	56
Figure 19 - Conf. A Canisters, Isometric View	56
Figure 20 - Conf. A Canisters, Front View.....	56
Figure 21 - Configuration B.....	57
Figure 22 - Conf. B Wing's Opening Principle	57
Figure 23 - Initial Configuration B, Opened.....	58
Figure 24 - Initial Configuration B, Closed.....	58
Figure 25 - Final Configuration B, Opened and Closed.....	59
Figure 26 - Internal Layout of Configuration B.....	60
Figure 27 - Conf. B Canisters, Isometric View	61
Figure 28 - Conf. B Canisters, Front View.....	61
Figure 29 - Configurations Side View Comparison	62
Figure 30 - Configurations Rear(Left) and Front(Right) View Comparison	63
Figure 31- IAI HARPY 18 Canisters Pack.....	64
Figure 32 - Final Combined Configuration	66
Figure 33 - 3W: 275 Xib2 TS	70
Figure 34 - Pitch Illustration	71
Figure 35 - Multi-Blade Illustraion.....	72
Figure 36 - Propeller Efficiency Vs. Propeller Advance Ratio.....	74
Figure 37 - Power Coefficient vs. Propeller Advance Ratio.....	75
Figure 38 - ABABIL Illustration.....	76
Figure 39 - Airfoils Comparison.....	76
Figure 40 - Airfoil's Lift And Drag Polar Comparisons	77
Figure 41 - Booster Angle.....	80
Figure 42 -Total Moment vs. Time	81
Figure 43 - PDR Final Configuration	82
Figure 44 - CDR Initial Configuration Improvenments	82
Figure 45 - CDR Final Configuration Improvements	83
Figure 46 - Geometry Improvements Description	83
Figure 47 - Typical Wing Torque Box Enclose Area.....	100
Figure 48 - Typical Transport and Fighter Wing Components	100

Figure 49 - Load Distribution on Trapeze Wing	101
Figure 50 - Parameters for Web Calculation	104
Figure 51 - Flanges Parameters	105
Figure 52 - Flange Area Along The Wing	105
Figure 53 - Flange Area Along The Canard	106
Figure 54 - Wing and Cantiliever Beam Cross-Sections	107
Figure 55 - Semi-Span Location Trade-Offs	114
Figure 56 - Vertical Pin Variations	114
Figure 57 - Spar Fibers Layers Angle Changing	115
Figure 58 - Pivot CAD Modeling	115
Figure 59 - Wing-Spar-Pivot Modeling	116
Figure 60 - Shear Stress Analysis, Isometric View	119
Figure 61 - Shear Stress Analysis, Closer View	119
Figure 62 - Von-Mises Stresses, Isometric View	120
Figure 63 - Von-Mises Stresses, Closer View	120
Figure 64 - Wing Deflection Analysis	121
Figure 65 - Wing and Canard Configuration Illustration	122
Figure 66 - Final Improved Configuration, Opened(left) and Semi-closed(right)	125
Figure 67 - Resultant Force Illustration	126
Figure 68 - Different Types of Bearings	128
Figure 69 - Spring Mechanism	128
Figure 70 - Mechanism Tension and Drag Illustration	130
Figure 71 - Spring Model	130
Figure 72 - Connecting Rods and Pins	131
Figure 73 - Limiters Operational States	132
Figure 74 - Limiter Model	132
Figure 75 - Final Improved Configuration, Isometric View	134
Figure 76 - Slots "Curtain"	134
Figure 77 - Internal Layout of The Improved Final Configuration	135
Figure 78 - Weights Table	136
Figure 79 - Wing's Aerodynamic Center Calculation	140
Figure 80 - Canard's Aerodynamic Center Calculation	141
Figure 81 - Lift Area as Function of The Wing Sweep Angle	142
Figure 82 - 25%/75% Stability Margin	146
Figure 83 - 40%/60% Stability Margin	146
Figure 84 - Wind Tunnel Description	148
Figure 85 - Experiment Cell Description	149
Figure 86 - Model Assembly Sketch	151
Figure 87 - Rod Adapter's Sketch	152
Figure 88 - Adapter's Location	153
Figure 89 - Printed Model, Semi-Close 1	154
Figure 90 - Printed Model, Semi-Close 2	154
Figure 91 - True Airspeed at Different Temperatures	155
Figure 92 - Opened, Closed and Open With Tufts Test Model	157
Figure 93 - Open Wing Only With Tufts, Body Only Test Model	157
Figure 94 - Lift Coefficient, Opened, 45 [m/s] - Test vs. Theory	158
Figure 95 - Lift Coefficient, Opened, 45[m/s] - Different Stages of The Test	159
Figure 96 - Moment Coefficient vs. Lift Coefficient, Opened	160
Figure 97 - Moment Coefficient vs. Lift Angle, Openend, 45[m/s]	161
Figure 98 - Drag Coefficient, Opened, 45[m/s]	162
Figure 99 - Lift coefficient, Closed, 45 [m/s]	163

Figure 100 - Moment Coefficient vs. Lift Coefficient, Closed, 45 [m/s]	164
Figure 101 - Body Reference Frame and Its Vectors	168
Figure 102 - Angles Definition in the XZ Plane	169
Figure 103 - Definition of Slide Angle β	170
Figure 104 - Root-Locus For \dot{q}	180
Figure 105 - Controller For θ_{com}	180
Figure 106 - θ and u Loops	181
Figure 107 - LAS - Loitering Attack Suicide UAV, GNC Tool	182
Figure 108 - Step Input For θ	183
Figure 109 - Step Input For \dot{u}	184
Figure 110 - Pitch-Rate Response	184
Figure 111 - u Response	185

LIST OF TABLES

Table 1 - UAV's Configurations.....	16
Table 2 - IAI UAVs and Required UAV Comparison.....	21
Table 3 - Sensors Comparison.....	23
Table 4 - Engines Comparison.....	24
Table 5 - Launchers Comparison.....	25
Table 6 - Dihedral Guidelines.....	34
Table 7 - Wing Vertical Location.....	35
Table 8 - Tail Geometry Comparison.....	38
Table 9 - Tail Aspect Ratio and Taper Ratio.....	39
Table 10 - Tail Volume Coefficient.....	41
Table 11 - Power to Weight Ratio.....	43
Table 12 - Wing Loading.....	45
Table 13 - Initail and Revised Evaluation Comparison.....	50
Table 14 - Configurations Geometric Comparison.....	62
Table 15 - Configurations Canisters Comparison.....	63
Table 16 - Configuration Advantages and Disadvantages.....	65
Table 17 - RCS Geometry Comparison.....	68
Table 18 - Airfoils Characteristics Comparison.....	77
Table 19 - NACA 0012 and EPPLER 560 Comparison.....	78
Table 20 - EPPLER 560 and NACA 4412 Comparison.....	78
Table 21 - Lift Characteristics.....	90
Table 22 - Drag Profile.....	91
Table 23 - Thrust Properties.....	93
Table 24 - Velocity Properties.....	94
Table 25 - Climb and Turn Properties.....	95
Table 26 - Range and Endurance Properties.....	97
Table 27 - Material Yield Stress.....	108
Table 28 - Tresca's Yield Criterion at Different Thicknesses.....	109
Table 29 - Rotary Joints Advantages and Disadvantages.....	111
Table 30 - Pivot Mechanisms Comparison.....	113
Table31 - Maximal Wing Deflection.....	121
Table 32 - 25%/75% Aerodynamic Calculations.....	144
Table 33 - 40%/60% Aerodynamic Calculations.....	145
Table 34 - Experiment Table.....	156

NOMENCLATURE

Sign & Symbol	Interpretation*
$x[ft]$	Longitudinal distance of a part from plane symmetry
$y[ft]$	Lateral distance from plane symmetry
$z[ft]$	Vertical distance from plane symmetry
$x_{w/c}, z_{w/c}[ft]$	Positions of the aerodynamic center in each axis
$\bar{c}[ft]$	Aerodynamic mean chord
$\bar{x} = \frac{x}{c}$	Distance from the reference point divided by the mean chord
$\alpha[^\circ] \text{ or } [rad]$	The attack angle of the plane (the angle between the flow and the plane axis)
$\alpha_{stall}[^\circ] \text{ or } [rad]$	The angle measured from the zero lift line in which the wing or canard stall. It is also the maximum angle of attack
$\varepsilon[^\circ] \text{ or } [rad]$	Induced angle
λ	Taper ratio, the ratio between the chord at the tip and the cord at the root
Λ	Sweep angle
i	Incidence angle
δ	The control surface's angle
i_{c0}	The incidence angle of the canard when the control surface's angle equal to zero
$\tau = \frac{\partial i_c}{\partial \delta}$	The ratio between the control surface to the canard's surface
AR / A	Aspect Ratio
$b[ft]$	Span
$S[ft^2]$	Lift area
$L[lbf]$	Lift
C_l	2D lift coefficient (lift coefficient of a section)
C_L	3D lift coefficient (lift coefficient of the whole wing or canard)
k_b	Span ratio correction factor
w, c, wc, wt	Wing, canard, wing-canard, wing-tail
$\rho \left[\frac{lb}{ft^3} \right]$	The density of the flow
$V \left[\frac{ft}{sec} \right] \text{ or } [knot]$	The velocity of the flow in compare to the velocity of the plane

Sign & Symbol	Interpretation*
C_D	Drag coefficient
C_{D_0}	Drag coefficient (at $\alpha = 0$)
$x_{wing/canard}, z_{wing/canard}$	Positions of the aerodynamic center in each axis
K	Lift- induced drag coefficient
$X_{y,\alpha} \left[\frac{1}{rad} \right]$	Derivation of a coefficient by the angle attack
$\eta_{canard} = \frac{\rho \cdot v_c^2}{\rho v^2},$ $\bullet \in \{wing, canard, body...\}$	The ratio between the flow conditions on a part of the plane and the flow conditions before the interferences
$T[lbf]$	Thrust of the engine
$g = 32.185 \left[\frac{ft}{sec^2} \right]$	Acceleration of gravity
$\gamma[^{\circ}] or [rad]$	Angle of climbing
$\phi[^{\circ}] or [rad]$	Angle of rolling
$R_{turn} [ft]$	The radius of the turn
$E[sec] or [hr]$	Endurance
$R[ft]$	Range
C_m x_{cg}	Moment coefficient around the center of gravity
C_m x_n	Moment coefficient around the center of pressure
n	Load factor

***Unless otherwise specified**

ABBREVIATIONS

UAV	Unmanned Aerial Vehicle
UCAV	Unmanned Combat Aerial Vehicle
IAI	Israel Aerospace Industries
EO	Electro Optic
IR	Infra-Red
FLIR	Forward Looking Infra-Red
CCD	Charged Coupled Device
RCS	Radar Cross Section
PDR	Preliminary Design Review
CDR	Critical Design Review
AOA	Angle Of Attack
GNC	Guidance Navigation and Control
FCS	Flight Control System
FC	Flight Computer
PPN	Pure Proportional Navigation
PN	Proportional Navigation
APN	Augmented Proportional Navigation
TPN	True Proportional Navigation
LOS	Line Of Sight
BLOS	Behind Line Of Sight
SISO	Single Input Single Output
MIMO	Multi Input Multi Output
GM	Gain Margin
PM	Phase Margin
OL	Open Loop
CL	Close Loop
SP	Short Period
TF	Transfer Function
IAS	Internal Standard Atmosphere
DOF	Degrees Of Freedom

1. INTRODUCTION

During the last decade, the use and the need for UAVs for many and varied purposes is increasing rapidly as technology get better. And it doesn't show any sign to slow down soon.

The main concentration is in the reconnaissance and combat territory.

If we put our focus on the combat side of UAVs, it is a side that has much more to discover. Nevertheless, there are several operational and very reliable combat UAVs on the market.

Let us divide them into two groups: suicide and multiple use UCAVs.

A multiple use UCAV is the Predator, manufactured by General Atomics for the USA Air Force. Suicide UCAVs for example are the HARPY and the HAROP manufactured by IAI, Israel.

The suicide UCAVs, as a result of their obvious purpose, doesn't need any major maintenance procedure, has a lower weight (usually doesn't have any landing gear) and designed for a low price per unit, which all comes to its advantage.

To focus on the reconnaissance side of UAVs, the aspiration is to be able to get the best quality of the image, recognize and detect from the longest range you can get, with the best azimuth and area coverage, for the lowest weight that can be in any light and climate conditions outside.

From the above we can conclude that there must be a combination between several systems to get the best performance available. Such as, day and night vision (EO/IR), rotating pod (360° coverage) etc.

"iCLEAN" is a loitering and suicide UCAV designed by the project's team members. The main purposes are reducing as much as possible the dimensions and costs of it.

During the following report the customer requirements are represented, the market survey and the work done in order to suffice those requirements, calculations, analysis, detailed design and wind tunnel test, and much more.

2. CUSTOMER SPECIFICATIONS

Operational capabilities:

- Suicide UAV
- Endurance: 5hr
- Range: 400 NM (~740km)
- Man in the loop
- Launching System: Mobile Ground Launcher with as many as possible UAV's ready to be launched

Target definition and acquisition:

- Target type: Static and mobile
- Truck Target: detection range of 30km, recognition of 12km
- Target acquisition: Day and Night Capabilities

Attack capabilities:

- Warhead: Approx. 20 Kg
- Attack capabilities: Any angle - vertical or horizontal
- Low Cost UAV unit

3. MISSION PROFILE

- Launch
- Climb to 5000ft
- Cruise at 5000ft at approx. 80 knots
- Loitering at 5000ft at approx. 60 knots
- Diving at 150 knots

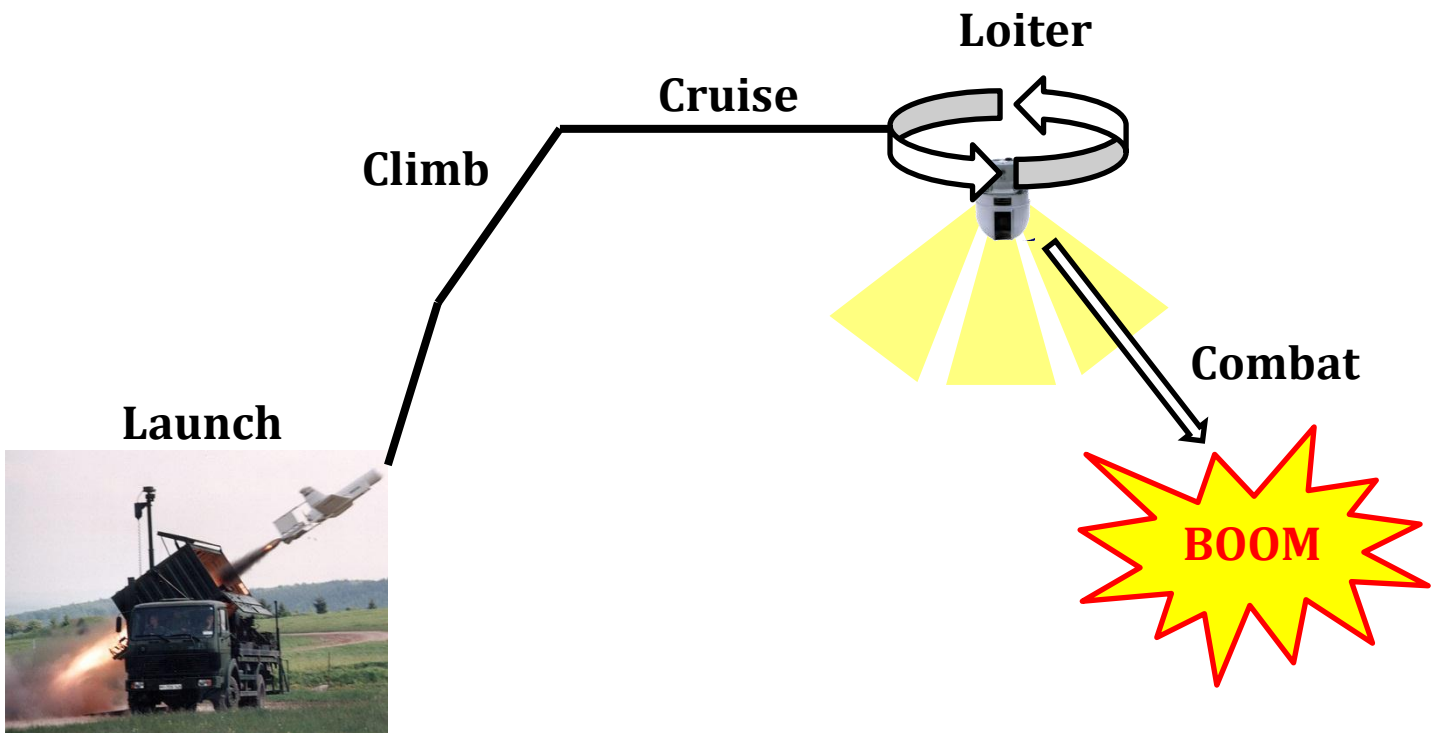


FIGURE 1 - MISSION PROFILE

4. MARKET SURVEY

4.1. MARKET SURVEY – CONFIGURATIONS

A UAV's configurations comparison has been made:

UAV	Special Characteristics	
Crecerlle, France	Delta wing, push-prop	
Taifun, Germany	Plus-tail, rectangular fuselage cross-section, push-prop	
Eitan, Israel	Boom tail, push-prop	
Skylark, Israel	Tractor-prop	
Harop, Israel	Canard, folding wings, push-prop	
Skyblade, Singapore	X-tail, winglets	
Switchblade, USA	Scissors wing's opening	
X47, USA	Flying wing	

TABLE 1 - UAV'S CONFIGURATIONS

Eventually, Two Israeli attack UAVs configurations, manufactured by IAI, HARPY and HAROP, which has purpose and characteristics similar to the customer specifications, were chosen to be assessed in order to try and improve the performances of this two.

4.1.1. HARPY

Characteristics:

- 1.) Delta wings
- 2.) Has an antenna that search a radar
- 3.) If target radar shouting off, when Harpy dives, it cancels the attack and continues patrolling
- 4.) Weight: 135 kg
- 5.) Performances: max speed of 185 km/hr and range of 500m.
- 6.) Propulsion: Rotor engine, AR731.

Harpy Manufactured by IAI, used by the Israeli air force, Turkey, India, China and South Korea. This UAV is designed to attack radar systems with 32 kg high explosive warhead at Power of 37hp.

Harpy Launched by a rocket.

How does it work: HARPY's flight path is planned in the ground station. After launch, HARPY flies to the patrol area and starts patrol independently until its antenna finds a location of radar radiation. When the antenna discovers a radar system, harpy dives and blows over it to cause maximum damage.

Advantages:

- Has a ground station and the ability to patrolling independently.
- Can be launched from a ground vehicle or a ship.
- Day/night autonomous weapon system.

Disadvantages:

- In a case the Harpy doesn't find an active radar it destroys itself.
- Any information about its price.

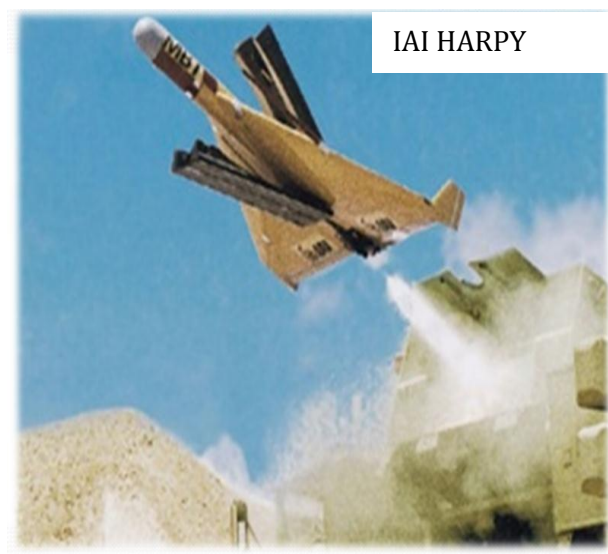


FIGURE 2 - IAI HARPY

4.1.2. HAROP

General Information

Manufactured by IAI, Israel

Used by the Israeli Air Force, India and Germany

Real-time access to control the platform ("Man in the Loop" Operation)

Equipped with: Loitering munition system, Radio anti-radar homing system, EO/IR sensors, FLIR and CCD, which supply a coverage of hemispherical 360 degrees view.

Main targets: In general, main to perform Suppression of Enemy Air Defense (SEAD) operations, such as radars whether it emits a signal or not. Low and high intensity conflicts, urban warfare and counter terror operations.

How does it work: The HAROP launched from transportable launcher. After launch it navigates and loiters in the combat area. Once target is detected, the HAROP strikes and destroys the spot target immediately before its activation. The operator monitors the attack until the target is hit. The operator can abort the attack in order to avoid collateral damage returning the HAROP to loitering mode

Estimated Price: 10 Million Dollars

General Characteristics

Delta wings + Rear wings extension

Canard front-plane

Length: 2.5m

Wingspan: 3.0m

Weight: 135kg

Armament: 23kg warhead

Propulsion: UEL AR-731, Wankel engine

Performance

Power: 37hp supplied by UEL AR-731, Wankel engine

Max speed: 190 km/hr

Range: 1000 km (625 miles)

Line-of-sight range: 150 km

Endurance: 6hr

Advantages:

- Can be launched from ground or. Can be adapted to air-launch
- Can be launched and attack in any angel, vertical or horizontal
- Can hit static and mobile targets
- Can be used to attack targets even if there are no radio signals
- High quality Day/Night system
- Have the option to add landing gear.

Disadvantages:

- High price



IAI HAROP

FIGURE 3 - IAI HAROP

4.1.3. HARPY, HAROP AND REQUIRED UAV COMPARISON

	Range	Control	Target type	Weight	Engine	Warhead	Endurance
HARPY	500km	Automated	Static + active	135kg	AR731	32kg	4hr
HAROP	1000km	Automated+ remote operator	Static, mobile + active	135kg	AR731	23kg	6hr
Required	~740km	Automated+ "man in the loop"	Static, mobile + active + passive	100kg	?	20kg	5hr

TABLE 2 - IAI UAVS AND REQUIRED UAV COMPARISON

4.2. MARKET SURVEY - SUB SYSTEMS

In order to satisfy the customer requirements three sub-systems has been compared:

Sensors, Engines and Launchers.

4.2.1. SENSORS

The sensor characteristics chosen according to the customer requirements and weight calculations that will introduce later, as follows

- Requirements: - Up to 10 kg
 - Day & night capability
 - Installed on operational systems
 - Detection range of 30km
 - Recognition range of 12km

- Over 15 companies and more than 70 Sensors compared

Four sensors, which suites best to the customer requirements, had been chosen:



Sensor	Weight	Dimensions	Installed on	Optical zoom +FOV	Angular coverage	
COBALT 190, Flir Sys.	8.2kg	Diameter 190mm	Boats mainly	Zoom x14.5 35deg	Azimuth 360deg	
		Height 270mm			Elevation -60 +20	
MINIPOP, TAMAM	8.5kg	Diameter 204mm	Many and varied UAVs	Zoom x12 42deg	Azimuth 360deg	
		Height 280mm			Elevation -100 +25	
ESP-600C, Controp	12.3kg	Diameter 300mm	Scout & Searcher UAVs	Zoom x15 25deg	Azimuth 360deg	
		Height 435mm			Elevation -90 +25	
Micro Compass, ELOP	9kg	Diameter 208mm	World leading armies	Zoom x12 42deg	Azimuth 360deg	
		Height 290mm			Elevation -85 +30	

TABLE 3 - SENSORS COMPARISON

The sensor that suites best to the requirements is **ESP-600C**.

It meets the requirements of detection and recognition, operationally proven on several platforms and manufactured by Israeli company, which settles down with our End-use requirements.

4.2.2. ENGINES

Similarly to the sensors characterization, the engines demands as follows:

- Requirements: - Installed on operational systems
 - Up to 12 kg
 - Fuel Consumption of 0.6-0.9 lib/Hp/hour
 - 22-28 Hp
- Over 7 companies and more than 20 engines examined

Four engines, which suites best to the customer requirements, had been chosen:


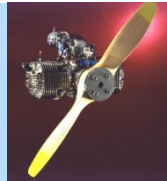


Engine	Power [hp]	Weight [kg]	Fuel consumption [g/hr/hp]	Capacity [cc]	Installed on	
305i, Zanzottera Tech.	25	10.8	340	287	New Engine in Market	
WAE-342, Meggit	26	7.5	363	342	Phoenix, BAE Sys.	
DYAD-290B, Herbrandson	25.5	7.7	354	290	Scout, IAI	
3W-275 XiB2	26	7	340	274	Elbit's UAV	

TABLE 4 - ENGINES COMPARISON

The chosen engine is **3W-275 XiB2** for its low weight and low fuel consumption.

4.2.3. Launcher Technology Selection

The main requirements for the launcher are:

- Low cost
- Mobile Ground Launcher
- Can carry as many units as possible
- ready to launch

There are two main types of launchers technologies. Rocket launch and catapult launch that can be pneumatic or hydraulic.

All the characteristics are summarized in the following tables:



Technology	Launch Velocity [kts.]	UAV Weight [kg]	Power [KPa]	Ease of Use	Operation Field	Budget	
Catapult	<30	<12	200 V 700	Easily assembled, disassembled by one person. Mostly requires no power source	Mountains, desert, sand, saltwater. Pier or ship deck.	Low cost	
Pneumatic	>60+	>23+	700 V 3500	Hard to design and manufacture. Leakage and temperature dangers	Can be transported to any area by vehicle. ready-to-use launch container.	Expensive	

TABLE 5 - LAUNCHERS COMPARISON

Based on the table, the rocket launch technology seems to be the best for the mission. Especially because the rocket engines have the highest exhaust velocities and the manufacturing materials are aluminum, magnesium or steel, which are easy to work with and common in the industry.

In comparison to the HARPY's launch vehicle, that able to carry up to 18 canisters, it concluded that the same vehicle can carry up to 100 units of our UAV (based on width-height calculations). Of course we do not need such a large number of canisters and therefore settle at 20 for our task. What able us to minimize our carrying vehicle.

5. PRELIMINARY DESIGN

5.1. INITIAL SIZING

5.1.1. INITIAL WEIGHT ESTIMATION

This part of the report will discuss the initial and revised calculations made in order to satisfy the customer and mission requirements.

According to Raymer, Chapter 3:

(Under the assumption of a Semi-Homebuilt Semi-General Aviation configuration)

- **Takeoff Weight Buildup Equation:**

$$W_0 = \frac{W_p}{1 - \frac{W_f}{W_0} - \frac{W_e}{W_0}}$$

$W_0 = \text{Design Takeoff Gross Weight} = 220\text{lb}$

$\frac{W_e}{W_0} = \text{Empty Weight Fraction}$

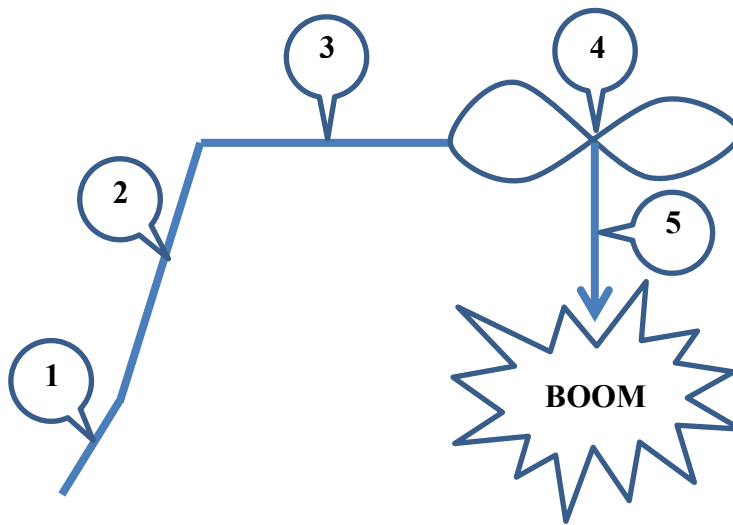
$\frac{W_f}{W_0} = \text{Fuel Weight Fraction}$

$W_p = \text{Payload Weight}$

- **Empty Weight Fraction Estimation:** $\frac{W_e}{W_0} = 1.03 \cdot W_0^{-0.09}$

- **Fuel-Fraction Estimation:**
 - Mission Profile
 - Fuel required as reserve

▪ Mission Selected Profile:



- 1. Takeoff**
- 2. Climb**
- 3. Cruise**
- 4. Loiter**
- 5. Combat/Landing**

Mission Segments Fuel-Fractions:

1. **Takeoff** Fraction: $\frac{W_1}{W_0} = 0.997$

2. **Climb** Fraction: $\frac{W_2}{W_1} = 0.985$

3. **Cruise** Fraction: $\frac{W_3}{W_2} = \exp\left(\frac{-RC}{V(L/D)}\right)$

4. **Loiter** Fraction: $\frac{W_4}{W_3} = \exp\left(\frac{-EC}{(L/D)}\right)$

5. **Landing** Fraction: $\frac{W_5}{W_4} = 0.995$

<p>$R = \text{Range}$ $E = \text{Endurance}$ $C = \text{Specific Fuel Consumption}$ $L/D = \text{Lift to Drag Ratio}$ $V = \text{Velocity}$</p>
--

Therefore:
$$\frac{W_x}{W_0} = \frac{W_5}{W_0} = \frac{W_1}{W_0} \times \frac{W_2}{W_1} \times \frac{W_3}{W_2} \times \frac{W_4}{W_3} \times \frac{W_5}{W_4}$$

Fuel required as reserve:

Allowing a fuel reserve of 10%:

Our Fuel Weight Fraction is:
$$\frac{W_f}{W_0} = 1.1 \left(1 - \frac{W_x}{W_0} \right)$$

Thus,
$$W_0 = \frac{W_p}{1 - 1.1 \left(1 - \frac{W_x}{W_0} \right) - 1.03 \cdot W_0^{-0.09}}$$

For a Given Mission Design Takeoff Weight, W_0 , we can now estimate our Empty Weight, W_e , Fuel Weight, W_f , and Payload Weight, W_p .

5.1.2. INITIAL WING GEOMETRY EVALUATION

According to Raymer, Chapter 4:

(Under the assumption of a Semi-Homebuilt Semi-General Aviation configuration)

▪ **Wing Geometry:**

$$(*) \quad S_{ref} = \frac{W_0}{\left(\frac{W}{S}\right)_{C.S.}} \left. \begin{matrix} AR \text{ from tables} \\ \end{matrix} \right\} \Rightarrow b = \sqrt{AR \cdot S_{ref}}$$

$$(**) \text{ For an arbitrary Main Wing } C_{root}, \lambda \Rightarrow C_{tip} = \lambda \cdot C_{root}$$

AR – Aspect Ratio

S_{ref} – Reference Surface

W/S – Wing Loading

b – Wing Width

C_{root} – Root Chord

C_{tip} – Tip Chord

λ – Taper Ratio

Finding Main Wing and Canard Geometry by iterative method:

$$(***) \quad S_{wing} = \frac{b_{wing} \cdot (1 + \lambda_{wing}) \cdot C_{root}}{2} \Rightarrow S_{canard} = S_{ref} - S_{wing}$$

$$(***) \text{ For chosen Canard } b, C_{root}, \lambda \Rightarrow S_{canard} = \frac{(C_{root} + C_{tip}) \cdot b_{canard}}{2}$$

To be more specific, in order to begin the layout of the wing, it is common to use the basic geometry - trapezoidal wing. The key geometric parameters of the trapezoidal wing are shown in the following figures:

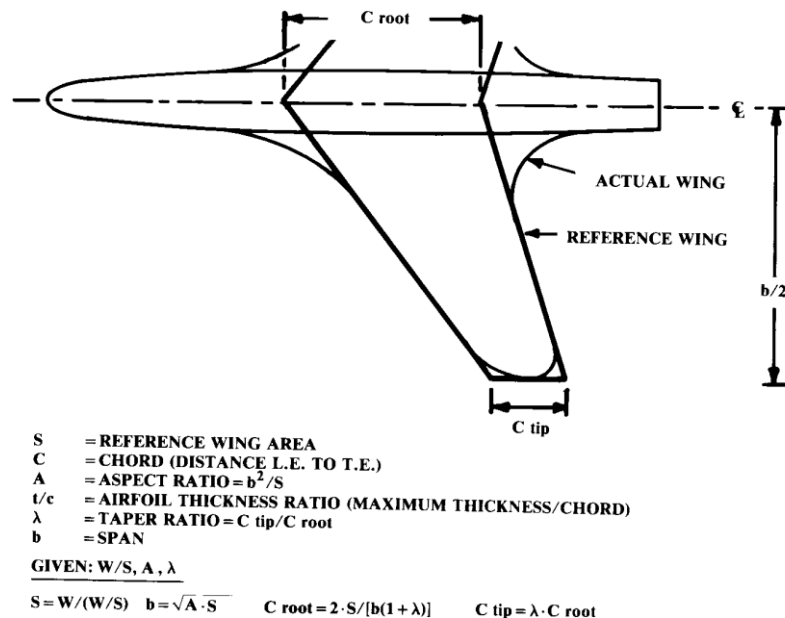


FIGURE 4 - WING GEOMETRY

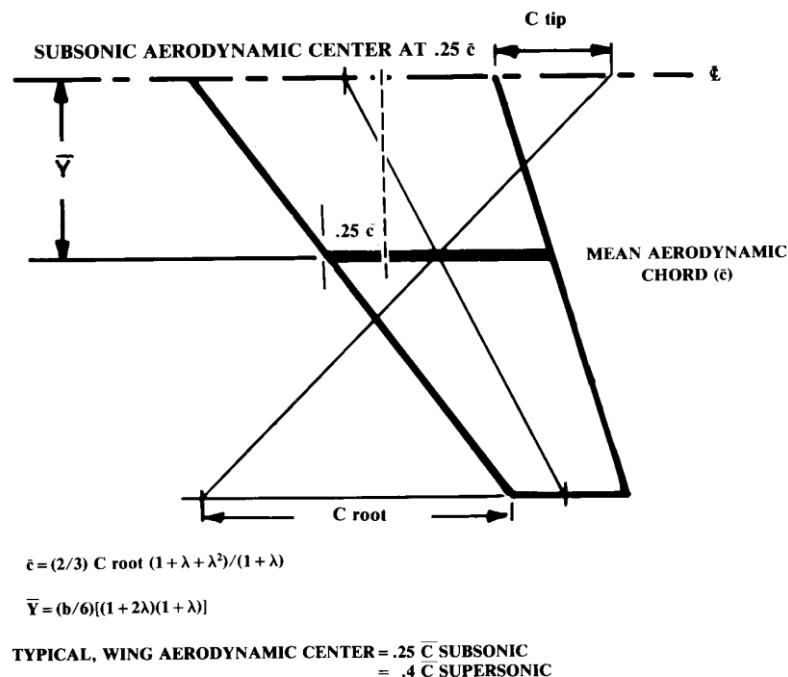


FIGURE 5 - WING AERODYNAMIC CHORD

The shape of the reference wing is determined by its aspect ratio, taper ratio, and sweep.

Aspect Ratio

Wing tunnel investigations shows that a long, skinny wing (high aspect ratio) has less drag for given lift than a short, fat wing (low aspect ratio).

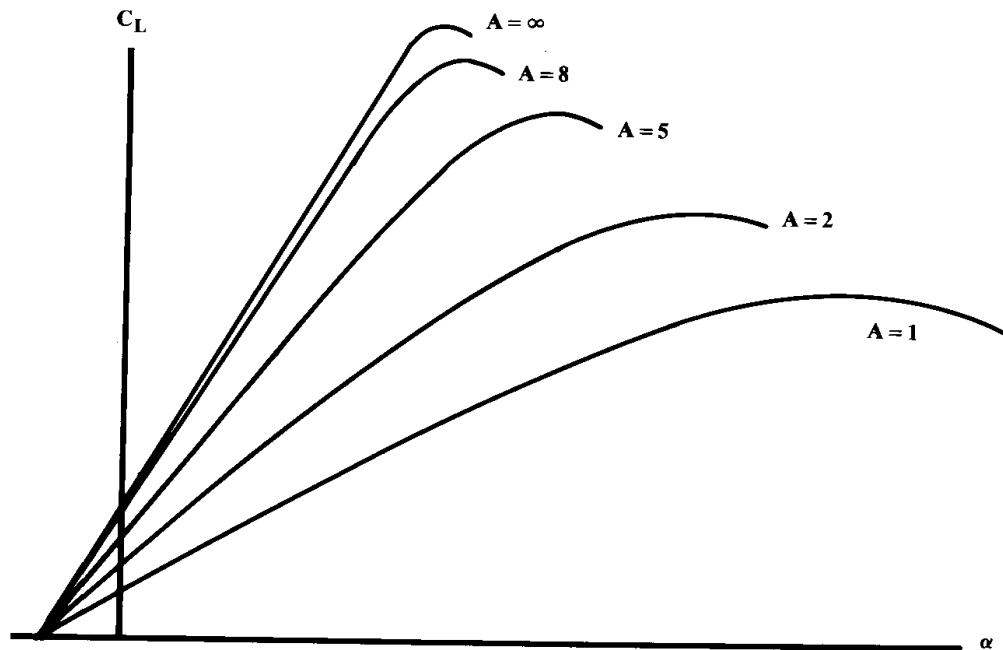


FIGURE 6 - EFFECT OF ASPECT RATION ON LIFT

The aspect ratio was chosen to answer the demands, such as lift and load number, of the conceptual design.

Wing Sweep and Taper Ratio

Wing sweep is the angle between the fuselage and the line connects the chords' quarter of the wing. It used primarily to reduce the adverse effect of transonic and supersonic flow. Taper ratio is the ratio between the tip chord and the centerline root chord.

Minimum drag to lift, or "induced" drag, occurs when the lift is distributed in an elliptical fashion.

The following graph illustrates the results of NACA wind tunnel tests to determine the taper ratio required to approximate the elliptical lift distribution of a swept untwisted wing.

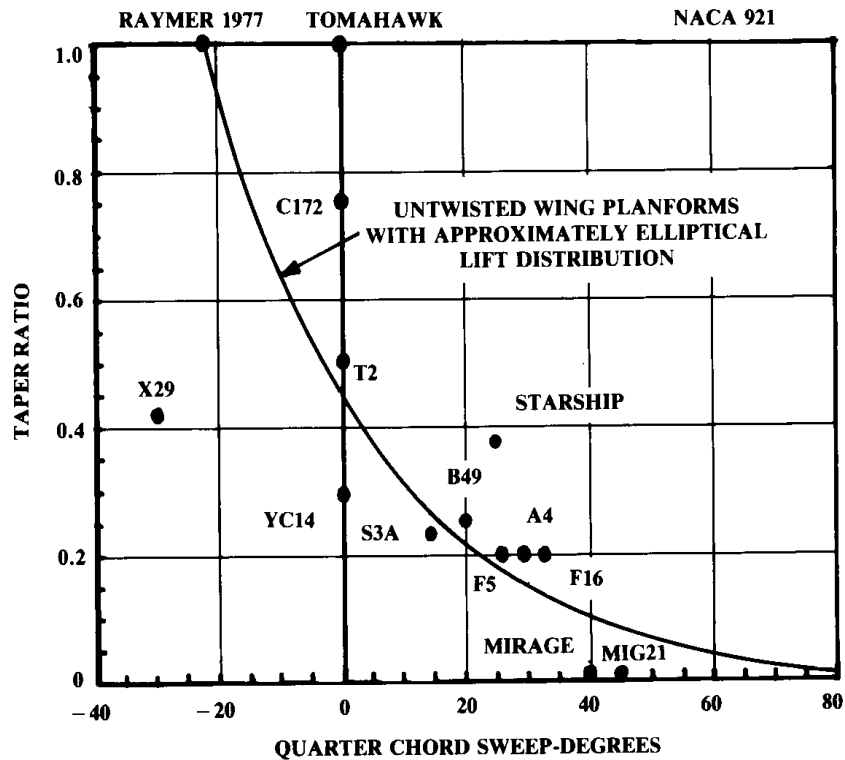


FIGURE 7 - EFFECT OF SWEEP ON DESIRED ASPECT RATIO

The graph also indicates that an untwisted wing with no taper ratio and a forward sweep of 22 degrees can approximate an elliptical lift distribution, however, cost analysis indicated that the weight increase caused by the wing thickness at the root caused this design to cost more than a tapered wing.

Twist

Wing twist is used to prevent tip stall and to approximate an elliptical lift distribution.

Optimizing the lift distribution by twisting the wing will be valid only at one optional lift coefficient. The more twist required to produce a good lift distribution at the design lift coefficient, the worse the wing will perform at other lift coefficients. The UAV ought to perform at cruising, loitering, and at diving, so its wing will not be twisted.

Wing Incidence

The wing incidence angle is the pitch angle of the wing with respect to the fuselage.

Wing incidence angle is chosen to minimize drag at some operating conditions, usually cruise. The UAV is used mostly for cruising (to the target, and only after finding it to dive). The calculation of this angle will be performed in the section of the performance of the UAV.

Dihedral

Wing dihedral is the angle of the wing with respect to the horizontal when seen from the front. Dihedral and sweep tends to roll the aircraft level whenever it is banked. Also, roughly speaking, 10 degrees of aft-sweep created 1 degree of effective dihedral.

The position of the wing on the fuselage has an influence on the effective dihedral. The greatest effect provided by a high and low – frequently creates a pendulum effect. That is the reason why many high-wing configurations have a negative geometric dihedral or an increased vertical tail area to reduce effects of Dutch roll.

Table 4.2 Dihedral guidelines

	Wing position		
	Low	Mid	High
Unswapt (civil)	5 to 7	2 to 4	0 to 2
Subsonic swept wing	3 to 7	– 2 to 2	– 5 to – 2
Supersonic swept wing	0 to 5	– 5 to 0	– 5 to 0

TABLE 6 - DIHEDRAL GUIDELINES

The wings of the UAV are ought to fold, and the sweep of the wings is very low. Therefore, we chose not to create a dihedral angle to the wings.

Wing Vertical Location

The following table compares between the three possibilities for the vertical location of the wing:

Criteria	High-wing	Mid-wing	Low-wing
Camera and vision abilities	Possible to put payloads such as cameras under the UAV.	Possible to put payloads such as cameras under the UAV.	Very difficult to add payload under the UAV. The wings can block the visibility.
Struts	Reduces the weight of the wing but add drag. Adding struts at the lower surface disturbs less to the airflow.	The fuselage carries the wings.	Reduces the weight of the wing but add drag. Adding struts at the higher surface disturbs more to the airflow.
Wing box	Doesn't add weight to the fuselage but adds drag.	Add weight to the fuselage.	Doesn't add weight to the fuselage but adds drag (more than a high-wing).
Fairing	Necessary in a circular fuselage.	Not necessary	Necessary in a circular fuselage.
Cargo	The wings does not take place in the fuselage.	The wing box takes place in the fuselage.	The wing box usually takes place in the fuselage to reduce drag.
Stresses	Apply normal stresses on the fuselage	Apply high bending moment on the fuselage. Solutions to this problem, eventually decreases the weight of the fuselage and disrupt the cargo.	Apply normal stresses on the fuselage
Flaps failure	For a non-dihedral wing, a one-piece flap is possible. This reduces complexity as well as reducing the risk for asymmetric lift caused by the failure of one flap.	Only two-piece flap is possible – increases the risk for asymmetric lift. A tow-piece wing reduces both lift and drag.	For a non-dihedral wing, a one-piece flap is possible. This reduces complexity as well as reducing the risk for asymmetric lift caused by the failure of one flap.

TABLE 7 - WING VERTICAL LOCATION

Wing-Tips

Wing-tips shape has two effects upon subsonic aerodynamic performances. It's determining the ease the air "escape" around the tip. The air which "escapes" creates an induced drag.

Wing-tips shaping increases the price of the wings. It's enough to make a sharp edge to reduce the induced drag of the wing.

Tail Geometry

Here are some of the possible variations in aft-tail arrangement:

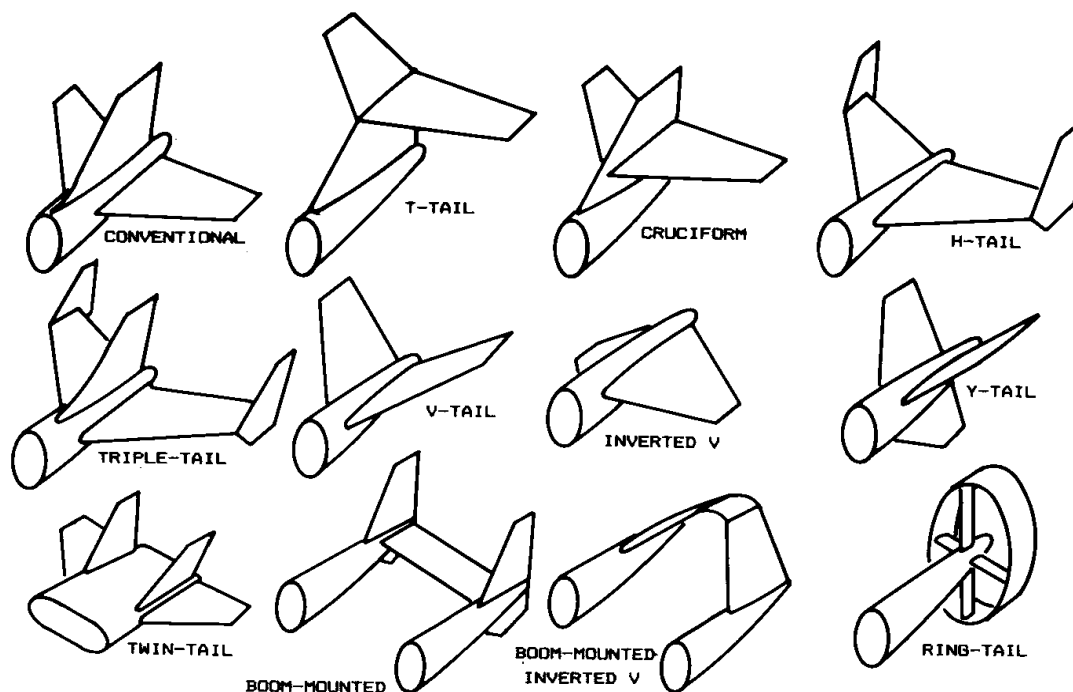


FIGURE 8 - TAIL GEOMETRY

The following table compares between the possible variations in aft-tail arrangement shown in the figure above:

Tail Configuration	Pros	Cons
Conventional	<ul style="list-style-type: none"> Provides adequate stability and control at the lightest weight. probably 70% or more of the aircraft in service have such tail arrangement. Easy to fold. 	<ul style="list-style-type: none"> Has big surfaces.
T-Tail	<ul style="list-style-type: none"> Widely used. Has smaller vertical tail. Has smaller horizontal tail. Has a reduced fatigue on the structure. Easy to fold. Stylish. 	<ul style="list-style-type: none"> Heavier than a conventional tail.
Cruciform	<ul style="list-style-type: none"> Does anything that T-tail can do, but more light-weighted. 	<ul style="list-style-type: none"> Doesn't have small surfaces as the T-tail. Can't be fold efficiently.
H-Tail	<ul style="list-style-type: none"> Smaller horizontal tail. Lower tail height. 	<ul style="list-style-type: none"> Heavier than a conventional tail. Can't be fold efficiently. Used mostly on multi-engine aircraft.
V-Tail	<ul style="list-style-type: none"> Reduced interference drag. 	<ul style="list-style-type: none"> Needs to go through a "mixer" in order to translate the desirable order into a proper movement of the V-tail. When the right rudder pedal is pressed, the nose goes to the right as desired, but it also produces a rolling moment to the left – in opposition to the desired direction of turn – "adverse roll-yaw coupling". Can't be fold efficiently.
Inverted V	<ul style="list-style-type: none"> Avoids the last problem and produces a desirable "proverse roll-yaw coupling". Reduces spiraling tendencies. 	<ul style="list-style-type: none"> Causes difficulties in providing adequate ground clearance. Can't be fold efficiently.

Y-Tail	<ul style="list-style-type: none"> • Similar to the V-tail, but avoids the complexity of the “mixer”. • Reducing interference drag. 	<ul style="list-style-type: none"> • Can’t be fold efficiently. • Interfering an existence of an aft motor .
Twin Tail	<ul style="list-style-type: none"> • Reduced height • More efficient that a centerline mounted single tail 	<ul style="list-style-type: none"> • Heavier than centerline mounted single tail
Boom-Mounted	<ul style="list-style-type: none"> • Allows a use of an aft pusher propeller. • Allows mid or high positioned horizontal tail and an inverted V arrangement. • Can be used with no connecting horizontal tail but with canard for pitch control. 	<ul style="list-style-type: none"> • Heavier than a conventional fuselage construction.
Ring-Tail		<ul style="list-style-type: none"> • Inadequate. • No one is using this type of tail.

TABLE 8 - TAIL GEOMETRY COMPARISON

In the more advanced levels of design, we'll use the next figure in order to determine the proper height of the horizontal tail (critical to the stall characteristics of the aircraft. If the tail enters the wing wake during the stall, control will be lost and pitch-up may be encountered) – low tails are best for stall recovery:

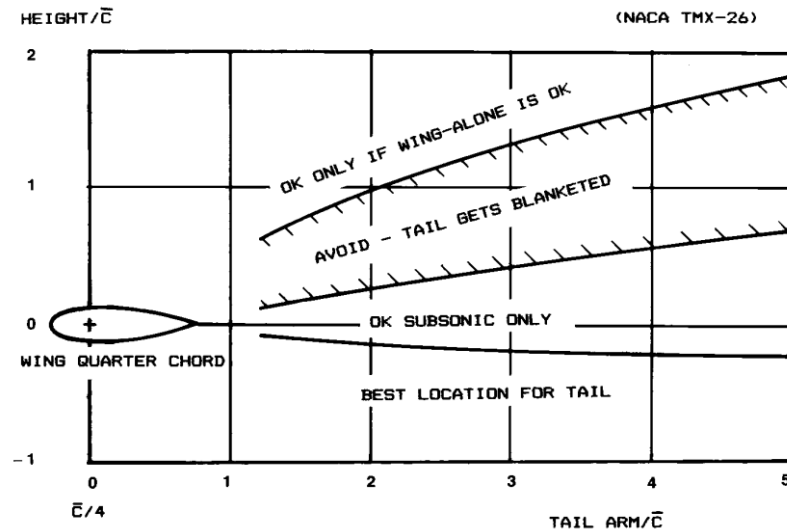


FIGURE 9 - AFT TAIL POSITIONING

A T-tail requires a wing designed to avoid pitch up without a horizontal tail. This requires an aircraft stable enough to recover from a stall even when the tail is blanked by the wing wake.

The following table shows the recommended aspect ratios and taper ratios:

Table 4.3 Tail aspect ratio and taper ratio

	Horizontal tail		Vertical tail	
	A	λ	A	λ
Fighter	3-4	0.2-0.4	0.6-1.4	0.2-0.4
Sail plane	6-10	0.3-0.5	1.5-2.0	0.4-0.6
Others	3-5	0.3-0.6	1.3-2.0	0.3-0.6
T-Tail	—	—	0.7-1.2	0.6-1.0

TABLE 9 - TAIL ASPECT RATIO AND TAPER RATIO

For the horizontal tail, we can use a non-tapered horizontal tail to reduce manufacturing costs.

Leading-edge sweep of the horizontal tail is usually set to about 5 degrees more than the wing sweep. This tends to make the tail stall after the wing. For low speed aircraft, the horizontal tail sweep is frequently set to provide a straight hinge line for the elevator, which is usually has the left and right sides connected to reduce flutter tendencies.

Vertical tail sweep varies between about 35-55 degrees. For a low speed aircraft, there is a little reason for vertical tail sweep beyond 20 degrees other than esthetics. Tail thickness ratio is usually similar to the wing thickness ratio.

Tail Area

The tail size will be determined by the Tail Volume Coefficient method – a historical approach that is used for the estimation of tail size. In order to determine the “vertical tail volume coefficient” and “horizontal tail volume coefficient” we’ll use these formulas:

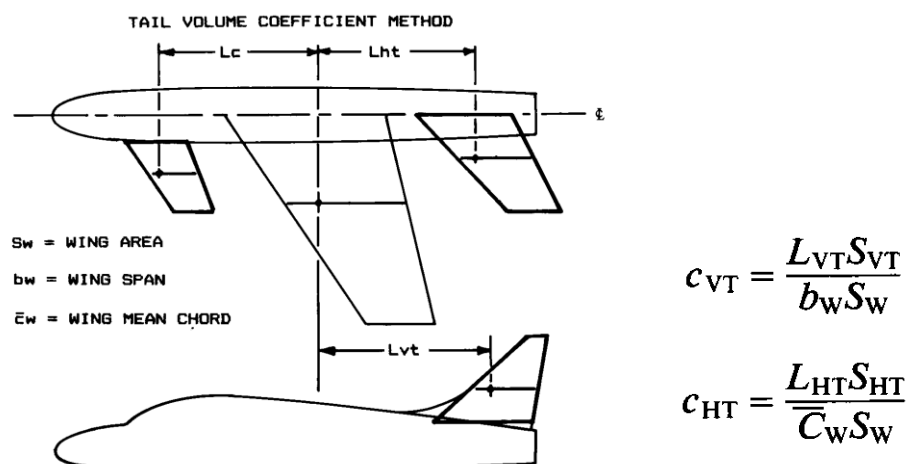


FIGURE 10 - INITIAL TAIL SIZING

Moment arm (L) is commonly approximated as the distance from the tail quarter chord to the wing quarter chord.

From the table below, the coefficients will be chose for a “general aviation – single engine” aircraft. Then, the next equations will be used in order to calculate tail area:

$$S_{VT} = c_{VT} b_W S_W / L_{VT}$$

$$S_{HT} = c_{HT} \bar{C}_W S_W / L_{HT}$$

Table 6.4 Tail volume coefficient

	Typical values	
	Horizontal c_{HT}	Vertical c_{VT}
Sailplane	0.50	0.02
Homebuilt	0.50	0.04
General aviation—single engine	0.70	0.04
General aviation—twin engine	0.80	0.07
Agricultural	0.50	0.04
Twin turboprop	0.90	0.08
Flying boat	0.70	0.06
Jet trainer	0.70	0.06
Jet fighter	0.40	0.07
Military cargo/bomber	1.00	0.08
Jet transport	1.00	0.09

TABLE 10 - TAIL VOLUME COEFFICIENT

For a T-tail, the vertical tail volume coefficient can be reduced by 5% due to end plate effect, and the horizontal tail volume coefficient can be reduced by 5% due to the clean air seen by the horizontal.

On the chosen UAV, where the engine is aft mounted, the tail arm is about 45%-50% of the fuselage length.

5.1.3. POWER-TO-WEIGHT RATIO AND WING LOADING

According to Raymer, Chapter 5:

(Under the assumption of a Semi-Homebuilt Semi-General Aviation configuration)

▪ **Power-to-Weight Ratio:**

Several Power-to-Weight estimation methods:

1. Competitor Study
2. Statistical Estimations – According to Raymer tables
3. Thrust Matching –
The required takeoff Power-to-Weight ratio can approximated by:

$$\left(\frac{hp}{W}\right)_{takeoff} = \left(\frac{V_{cruise}}{550\eta_p}\right) \cdot \left(\frac{1}{(L/D)_{max}}\right) \left(\frac{W_{cruise}}{W_{takeoff}}\right) \left(\frac{hp_{takeoff}}{hp_{cruise}}\right); \eta_p = \text{Engine Efficiency}$$

4. Sustained Turn –
To perform sustained turn with given parameters the following must be satisfied:

$$\left(\frac{hp}{w}\right)_{sustained} \geq 2n \cdot \sqrt{\frac{C_{D0}}{\pi \cdot e \cdot AR}} \cdot \left(\frac{V_{cruise}}{550\eta_p}\right)$$

n – <i>Sus. Turn Factor</i> C_{D0} – <i>Zero Lift Drag Coeff.</i> e – <i>oswald efficiency No.</i>
--

In order to convert this condition to Sea-Level terms:

$$\left(\frac{hp}{w}\right)_{takeoff} = \left(\frac{hp}{w}\right)_{sustained} \cdot \left(\frac{W_{cruise}}{W_{takeoff}}\right) \left(\frac{hp_{takeoff}}{hp_{cruise}}\right)$$

Our goal is to perform well during each and every part of the mission profile segments, therefore we will have to choose the maximum Power-to-Weight ratio we obtain from the estimation methods above.

Final values calculated:

Estimation Method	Method Description	Value
Competitor Study		0.085
Statistical Estimation	According to 2 different Raymer tables	0.08 0.053
Thrust Matching	$\left(\frac{hp}{W}\right)_{takeoff} = \frac{1}{\left(\frac{L}{D}\right)_{max}} \cdot \left(\frac{V_{cruise}}{550\eta_p}\right) \left(\frac{W_{cruise}}{W_{takeoff}}\right) \left(\frac{hp_{takeoff}}{hp_{cruise}}\right)$ $\eta_p = \text{Engine Efficiency}$	0.03
Sustained Turn	$\left(\frac{hp}{w}\right)_{sustained} \geq 2n \cdot \sqrt{\frac{C_{D0}}{\pi \cdot e \cdot AR}} \cdot \left(\frac{V_{cruise}}{550\eta_p}\right)$ $n - \text{Sus. Turn Factor}$ $C_{D0} - \text{Zero Lift Drag Coeff.}$ $e - \text{oswald efficiency No.}$	0.114
Selected Method	Maximum Power-to-Weight ratio (Better segments performance)	0.114

TABLE 11 - POWER TO WEIGHT RATIO

▪ **Wing Loading:**

Several Wing Loading estimation methods:

1. Competitor Study
2. Statistical Estimations – According to Raymer tables
3. Stall Speed – Major contributor to safety flying.
Can be determined directly by the Wing Loading and maximum lift coefficient:

$$V_{stall} = \sqrt{\frac{2W}{\rho S C_{L_{max}}}} \Rightarrow \frac{W}{S} = \frac{1}{2} \rho \cdot V_{stall}^2 \cdot C_{L_{max}}$$

$C_{L_{max}}$ – Max. Lift Coeff.
 ρ – Density

4. Cruising – To maximize range the Wing Loading should be selected to provide high L/D at cruise condition.

In order to do so:

$$\left(\frac{W}{S}\right)_{cruise} = q \cdot C_L = \frac{1}{2} \rho_{cruise} \cdot V_{cruise}^2 \cdot \sqrt{\pi \cdot AR \cdot e \cdot C_{D0}}$$

In order to convert this condition to Sea-Level terms:

$$\left(\frac{W}{S}\right)_{take\ off} = \frac{(W / S)_{cruise}}{W_{cruise} / W_{take\ off}}$$

5. Loitering - To maximize endurance the Wing Loading should be selected to provide high L/D at loiter condition.

In order to do so:

$$\left(\frac{W}{S}\right)_{loiter} = \frac{1}{2} \rho_{cruise} \cdot (V_{cruise})^2 \sqrt{3\pi \cdot AR \cdot e \cdot C_{D0}}$$

In order to convert this condition to Sea-Level terms:

$$\left(\frac{W}{S}\right)_{takeoff} = \frac{(W/S)_{loiter}}{W_{loiter} / W_{takeoff}}$$

In final selection, we want the wing to be large enough for all flight conditions. Therefore we will have to choose the lowest Wing Loading we obtain from the estimation methods above.

Final values calculated:

Estimation Method	Method Description	Value
Competitor Study		16.59
Statistical Estimation	According to 2 different Raymer tables	14
Stall Speed	$V_{stall} = \sqrt{\frac{2W}{\rho S C_{L_{max}}}} \Rightarrow \frac{W}{S} = \frac{1}{2} \rho \cdot V_{stall}^2 \cdot C_{L_{max}} ; C_{L_{max}} - \text{Max. Lift Coeff.}$ $\rho - \text{Density}$	15.23
Cruising	$\left(\frac{W}{S}\right)_{cruise} = \frac{1}{2} \rho_{cruise} \cdot V_{cruise}^2 \cdot \sqrt{\pi \cdot AR \cdot e \cdot C_{D0}} \Rightarrow \left(\frac{W}{S}\right)_{take\ off} = \frac{(W/S)_{cruise}}{W_{cruise} / W_{take\ off}}$	12.74
Loitering	$\left(\frac{W}{S}\right)_{loiter} = \frac{1}{2} \rho_{cruise} \cdot (V_{cruise})^2 \sqrt{3\pi \cdot AR \cdot e \cdot C_{D0}}$	12.98
Selected Method	Minimum Wing Loading (Large enough wing)	12.74

TABLE 12 - WING LOADING

5.1.4. REVISED WEIGHT ESTIMATION

According to Raymer, Chapter 6:

(Under the assumption of a Semi-Homebuilt Semi-General Aviation configuration)

Rubber Engine Sizing: (New Design Engine)

- **Takeoff Weight Buildup Equation:**
$$W_0 = \frac{W_p}{1 - \frac{W_f}{W_0} - \frac{W_e}{W_0}}$$
- **Empty Weight Fraction Estimation:**
$$\frac{W_e}{W_0} = 0.59 \cdot W_0^{-0.1} \cdot AR^{0.05} \cdot \left(\frac{hp}{W_0} \right)^{0.1} \cdot \left(\frac{W_0}{S} \right)^{-0.05} \cdot V_{cruise (mph)}^{0.17}$$

Mission Segments Fuel-Fractions:

1. **Takeoff** Fraction: $\frac{W_1}{W_0} = 0.985$
2. **Climb** Fraction: $\frac{W_2}{W_1} = 1.0065 - 0.325 \cdot M_{@ \text{ the end of climb}}$
3. **Cruise** Fraction: $\frac{W_3}{W_2} = \exp \left(\frac{-RC}{V \left(\frac{L}{D} \right)} \right)$

4. **Loiter** Fraction:
$$\frac{W_4}{W_3} = \exp\left(\frac{-EC}{\left(\frac{L}{D}\right)}\right)$$

But now:
$$\left(\frac{L}{D}\right) = \frac{1}{\frac{q \cdot C_{D0}}{\left(\frac{W}{S}\right)} + \left(\frac{W}{S}\right) \cdot \frac{1}{q \cdot \pi \cdot AR \cdot e}}$$

5. **Combat** Fraction:
$$\frac{W_5}{W_4} = 1 - C \cdot \left(\frac{550\eta_p}{V}\right) \cdot \left(\frac{hp}{W}\right) \cdot (d)$$

As demonstrated earlier:
$$\frac{W_x}{W_0} = \frac{W_5}{W_0} = \frac{W_1}{W_0} \times \frac{W_2}{W_1} \times \frac{W_3}{W_2} \times \frac{W_4}{W_3} \times \frac{W_5}{W_4}$$

And for a reserve fuel of 10% :

Our Fuel Weight Fraction is:
$$\frac{W_f}{W_0} = 1.1 \left(1 - \frac{W_x}{W_0}\right)$$

Thus,
$$W_0 = \frac{W_p}{1 - 1.1 \left(1 - \frac{W_x}{W_0}\right) - 0.59 \cdot W_0^{-0.1} \cdot AR^{0.05} \cdot \left(\frac{hp}{W_0}\right)^{0.1} \cdot \left(\frac{W_0}{S}\right)^{-0.05} \cdot V_{cruise}^{0.17}}$$

For a given W_0 and calculated or chosen $AR, \left(\frac{hp}{W_0}\right), \left(\frac{W_0}{S}\right), V_{cruise}$, we can now estimate our **NEW** Empty Weight, W_e , Fuel Weight, W_f , and Payload Weight, W_p .

Fixed Engine Sizing: (Existing Engine)

- Similar to the Rubber Engine Sizing with several exceptions:
 - Range/Performance - a fallout parameter
 - An iterative method is used to find the fallout parameter
 - Range requirements \Rightarrow Performance is the fallout \Rightarrow Combat Fraction cannot be used \Rightarrow Fuel burned in combat is treated as weight drop!

Therefore, our new **Takeoff Buildup Weight** calculated by:

$$W_0 = \frac{W_{p, fixed} + W_{p, dropped}}{1 - \cancel{W_f / W_0} - \cancel{W_e / W_0}}$$

The weight drop is: $W_{p, dropped} = C \cdot \left(\frac{550\eta_p}{V} \right) \cdot \left(\frac{hp}{W_0} \right) \cdot W_0 \cdot (d)$

Remember that:

$$\cancel{W_e / W_0} = 0.59 \cdot W_0^{-0.1} \cdot AR^{0.05} \cdot \left(\frac{hp}{W_0} \right)^{0.1} \cdot \left(\frac{W_0}{S} \right)^{-0.05} \cdot V_{cruise (mph)}^{0.17}$$

An iterative method is used to find the chosen fallout parameter, $\left(\frac{hp}{W}\right)$.

⇓

$$\left(\frac{hp}{W}\right)_{new} = 0.115 \left[\frac{HP}{lb} \right]$$

⇓

Required Power Final Evaluation by :

$$HP_{req} = \left(\frac{hp}{W_0}\right) \cdot W_0 \cong 25.1 [HP]$$

Required Fuel Weight Final Evaluated by: $W_f = \left(\frac{W_f}{W_0}\right) \cdot W_0$

Required Empty Weight Final Evaluated by: $W_e = \left(\frac{W_e}{W_0}\right) \cdot W_0$

5.1.5. INITIAL AND REVISED EVALUATION COMPARISON

Initial	Revised
$W_0 = \frac{W_p}{1 - \frac{W_f}{W_0} - \frac{W_e}{W_0}}$	$W_0 = \frac{W_{p, fixed} + W_{p, dropped}}{1 - \frac{W_f}{W_0} - \frac{W_e}{W_0}}$
$W_0 = \text{Design Takeoff Gross Weight} = 220\text{lb}$	
$\frac{W_e}{W_0} = \text{Empty Weight Fraction} ; \frac{W_f}{W_0} = \text{Fuel Weight Fraction}$	
$W_p = W_{p, fixed} = \text{Payload Weight} ; W_{p, dropped} = \text{Dropped Payload}$	
$W_e = 140\text{lb} ; W_f = 16\text{lb}$ $W_p = 64\text{lb}$	$W_e = 110\text{lb} ; W_f = 25\text{lb}$ $W_{p, fixed} = 65\text{lb} ; W_{p, dropped} = 20\text{lb}$

TABLE 13 - INITIAL AND REVISED EVALUATION COMPARISON

5.1.6. REVISED GEOMETRY EVALUATION

According to Raymer, Chapter 6:

(Under the assumption of a Semi-Homebuilt Semi-General Aviation configuration)

Using the geometry equations shown earlier and the new values we calculated:

$$(*) \quad \left. \begin{array}{l} AR \text{ from tables} \\ S_{ref} = \frac{W_0}{\left(\frac{W}{S}\right)_{Chosen}} \end{array} \right\} \Rightarrow b = \sqrt{AR \cdot S_{ref}}$$

$$(**) \text{ For an arbitrary Main Wing } C_{root}, \lambda \Rightarrow C_{tip} = \lambda \cdot C_{root}$$

Finding Canard and Tail Geometry by iterative method:

$$\text{For: } MAC = \bar{C}_w = \frac{2}{3} \cdot C_{root} \cdot \left(\frac{1 + \lambda + \lambda^2}{1 + \lambda} \right)$$

$$(***) \quad \left. \begin{array}{l} L_{canard} = 50\%(\text{Length}) \\ \text{From tables: } C_{canard} = 0.5 \end{array} \right\} \Rightarrow S_{canard} = \frac{C_{canard} \cdot \bar{C}_w \cdot S_{wing}}{L_{canard}}$$

$$(***) \quad \left. \begin{array}{l} L_{VT} = 35\%(\text{Length}) \\ \text{From tables: } C_{VT} = 0.04 \end{array} \right\} \Rightarrow S_{VT} = \frac{C_{VT} \cdot b_{wing} \cdot S_{wing}}{L_{VT}}$$

To find C_{root}, C_{tip} for both, Canard and Tail, we used an iterative method:

$$b = \sqrt{AR \cdot S} \Rightarrow \bar{C}_{w,new} = \frac{S}{b} \Rightarrow \text{Chosen Iterative Condition} \Rightarrow (C_{root}, C_{tip})$$

5.2. CONFIGURATIONS REVIEW

This part of the report will discuss the two configurations that were designed and evaluated during the first semester:

To optimize the development process of the UAV, it was decided to divide the group into two teams which will grow ideas and will develop simultaneously, each in its own way.

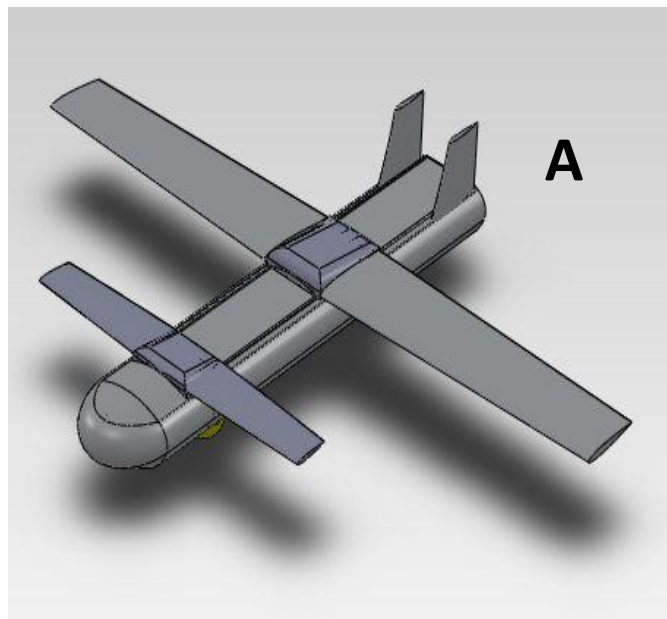


FIGURE 11 - CONFIGURATION A, ISOMETRIC

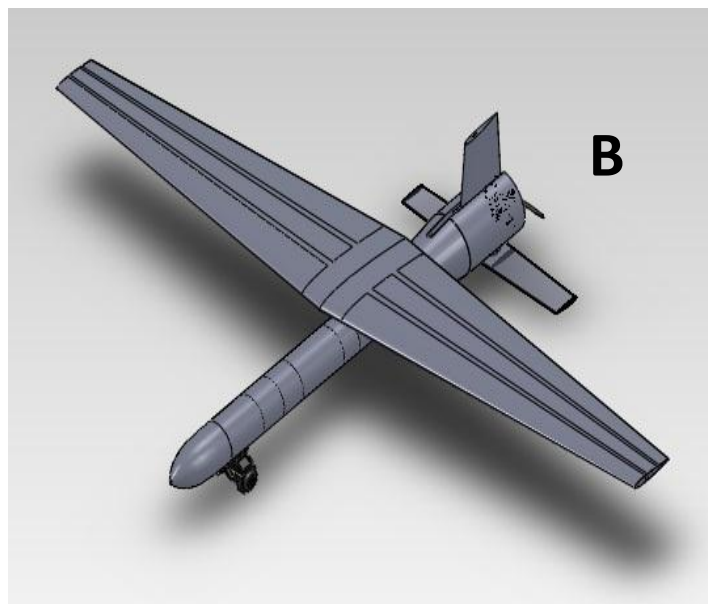


FIGURE 12 - CONFIGURATION B, ISOMETRIC

5.2.1. CONFIGURATION A

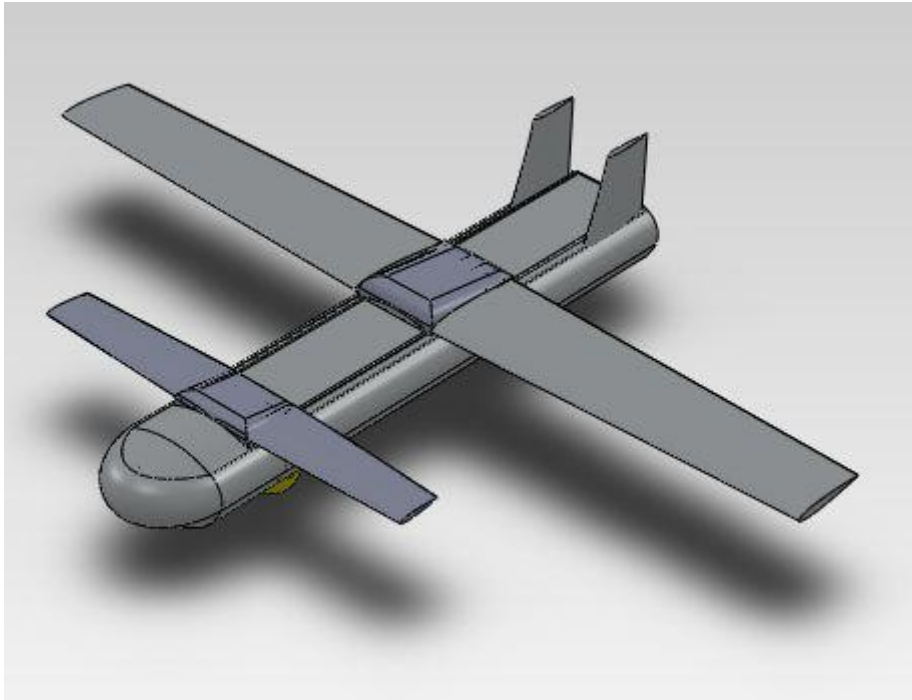


FIGURE 13 - FINAL CONFIGURATION A

The basic principles on which configuration A was based on symmetric unfolding method, hence the idea for two wings that open symmetrically, because that way asks for a large wing span, to minimize it, and for adding maneuver ability, we added a canard. The body of this configuration is round, with flat surfaces where the wings or the canards are when the UAV closed.

The inspiration to that configuration came from the Lockheed 'Minion' plane (picture below), which is supersonic, so we added few changes, like described above.



FIGURE 14 - LOCKHEED MARTIN'S MINION

At the beginning, configuration A was looked like this:

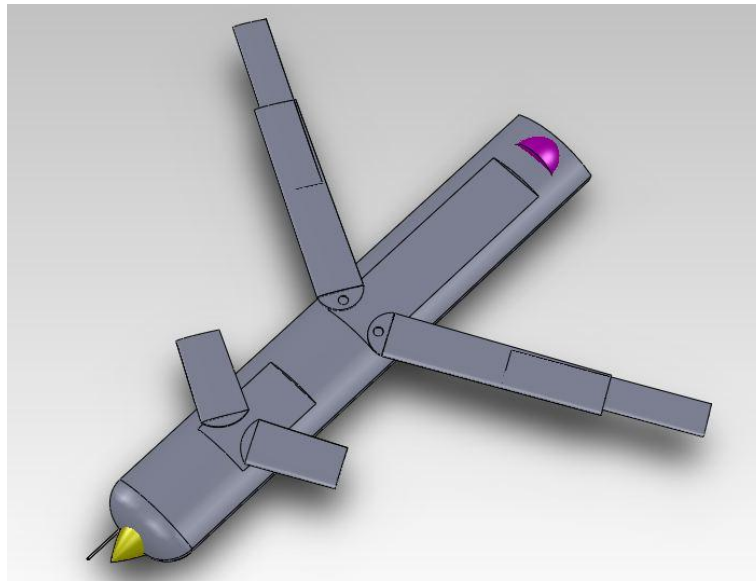


FIGURE 15 - INITIAL CONFIGURATION A, OPENED

As the picture tells, the canard span is very short, the wings has a telescopic part, for extra compactness and the body itself is not round but more flattened then the final version. The tail was added later, so it is doesn't appear in the picture. The purple cone symbolizes the engine and the yellow one symbolizes the sensor, which is first designed to be at the front.

When this version was close, it was looked like this:

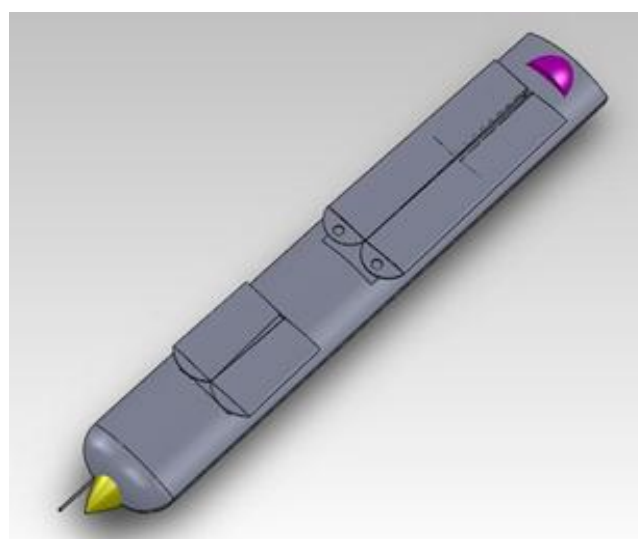


FIGURE 16 - INITIAL CONFIGURATION A, CLOSED

All of that was taken into account and improvements were made, making the final configuration A look like this:

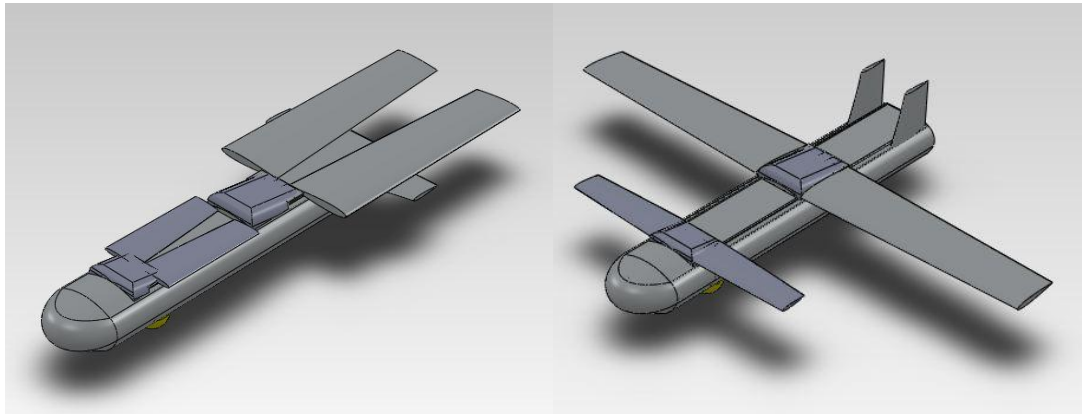


FIGURE 17 - FINAL CONFIGURATION , OPENED AND CLOSED

The wing span and the canard span were recalculated. The sensor was reshaped to more similar form to the real one. The wing is no more telescopic which adds to the canister length, and wings and canards axis were covered for more aerodynamic shape. A horizontal wing was added, for better folding, it was split.

$$b_w = 3.2[m]$$

$$C_{R_w} = 44[cm]$$

$$C_{t_w} = 33[cm]$$

Some data: $b_c = 1.88[m]$

$$C_{R_c} = 25[cm]$$

$$C_{t_c} = 18.8[cm]$$

$$L_{fuselage} = 2.2[m]$$

$$R_{\max_{fuselage}} = 55[cm]$$

Internal layout of the components:

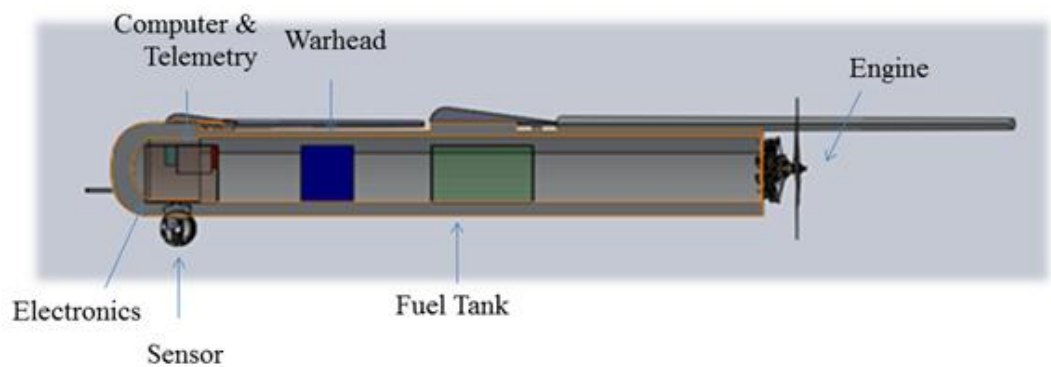


FIGURE 18 - INTERNAL LAYOUT OF CONFIGURATION A

The electronics are in the front, away from the motor’s noise and the fuel tank is in the C.G area, in order to prevent the C.G movement along the body because of the fuel consumption.

Illustration of 18 canisters:

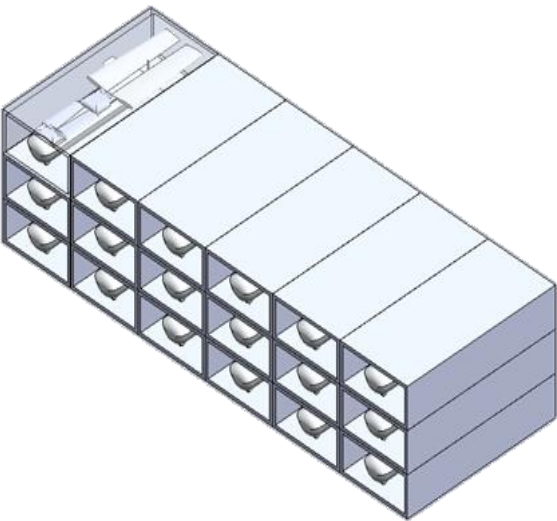


FIGURE 19 - CONF. A CANISTERS, ISOMETRIC VIEW

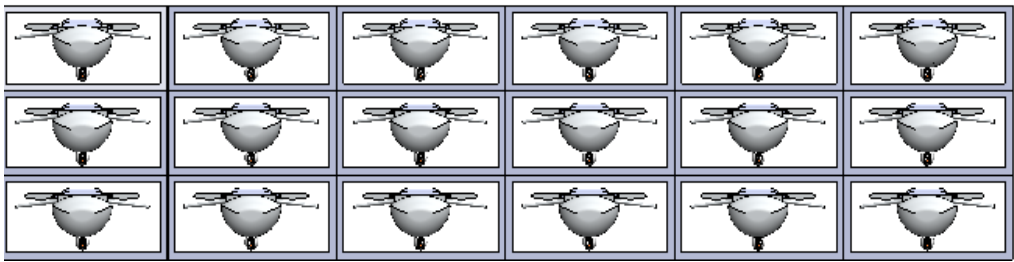


FIGURE 20 - CONF. A CANISTERS, FRONT VIEW

5.2.2. CONFIGURATION B

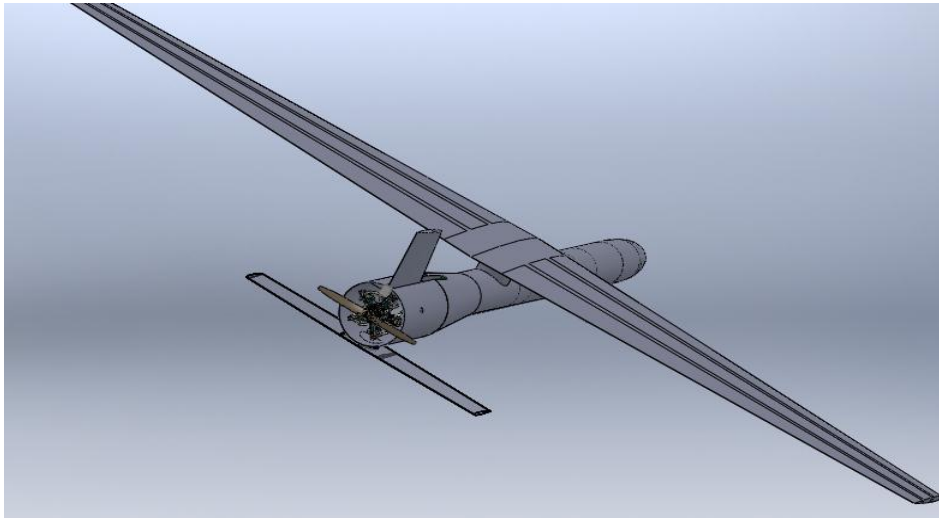


FIGURE 21 - CONFIGURATION B

The basic principles on which configuration B was based on were compactness the simplicity of the unfolding method, hence the idea for simple cross wing in which the wing unfolds by a 90 degrees rotation:

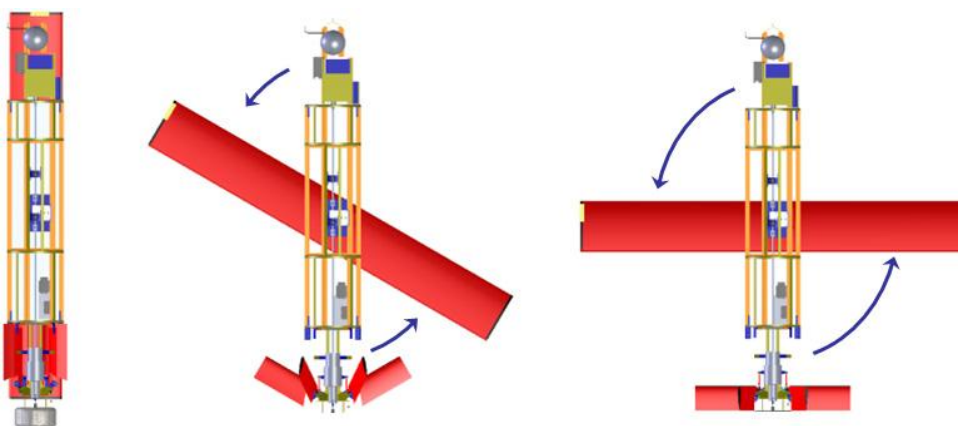


FIGURE 22 - CONF. B WING'S OPENING PRINCIPLE

At the beginning, configuration B looked like this:

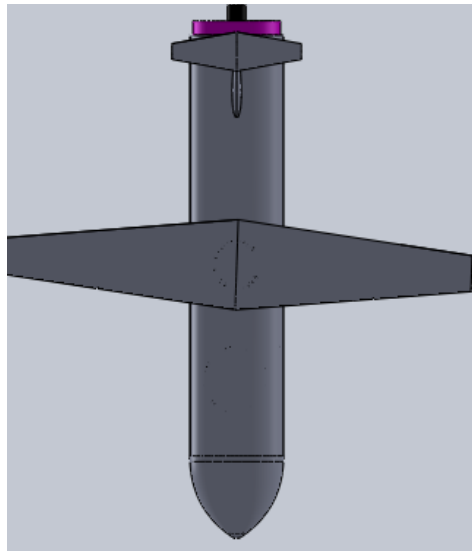


FIGURE 23 - INITIAL CONFIGURATION B, OPENED

The body has a large diameter (so the motor fit the body)/length ratio which makes it look a bit “fat” and short and not so aerodynamic. Also, when the wing had to be positioned in the folded position, the tail interrupted it, making it impossible to fold completely:

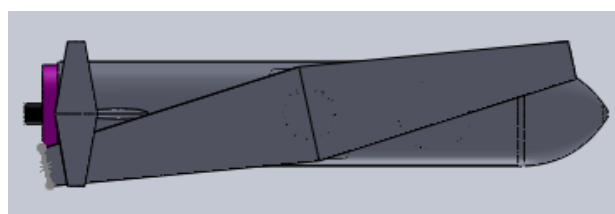


FIGURE 24 - INITIAL CONFIGURATION B, CLOSED

All of that was taken into account and improvements were made, making the final configuration B look like this:

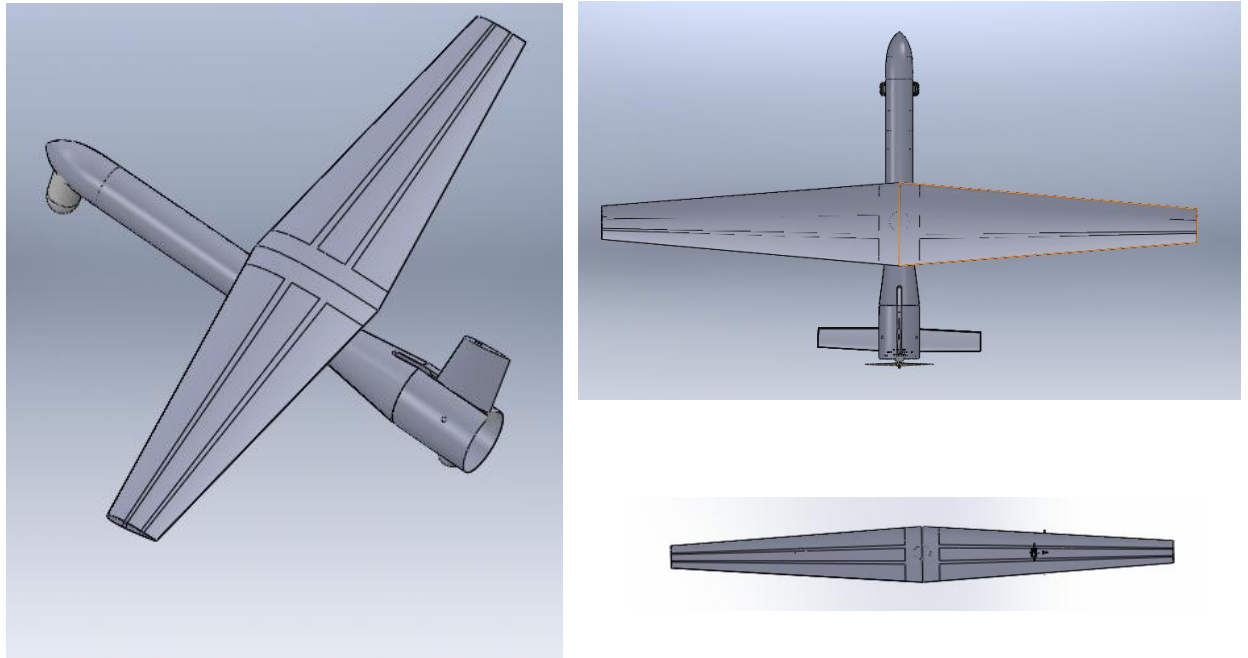


FIGURE 25 - FINAL CONFIGURATION B, OPENED AND CLOSED

Body's length and wing span got extended, while the diameter of the body was reduced along most of the body, and close to the motor area it got expended only in the rear in order to have enough room for the motor. Body's cylindrical symmetry was kept in order to prevent any affection on lift and keeping the aerodynamic shape.

Also, the tails were separated and now the vertical tail folds into the body which enables a full folding of the wing (and hence enables a smaller canister) and the horizontal tail is located at the lower side of the body and rotates in the opposite direction to the wing rotating direction while unfolding, in order to resist each other's yawing torque that comes from the rotational motion of each of them.

Some data:

$$b_w = 4.4[m]$$

$$C_{R_w} = 62.5[cm]$$

$$C_{t_w} = 25[cm]$$

$$L_{fuselage} = 2.5[m]$$

$$R_{\max_{fuselage}} = 30[cm]$$

Internal layout of the components:

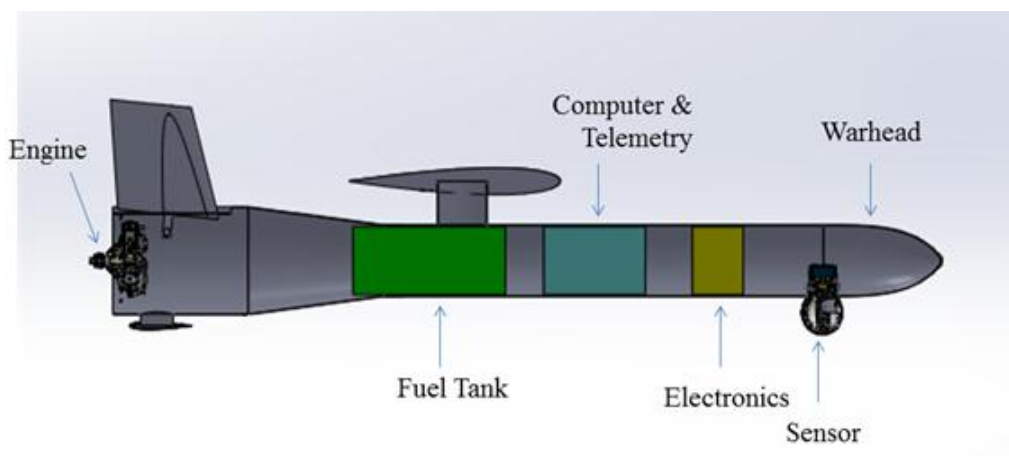


FIGURE 26 - INTERNAL LAYOUT OF CONFIGURATION B

Similar to the internal layout of configuration A: The electronics are in the front, away from the motor's heat and noise. The fuel tank is in the C.G area, in order to prevent the C.G movement along the body because of the fuel consumption.

Illustration of 18 canisters:

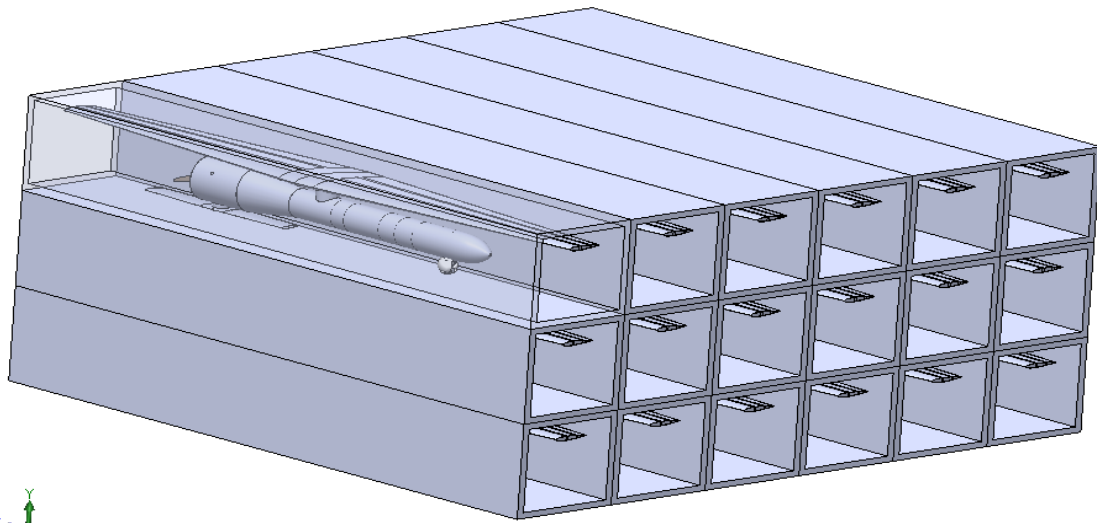


FIGURE 27 - CONF. B CANISTERS, ISOMETRIC VIEW

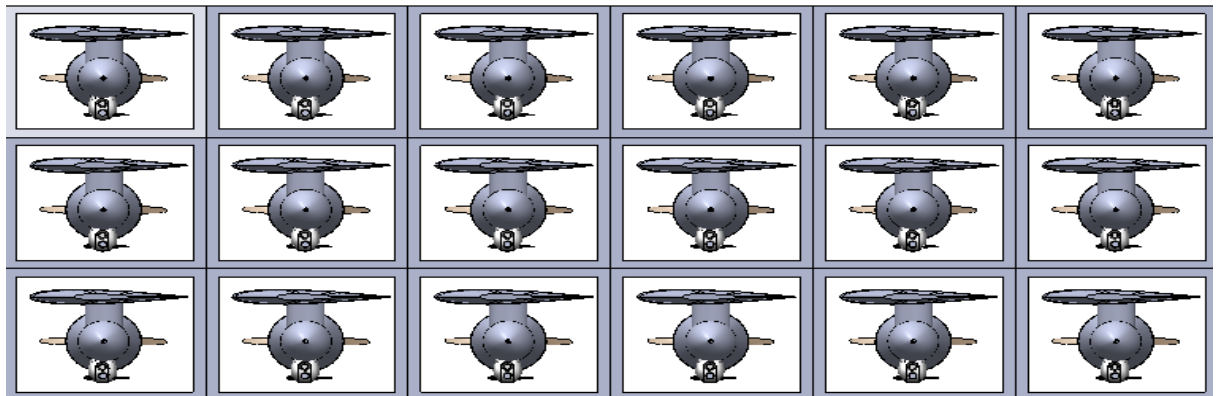


FIGURE 28 - CONF. B CANISTERS, FRONT VIEW

5.2.3. CONFIGURATIONS COMPARISON

Having seen both configuration A and configuration B the 2 teams have decided to Join forces and create the ultimate plane that will contain the better properties of each of configuration.

The comparison was made according to several criteria's that were set prior to the design and that had to meet the product requirements.

The table below describes the main geometric elements that will be discussed:

Configuration	Height [cm]		Width [cm]		Length [cm]		Wingspan [cm]
	Close	Open	Close	Open	Close	Open	
A – Pivoted Canard and Wings	50	55	100	320	290	220	320
B – Rotate Wing	48	68	62.5	400	400	250	400

TABLE 14 - CONFIGURATIONS GEOMETRIC COMPARISON

The most significant difference is in fact the wing length of configuration A relative to configuration B. The latter one has much longer wing The canard even compensates of that length and even adds more lift.

The side view shows that the 'Canard-body' is indeed more "fat" compared to the rotating wing body with a more aerodynamic structure and shape. (Later on that t will be taken into account).

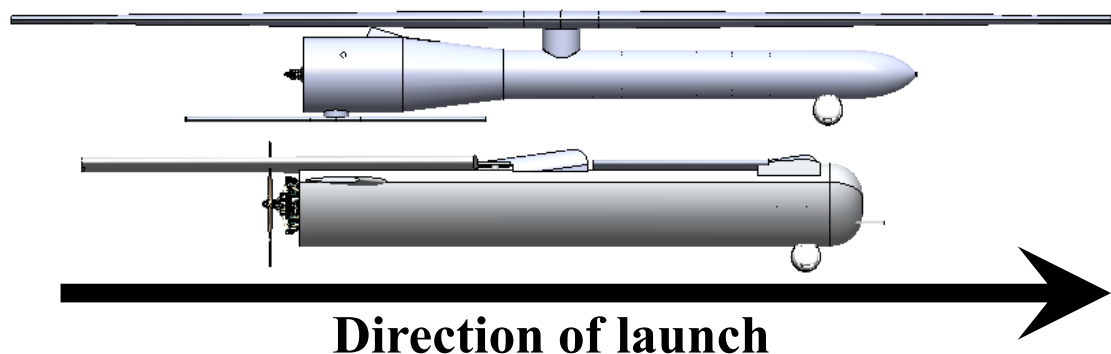


FIGURE 29 - CONFIGURATION SIDE VIEW COMPARISON

At the front it may be noticed that the height is indeed almost identical at both of the configurations. Comparison of both, shows that there is a significant addition to the width in the configuration of the canard.

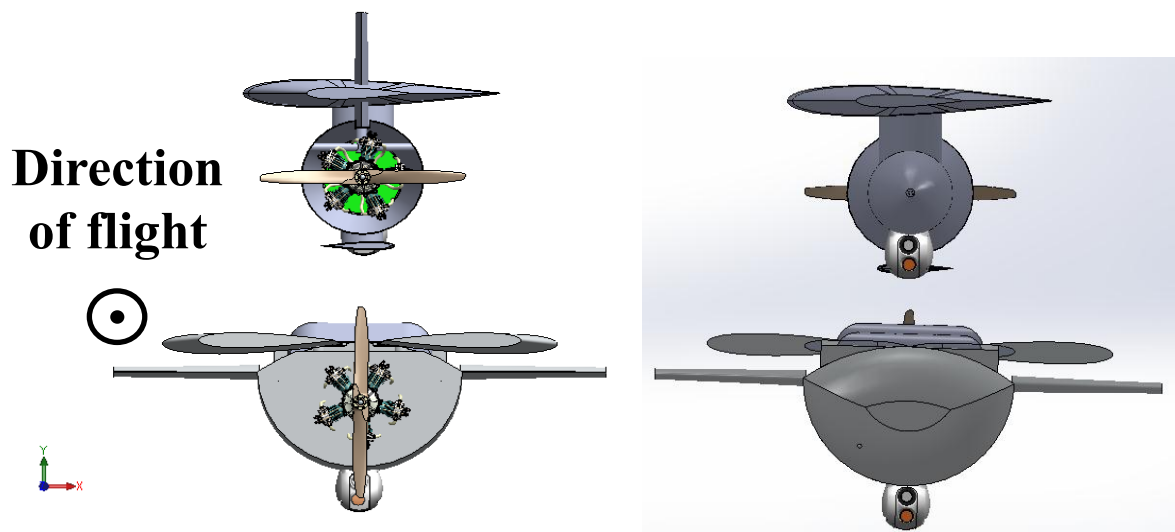


FIGURE 30 - CONFIGURATIONS REAR(LEFT) AND FRONT(RIGHT) VIEW COMPARISON

The dimensions of the containers (or canisters, the cell containing the UAV), appear in the following table:

<u>Configuration</u>	<u>Height [cm]</u>	<u>Width [cm]</u>	<u>Length [cm]</u>	<u>Canisters No for the Harpy vehicle</u>	<u>Vehicle surface area for 18 canisters</u>
<u>A – Pivoted Canard and Wings</u>	<u>60</u>	<u>90</u>	<u>300</u>	<u>60</u>	<u>3.6X3</u>
<u>B – Rotating Wing</u>	<u>55</u>	<u>70</u>	<u>450</u>	<u>72</u>	<u>3.3X2</u>

TABLE 15 - CONFIGURATIONS CANISTERS COMPARISON

It can be seen the length and width dimensions of the rotating wing canister, (which is actually the thing that interests us), is quite small compared to the canard drone.

The cross section area of harpies' carrier on top of the truck is 32.4 square meters. The truck height is 4 and its width is 9, as can be seen in the picture below:



FIGURE 31- IAI HARPY 18 CANISTERS PACK

In fact that the truck can carry about 60 such drones (canard type) and even more drones of the Rotating wing type (approximately 72 items). The size of a vehicle carrying 18 items is about the size of Hammer, which would give us more transferability and would be less dependent on rough terrain.

The next chart summarizes the main advantages raised while developing the configurations.

Configuration	A – Pivoted Canard and Wings	B – Rotate Wing
Advantages	<ul style="list-style-type: none"> ▪ Optional Variable sweep of the wing during different parts of the flight ▪ Better steering , Thanks to canard ▪ Wings common opening system ; Makes it cheaper 	<ul style="list-style-type: none"> ▪ Axisymmetric Body ; minimized effect on lift ▪ Only three folded objects ; Main wing and stabilizers ▪ Simple and cheap wing opening
Disadvantages	<ul style="list-style-type: none"> ▪ Four folded objects 	<ul style="list-style-type: none"> ▪ Unsymmetrical opening

TABLE 16 - CONFIGURATIONS ADVANTAGES AND DISADVANTAGES

The wing's opening systems are both common systems and do not constitute an obstacle while choosing one configuration over another.

However, the canard has the ability to maneuver faster than the rotating wing.

The opening of the wings is symmetrically at the canard, while it is asymmetric at the rotating wing type, which may affect the aerodynamic performance at launch.

The canard has the possibility to change the angle of the wing while the rotating platform has no option to create a variable wing angle.

5.2.4. FINAL COMBINED CONFIGURATION

Good results were obtained for both of the configurations, and each group found the most important benefits of its configuration. It was decided to take the body shape of the canard, improve it and give it the aerodynamic capabilities of the narrow body of the rotating wing. Advantages of each configuration were combined into one, and the planned UAV body actually began to shape into its final combined design.

Combination of all the benefits above with a few more improvements, result in the following combined configuration:

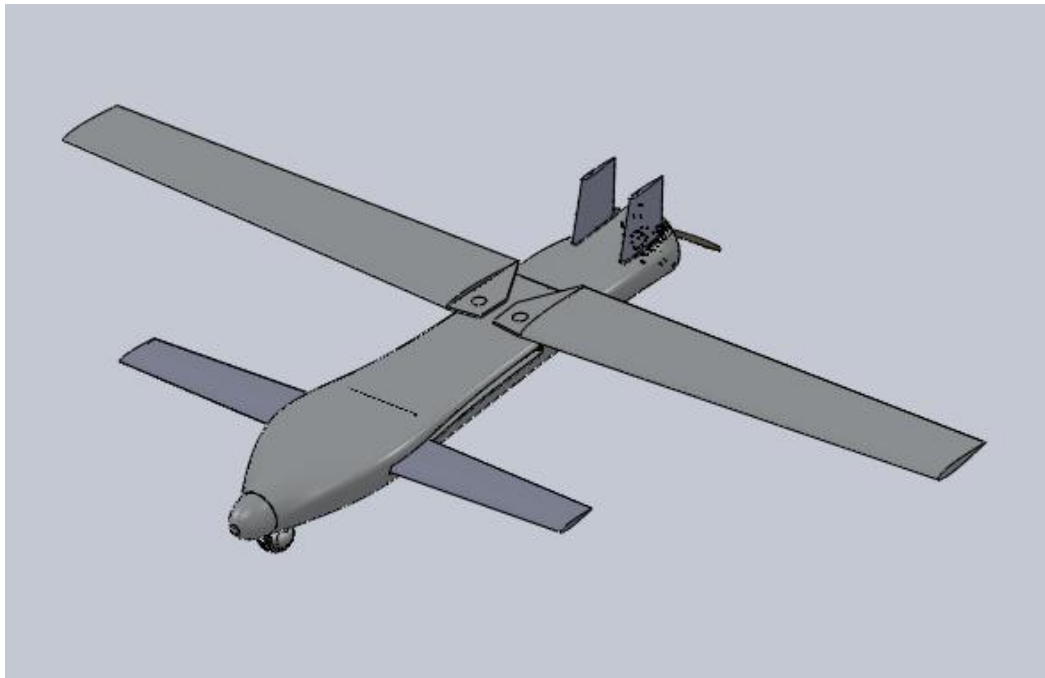


FIGURE 32 - FINAL COMBINED CONFIGURATION

5.3. RADAR CROSS SECTION- RCS

Radar Cross Section (RCS) is a measure of how detectable an object is with radar.

A larger RCS indicates that an object is more easily detected.

Most military aircraft these days are made and designed to have a smaller RCS as possible.

The Stealth Challenge is:

- Survive and prosper in the future environment of improved sensors, dense counter-measures, anti-radiation weapons, and emitter locations.
- Become invulnerable or invisible.

5.3.1. RCS CALCULATED

$RCS = \sigma = \text{Geometric Cross Section} \times \text{Reflectivity} \times \text{Directivity}$

$$RCS = \sigma = A \times \frac{P_{scatter}}{(A)(P_{intercepted})} \times \frac{P_{backscatter}}{\left(\frac{1}{4\pi}\right)P_{scatter}}$$

Simplifying that expression yields the following relationship for radar cross section.

$$\sigma = 4\pi \frac{P_{backscatter}}{P_{intercepted}}$$

The importance of radar cross section can best be understood by

Looking at an equation relating the RCS of the target to the energy received by the radar .

$$S \cong \frac{P_{avg} G \sigma A_e t_{ot}}{(4\pi)^2 R^4}$$

S = signal energy received by the radar

P_{avg} = average power transmitted by the radar

G = gain of the radar antenna

Where:

A_e = effective area of the radar antenna, or "aperture efficiency"

t_{ot} = time the radar antenna is pointed at the target (time on target)

R = range to the target

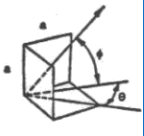
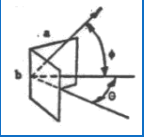
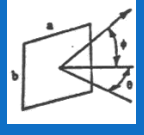
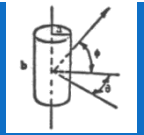
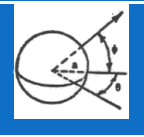
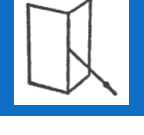
Geometry	Description	Max RCS	Comment
	Square trihedral corner reflector	$\sigma = \frac{12\pi a^4}{\lambda^2}$	Strongest radar return due to triple reflection of incident wave
	Right dihedral corner reflector	$\sigma = \frac{8\pi a^2 b^2}{\lambda^2}$	Second strongest radar return due to double reflection of incident wave; decreases from maximum slowly with changing θ and rapidly with changing ϕ
	Flat plate	$\sigma = \frac{4\pi a^2 b^2}{\lambda^2}$	Third strongest radar return due to direct reflection of incident wave; decreases rapidly as incidence angle changes from perpendicular
	Right circular cylinder	$\sigma = \frac{2\pi a b^2}{\lambda}$	Strong radar return as aspect (θ) changes, but decreases rapidly as azimuth (ϕ) changes
	Sphere	$\sigma = \pi a^2$	Produces the same isotropic return in all directions
	Straight edge	$\sigma = L^2 f(\theta, \theta_{int})$	Perpendicular incidence wave creates a strong but narrow RCS peak

TABLE 17 - RCS GEOMETRY COMPARISON

At the time a thought to make the bottom of the UCAV in a wedge shape because we thought it will have better RCS but after looking at the table we saw that round shape has better RCS than flat plate so that made us drop the idea and keep the oval shape we have.

6. PDR REMARKS

During the PDR a concern was raised as per a possible pitch-up which may happened during the UAV launch.

The wing's unfolding direction determine with the flow direction. In small opening angles, the aerodynamic center of the wing is very close to the nose of the plane. The wing has the biggest lift area and causes the aerodynamic center of the whole UAV to be in front of the center of gravity. The moment causes from the lift of the plane will be positive and will be enlarged with the enlargement of the angle of attack. This is the pitch-up effect.

In order to overcome the pitch-up problem two solutions was examined, as follows:

- Changing the wing and canard lengths (changing the wings and canards wet area ratio).
- Changing the booster rocket positioning angle (changing the thrust flow line direction)

These solutions will be described broadly in the following Detailed Design chapter.

7. DETAILED DESIGN

7.1. PROPELLER SELECTION

The first thing we wish to do is to consult the engine data and information. Each engine has its propeller recommended by the manufacturer. As seen before the chosen engine was 3W:275 XiB2 TS (as seen in picture number 1).



FIGURE 33 - 3W: 275 XiB2 TS

The Information that will help us is as followed:

- A. Engine rotation speed – 1000-7000 RPM
- B. power is 26 horsepower = ~ 19300 watts.
- C. 15.5 lbs= 7 Kg.
- D. Fuel consumption – 0.75 lb/hr/hp.

The manual for every engine will give you a range of propellers that are safe to use with that engine. The manual does not specify the exact size propeller because the propeller must be sized for the airplane that it is used with. It is very important to stay within this recommended range.

Later to the foregoing, the propeller recommended by the manufacturer is a two blade propeller of 26X16 or 26X14 (") or 3 blade propeller of 22X14 or 24X14 (").

As mentioned in previous pages, the weight of our plane is 100 kg and has a pusher propeller that will exceed it to maximal velocity of: 90 [knots] ($180 \left[\frac{ft}{sec} \right]$).

The characteristics of a propeller are defined by the diameter and the pitch. The diameter is the distance from one tip to the other. The pitch is defined as the distance the propeller would move the airplane forward in one rotation in a “perfect” world. Perfect world meaning that the propeller is 100% efficient and the air does not compress, neither of which is practical in the real world. The “*twist*” of the propeller is what determines the pitch. Basically the length of the propeller and its twist defines its characteristics

Generally speaking, before we pick a propeller we need to remember this rule of thumb: the larger the diameter of the propeller the more thrust will be produced by the engine. The larger the pitch the more speed you will get out of your engine. A small diameter large pitch propeller will move a small volume of air really fast! A large diameter small pitch propeller will move a large volume of air at a slower speed.

In the illustration below, the two arrow lines represent the path of each propeller tip. You can see that the higher pitch prop (EG 10x8) takes only one and a half turns to cover the same distance that the lower pitch prop (EG 10x4) takes 3 turns to. So, with both engines and props spinning at identical RPM, the higher pitch prop will travel further in the same amount of time - hence a faster flying plane.

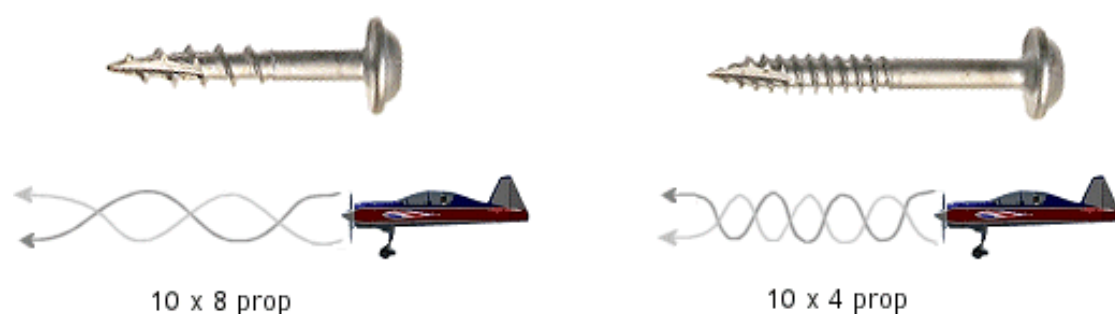


FIGURE 34 - PITCH ILLUSTRATION

If we want to change the maximum RPM, then we need to change the load on the engine. Replacing a 11x6 prop with a 10x6 prop, or replacing a 11 X 6 prop with a 11 x 5 prop will decrease the load on the engine and raise the max RPM. Changing from a 10 x 6 to 10 x 7 prop, or changing from a 10 x 6 prop to a 11 x 6 prop will increase the load and lower the max RPM.

If the propeller load is too large the engine will not turn fast enough to fly the airplane and could cause the engine to overheat. If the load is too small the engine will turn too fast damaging the engine. So it is important to stay within the window recommended by the engine manufacturer.

Let us compare the main propeller properties to those of a car.

Low pitch propellers = low gear in your car. It will get you up hills well but will not take you anywhere fast.

High pitch propellers = Beginning your drive in fifth gear It will take forever to accelerate to speed but the plane is cruising when it gets there.

High Pitch Propeller properties: High speed flight, poor acceleration, poor climb, can be difficult to slow down for landing.

Low Pitch Propeller properties: Low speed flight, good acceleration, good climb, finer speed control throughout throttle range — particularly at low throttle settings.

Multi-blade Model Airplane Propellers

Three bladed model airplane propellers are less efficient than two bladed propellers. In fact, the more blades that are added, the less efficient the propeller becomes. The only advantage of a multi-blade prop is a smaller diameter.



FIGURE 35 - MULTI-BLADE ILLUSTRATION

Multi-blade propellers are used with full-scale airplanes when ground clearance is an issue (NOT our case). WWII fighter planes are a good example. For this reason many pilots use multi-blade props on their scale model airplanes to make it look more like the full-scale airplane.

Twin engine airplanes often use multi-blade propellers because the smaller diameter is needed for the propeller to clear the fuselage.

Now we shall discuss how to choose the right pitch and diameter alongside the manufacturer recommendation.

Calculations – Needed Pitch

The calculation is quite simple to determine the right pitch for our plane.

From our engine data: engine max RPM is 7000 RPM, that is 116.67 round per second.

To cruise at speed $180 \frac{ft}{sec}$, we will need

$$\frac{55}{116} = 0.34 \left[\frac{m}{round} \right] = 18 \left[\frac{inch}{round} \right]$$

Now let us compare it to the recommended pitch:

$$14'' \text{ pitch will give us } 14 \left[\frac{inch}{round} \right] = 1.167 \left[\frac{ft}{round} \right]$$

Hence, for speed of $180 \frac{ft}{sec}$, we'll need 231.36 RPS = 13882 RPM = 198% of max RPM.

Calculations – Choose the Needed Diameter

Let us define some needed variables:

D – diameter

V = velocity

n = RPM value

ρ = Density

P = power

β = Step angle

advanced ratio – $J = \frac{V}{nD}$

power coefficient – $C_p = \frac{P}{\rho n^3 D^5}$

if β is const then – $\beta = \tan^{-1} \frac{p/D}{\pi r}$

We use these equations in an iterative manner to find the average diameter that fits us best. Accordingly to the graph below

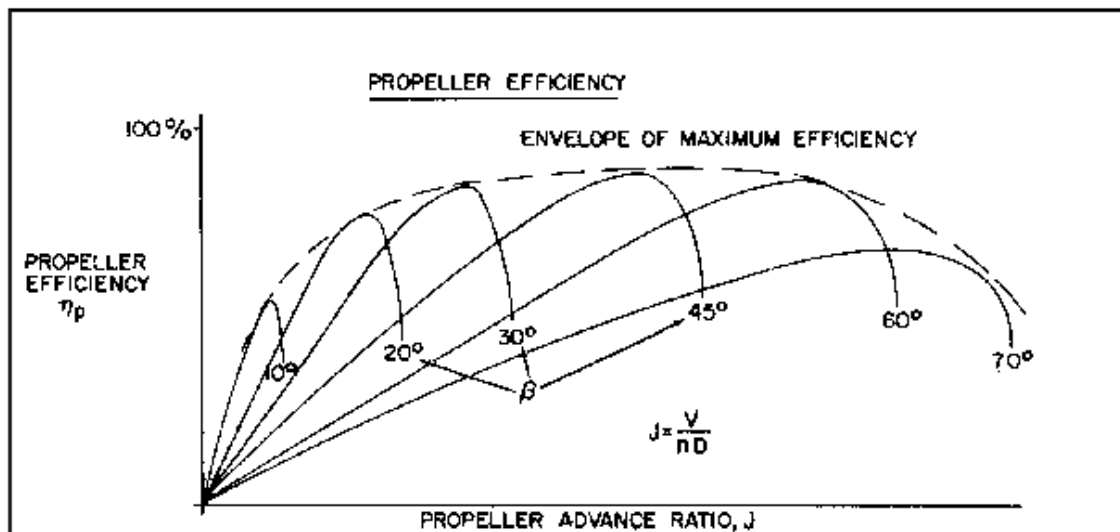


FIGURE 36 - PROPELLER EFFICIENCY VS. PROPELLER ADVANCE RATIO

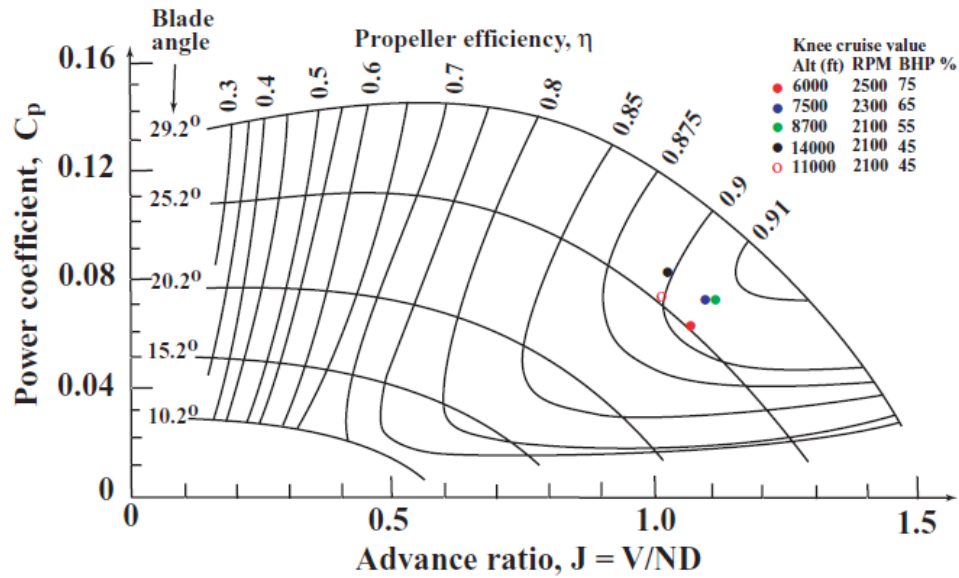


FIGURE 37 - POWER COEFFICIENT VS. PROPELLER ADVANCE RATIO

These graphs were taken from an article that shows how to choose a propeller. A specific propeller had been chosen which has a specific airfoil. That is because there are lots of elements in the iteration, we cannot name them all.

At the end, our prop is a 2 bladed-back-folding prop at the size of 25X18.

7.2. AIRFOIL SELECTION

First of all, the airfoil has to be not extremely thin and with no extremely high camber, so it'll be easy to manufacture.

The stall angle was the most important feature taken into account, since in this case, where the UAV is maneuvering at high angles of attack, it's important to have an airfoil with a high stall angle.

Also, the chosen EPPLER 560 airfoil has a high max L/D and lift coefficient.

A canard airfoil will usually have a greater camber, but it's not always necessary. Hence, the same airfoil will be used for the canards, because of stall considerations and because of performance considerations.

This airfoil will be the airfoil of both wings and canards, since it's the best of more than 1000 airfoils analyzed. The vertical tails' airfoil will remain symmetric – NACA 0012.

In addition, the Iranian UAV ABABIL has the same configuration (wing-canard) and it's airfoil is NACA 4412.

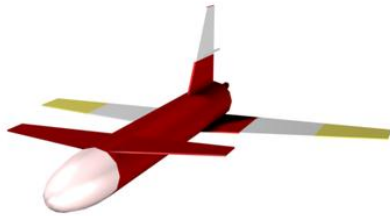


FIGURE 38 - ABABIL ILLUSTRATION

A comparison made between a simple NACA 0012 airfoil, NACA 4412 and the selected EPPLER 560:

naca-4412

EPPLER 560

naca-0012

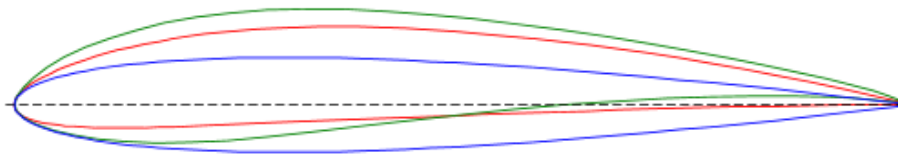


FIGURE 39 - AIRFOILS COMPARISON

A comparison between the three above airfoils in aspects of lift, moment and drag coefficients:

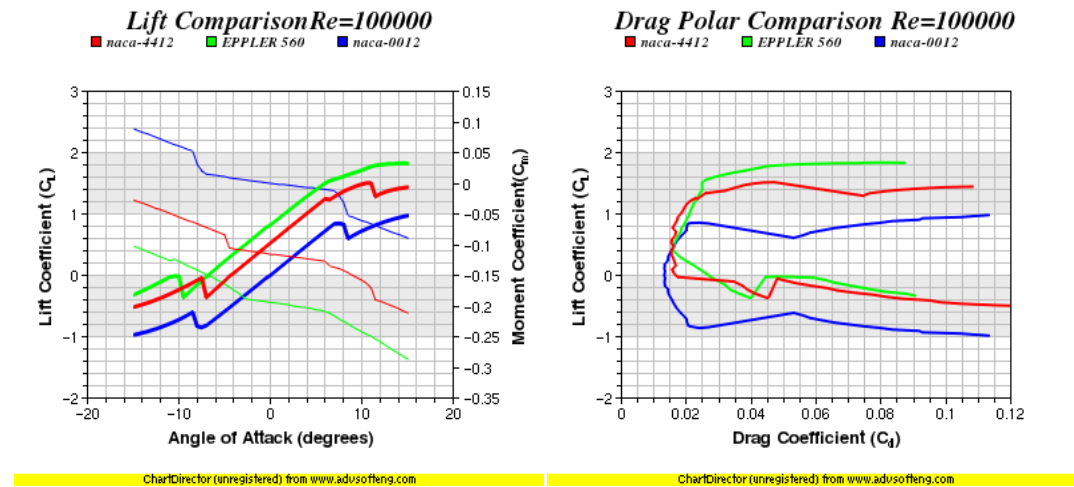


FIGURE 40 - AIRFOILS' LIFT AND DRAG POLAR COMPARISONS

	NACA 4412	EPPLER 560	NACA 0012
Thickness (%)	11.979	16.067	11.979
Camber (%)	3.999	4.859	0.000
Trailing Edge Angle (%)	14.394	13.703	14.571
Lower Surface Flatness	76.1	57.465	17.064
Leading Edge Radius (%)	1.683	3.009	1.686
Maximum Lift (C_L)	1.507	1.827	0.972
Maximum Lift Angle-of-Attack (deg)	11.000	14.500	7.500
Maximum Lift-to-drag (L/D)	57.209	60.080	40.563
Lift at Maximum Lift-to-drag	1.188	1.504	0.840
Angle-of-Attack for Maximum Lift-to-drag (L/D)	5.500	6.000	7.000

TABLE 18 - AIRFOILS CHARACTERISTICS COMPARISONS

The tables above and below shows a comparison between the three airfoils described above, while the three most important features for us were the underlined ones:

If we focus on those three main features and compare between the NACA 0012 and EPPLER 560:

	NACA 0012	Eppler 560	Improvement (%)
Max C_L	0.972	1.827	88
Max L/D	40.63	60.08	48
Stall angle	7.5	14.5	93

TABLE 19 - NACA 0012 AND EPPLER 560 COMPARISON

If we focus on those three main features and compare between the NACA 4412 and EPPLER 560:

	Eppler 560	NACA 4412	Improvement (%)
Max C_L	1.827	1.507	21
Max L/D	60.08	57.209	5
Stall angle	14.5	6	142

TABLE 20 - EPPLER 560 AND NACA 4412 COMPARISON

All parameters combined, the EPPLER 560 is the best airfoil analyzed.

7.3. ROCKET BOOSTER

7.3.1. BOOSTER DESIGN AND SIZING

Now we'll calculate rocket's (booster) estimated path.

The angle of launch is 45° :

$$du = -u_{eq} \cdot \frac{dm}{m} - \frac{D}{m} dt - g \cdot dt ; \quad u_{eq} = I_{sp} \cdot g_o$$

Let's integrate this equation numerically with steps of Δt :

$$\Delta u = u_{eq} \cdot \ln \frac{m_1}{m_2} - \frac{\bar{D}}{\bar{m}} \Delta t - g \cdot \Delta t$$

$$m_2 = m_1 - \dot{m} \cdot \Delta t ; \quad \bar{m} = \frac{m_1 + m_2}{2} ; \quad \bar{D} = 0.5 \rho_1 u_1^2 C_D A_f ;$$

$\Delta u_x, \Delta t \rightarrow \Delta x ; \Delta u_y, \Delta t \rightarrow \Delta y \Rightarrow$ The path of the rocket.

$\left. \begin{array}{l} t_b = 3[\text{sec}] \\ m_p = 3[\text{kg}] \end{array} \right\} \Rightarrow$ This information was found by iterations (in Matlab) of the flight path.

$$\dot{m} = \frac{m_p}{t_b} = 1[\text{kg}/\text{sec}] ;$$

$$\Rightarrow A_t = \frac{C^* \cdot \dot{m}}{P_c} = 1.964 \cdot 10^{-4}[\text{m}^2] ;$$

$$\Rightarrow d_t = 15.8[\text{mm}] \Rightarrow d_e = d_t \cdot \sqrt{8.87} = 47.1[\text{mm}] ;$$

7.3.2. MOMENT VS. TIME FOR DIFFERENT BOOSTER ANGLES

In order to complete the pitch-up solution, placing the booster in an angle was tested. This angle should cause negative moment and by this will cancel the pitch.

After modifying the wing dimensions at the beginning of the semester, the positive moment needs to be much smaller. To examine this solution, we plotted graphs of the moment vs. time (while the unfolding of the wings) for different angles. We had to confront with the change of mass and pressure centers due to wings opening.

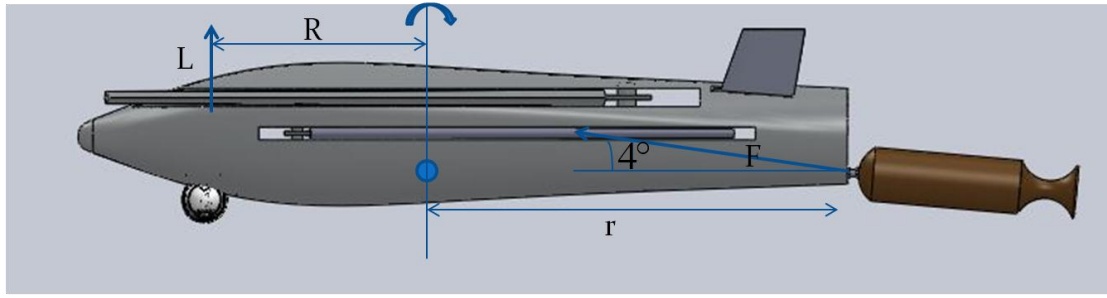


FIGURE 41 - BOOSTER ANGLE

At the sketch r, R –are distances that changing in time.

Assumptions and datas:

Time of opening the wings: $t = 1.5[\text{sec}]$

Velocity: $v = 60 \left[\frac{m}{s} \right]$

Density: $\rho = 1.225 \left[\frac{kg}{m^3} \right]$

The mass: $m = 100[kg]$

The acceleration of the booster: $a = 40 \left[\frac{m}{s^2} \right]$

Distance from the lift to the center of mass: $R[m]$

Distance from the thrust of booster to the center of mass: $r[m]$

Area of wing that creates the lift: $S[m^2]$

The force that booster applies: $F[N] = m \cdot a \cdot \sin \alpha$

The lift: $L = \frac{1}{2} \rho v^2 S C_l$

The total moment at the UAV at time of launch:

$$\sum M = L \cdot R - F \cdot r = \frac{1}{2} \rho v^2 S C_l R - m a r$$

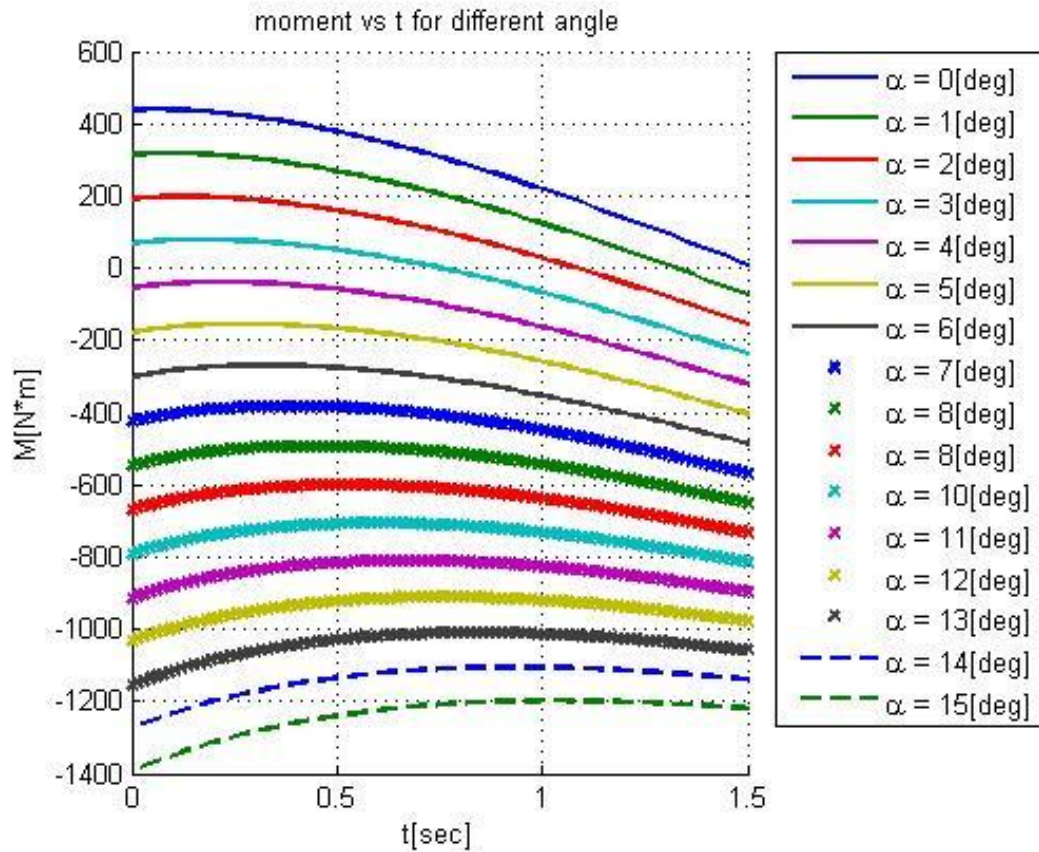


FIGURE 42 -TOTAL MOMENT VS. TIME

The above graph shows how the moment changes with time at different angles from 1° to 15° .

The conclusion is: when the angle equals 4° the moment's sum is zero, so by placing the booster at this angle there will be no pitch.

7.4. PLANE GEOMETRY IMPROVEMENTS

Plane geometry design as shown at PDR:

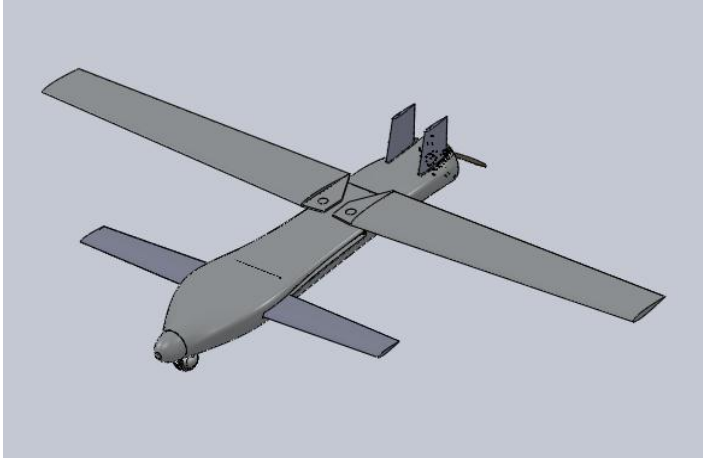


FIGURE 43 - PDR FINAL CONFIGURATION

Most of the aerodynamic drag was cost due to wrong body geometry design. That drag is caused mainly from the "come and back" geometry – meaning that the body becomes thinner in the middle of it and then expands until it reaches the engine diameter. To resolve that issue, we made the guideline of the body as much as monotonic as possible, because of the limitation of the root of the canard at the front of the plane. The first iteration in this process is in the pictures below:

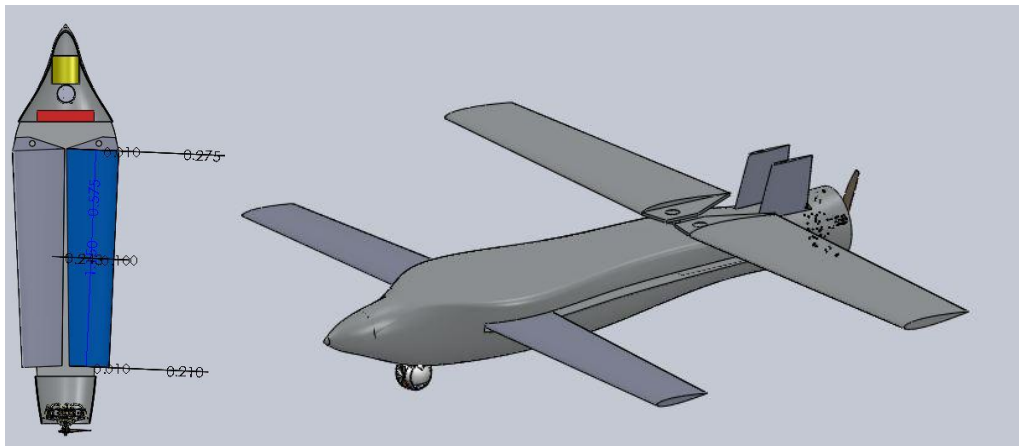


FIGURE 44 - CDR INITIAL CONFIGURATION IMPROVEMENTS

In this iteration we already fitted the plane with the larger 40:60 canard and gave the plane a more continuous and smooth fuselage but still had the "come and back" effect.

In order to improve more the aerodynamic of the plane, we redesign the nose and cover the wings axis. That was last iteration, and it is shown in the pictures below:

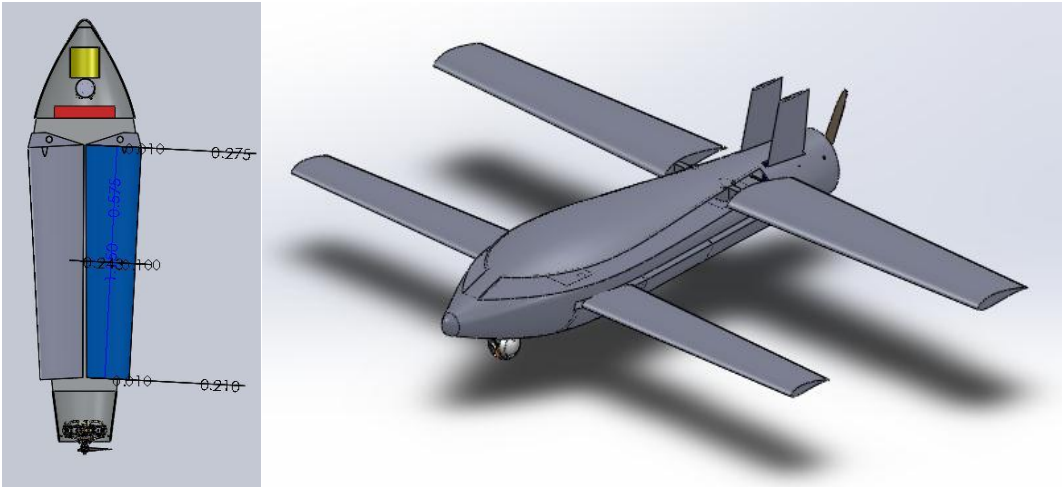


FIGURE 45 - CDR FINAL CONFIGURATION IMPROVEMENTS

In the final configuration we put on the plane the right airfoil on the wings gave it a propeller in the right size according to the calculations.

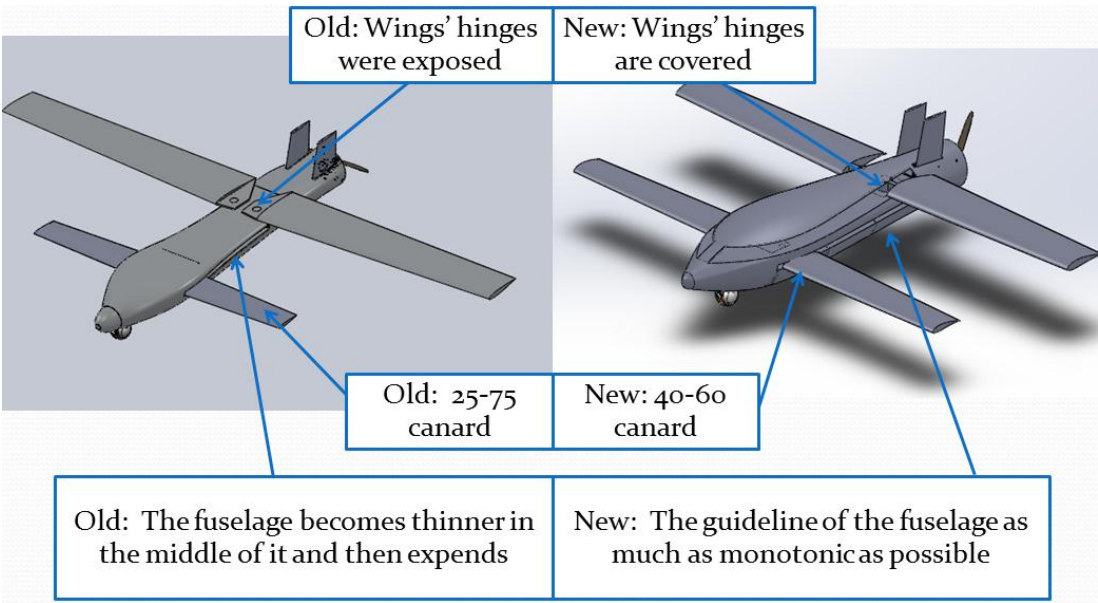


FIGURE 46 - GEOMETRY IMPROVEMENTS DESCRIPTION

Adding a cover to the wings also gave us a smoother fuselage and gut rid of the "come and back" effect, but it gave us another slot for the main wing as can be seen in the picture above.

The idea in how to fix it was a strong rubber "curtain" as shown in the final configuration chapter.

7.5. AERODYNAMIC

7.5.1. LIFT COEFFICIENT

Data:

Plane & engine:

$$W = 220g[poundal]$$

$$\rho_{height=0} = 0.0765 \left[\frac{lb}{ft^3} \right], \rho_{height=5000\ ft} = 0.0613 \left[\frac{lb}{ft^3} \right]$$

The airfoils chosen for the wing and canard: EPPLER 560.

Primary properties:

$$C_{l\max} = 1.827$$

$$\alpha_{stall} = 14.5^\circ = 0.367[rad]$$

$$\alpha_{zero\ lift\ line} = -6.5^\circ = 0.113[rad]$$

$$C_l = 0.8$$
$$\alpha=0$$

$$C_{l,\alpha} = 4.1 \left[\frac{1}{rad} \right]$$

The distances of the wing and the canard from the reference point:

$$x_w = 4.921[ft], x_c = 2.034[ft]$$

$$z_w = 0.427[ft], z_c = 0.131[ft]$$

Aspect ratio:

$$A_{wing} = 9, A_{canard} = 11, A_{body} = 0.5$$

Lift areas:

$$S_{ref} = 17.586[ft^2]$$

$$S_{wing} = 10.471[ft^2], S_{canard} = 7.116[ft^2], S_{body} = 8.739[ft^2]$$

Spans:

$$b_{wing} = 9.843[ft], b_{canard} = 8.858[ft]$$

Assumptions:

- C_l, C_L Are Linear with α .
- The wing and the canard's effects on each other are distributed constantly along their span.
- The dynamic pressure is constant along the plane ($\eta_c = 1, \eta_b = 1$).
- The body, as a lift generator, has a very small aspect ratio, but it can still affect the lift. As an aerodynamic airfoil, the assumptions will be:

$$C_{l_b, \alpha} = 2\pi \left[\frac{1}{rad} \right], C_{L_b} \approx 0_{\alpha=0}$$

(In zero angle of attack, the body generates approximately zero lift).

Minimum lift coefficient (for cruise flight):

$$V_{\max} = 110[knots] = 182.3 \left[\frac{ft}{sec} \right], L = W$$

$$\Rightarrow C_{L_{\min}^{height=0 ft}} = \frac{L}{\frac{1}{2} \rho S V_{\max}^2} = \frac{220 \cdot 32.185}{\frac{1}{2} \cdot 0.0765 \cdot 17.59 \cdot 182.3^2} = 0.317$$

$$C_{L_{\min}^{height=5000 ft}} = \frac{L}{\frac{1}{2} \rho S V_{\max}^2} = \frac{220 \cdot 32.185}{\frac{1}{2} \cdot 0.0613 \cdot 17.59 \cdot 182.3^2} = 0.395$$

Lift coefficient as function of angle of attack:

In general, the components of the UAV which generates lift will induce one another. In the case of a conventional plane with a configuration of wing-tail, the wing will influence the tail because the wing generates a wake. The following equation is modified to include the effect of the downwash field in a wing-tail configuration:

$$C_{L_{wt}, \alpha} = C_{L_w, \alpha} + C_{L_t, \alpha} \eta_t \frac{S_t}{S_w} \left(1 - \frac{d\varepsilon_t}{d\alpha} \right) + C_{L_b, \alpha} \eta_b \frac{S_b}{S_w}$$

In principle, the horizontal tail will influence the wing as well. However, in practice this effect is very small and neglected because of the small

reference surfaces ratio $\left(\frac{S_t}{S_w} \ll 1 \right)$.

The equation for the lift curve slope for configuration of wing-canard is similar to the equation for a wing-tale configuration:

$$C_{L_{wc},\alpha} = C_{L_w,\alpha} \left(1 - \frac{d\varepsilon_w}{d\alpha}\right) + C_{L_c,\alpha} \eta_c \frac{S_c}{S_w} \left(1 + \frac{d\varepsilon_c}{d\alpha}\right) + C_{L_b,\alpha} \eta_b \frac{S_b}{S_w}$$

It is seen that the influence up-wash at the canard due to the wing is also included, because of the big reference surfaces ratio $\left(\frac{S_c}{S_w} = 0.68\right)$.

Now, the expression $\left(1 - \frac{d\varepsilon_w}{d\alpha}\right)$ is interpreted as the effective or average value of interference from the up-wash.

From Etkin and Reid's book:

$$C_{L_w,\alpha} = \frac{C_{l,\alpha}}{\frac{C_{l,\alpha}}{\pi A_w} + \sqrt{1 + \left(\frac{C_{l,\alpha}}{\pi A_w}\right)^2}} = \frac{4.2}{\frac{4.2}{\pi \cdot 9} + \sqrt{1 + \left(\frac{4.2}{\pi \cdot 9}\right)^2}} = 3.62 \left[\frac{1}{rad} \right]$$

$$C_{L_c,\alpha} = \frac{C_{l,\alpha}}{\frac{C_{l,\alpha}}{\pi A_c} + \sqrt{1 + \left(\frac{C_{l,\alpha}}{\pi A_c}\right)^2}} = \frac{4.2}{\frac{4.2}{\pi \cdot 11} + \sqrt{1 + \left(\frac{4.2}{\pi \cdot 11}\right)^2}} = 3.72 \left[\frac{1}{rad} \right]$$

$$C_{L_b,\alpha} = \frac{C_{l_b,\alpha}}{\frac{C_{l_b,\alpha}}{\pi A_b} + \sqrt{1 + \left(\frac{C_{l_b,\alpha}}{\pi A_b}\right)^2}} = \frac{2\pi}{\frac{2\pi}{\pi \cdot 0.5} + \sqrt{1 + \left(\frac{2\pi}{\pi \cdot 0.5}\right)^2}} = 0.774 \left[\frac{1}{rad} \right]$$

To find the downwash effect will be estimate from flight mechanics, while the value is multiplied by a correction factor which is depends on the ratio of the wing span to the canard span.

$$\Lambda_{c/4} = 3^\circ = \frac{1}{60} \pi [\text{rad}]$$

$$K_A = \frac{1}{A_{canard}} - \frac{1}{1 + A_{canard}^{1.7}} = \frac{1}{11} - \frac{1}{1 + 11^{1.7}} = 0.0742$$

$$K_\lambda = \frac{10 - 3\lambda}{7} = \frac{10 - 3 \cdot 0.75}{7} = 1.1071$$

$$K_H = \frac{1 - |z_{canard} - z_{wing}| / b_{canard}}{\sqrt[3]{2(x_{wing} - x_{canard}) / b_{canard}}} = \frac{1 - |0.131 - 0.427| / 8.858}{\sqrt[3]{2(4.921 - 2.034) / 8.858}} = 1.1149$$

$$\Rightarrow \frac{d\varepsilon_w}{d\alpha} \cong k_b \cdot 4.44 \left[K_A K_\lambda K_H (\cos \Lambda_{c/4})^{0.5} \right]^{1.19}$$

$$k_b = \frac{b_c}{b_w} = \frac{8.858}{9.843} = 0.9$$

$$\frac{d\varepsilon_w}{d\alpha} = 0.9 \cdot 4.44 \left[0.0742 \cdot 1.1071 \cdot 1.1149 (\cos \frac{1}{60} \pi)^{0.5} \right]^{1.19} = 0.232 \left[\frac{1}{\text{rad}} \right]$$

The up-wash effect is much smaller than the downwash effect (the direction of the trace is with the flight direction). It can be assumed that the average up-wash effect is: $\frac{d\varepsilon_c}{d\alpha} \cong 0.05$.

Therefore:

$$C_{L,\alpha} = 3.62(1 - 0.232) + 3.72 \cdot 1 \cdot 0.68 \cdot (1 + 0.05) + 0.774 \cdot 1 \cdot \frac{8.793}{10.471} = 6.086 \left[\frac{1}{\text{rad}} \right]$$

From flight mechanics:

$$C_L = C_{L,\alpha=0} + C_{L,\alpha} \alpha$$

While $C_{L,\alpha=0}$ is calculated with respect to the incidence angles:

$$C_{L,\alpha=0} = C_{L,\alpha_w} \left(i_w - \varepsilon_w \right) + C_{L,\alpha_c} \eta_c \frac{S_c}{S_w} \left(i_c + \varepsilon_c \right)$$

Calculating the induced angles:

The induced angle of the wing is caused by the canard. Therefore, the angle is calculated with respect to the angle of attack of the canard (and vice versa).

$$\begin{cases} \varepsilon_w = \frac{d\varepsilon_w}{d\alpha} \alpha_c = \frac{d\varepsilon_w}{d\alpha} (\alpha + i_c) \rightarrow \varepsilon_w = \frac{d\varepsilon_w}{d\alpha} i_c = 0.232 i_c \\ \varepsilon_c = \frac{d\varepsilon_c}{d\alpha} \alpha_w = \frac{d\varepsilon_c}{d\alpha} (\alpha + i_w) \rightarrow \varepsilon_c = \frac{d\varepsilon_c}{d\alpha} i_w = 0.05 i_w \end{cases}$$

Therefore:

$$C_{L_{\alpha=0}} = 3.62(i_w - 0.232i_c) + 3.72 \cdot 1 \cdot 0.68(i_c + 0.05i_w) = 3.746i_w + 1.69i_c$$

$$\Rightarrow C_L = 3.746i_w + 1.69i_c + 6.086 \cdot \alpha$$

The incidence angles are the pitch angle of the wing with respect to the fuselage. The chosen wing is untwisted; therefore the incidence is simply the angle between the fuselage longitudinal axis and the wing's airfoil chord's line.

Wing incidence angle is chosen to create the required lift in some operating conditions. The UAV has a long segment of cruise and therefore the chosen angles of the wing have to create stall of the plane in horizontal flight.

For cruise flight:

$$L = W \rightarrow C_L = C_{L_{\text{cruise}}}$$

Therefore:

$$V_{\text{cruise}} = 80[\text{knots}] = 135 \left[\frac{\text{ft}}{\text{sec}} \right]$$

$$\alpha_{\text{plane}} = 0 \text{ (horizontal flight)}$$

$$C_{L_{\text{cruise}}} = \frac{W}{\frac{1}{2} \rho S V_{\text{cruise}}^2} = \frac{220 \cdot 32.185}{\frac{1}{2} \cdot 0.0613 \cdot 17.59 \cdot 135^2} = 0.721$$

$$C_{L_{\text{cruise}}} = 3.746i_w + 1.69i_c = 0.721$$

The wing and the canard have the same airfoil, and therefore stall at the same angle. In order to prevent stall of the canard before the stall of the wing, the wing should be placed with a bigger incident angle.

$$\alpha_w = \alpha + i_w - \varepsilon_w = \alpha_c + 3^\circ = \alpha + i_c + \varepsilon_c + \frac{\pi}{60} [rad]$$

$$i_w - 0.232i_c = i_c + 0.05i_w + \frac{\pi}{60} \Rightarrow 0.95i_w \Rightarrow i_w = 1.297i_c + \frac{\pi}{57}$$

$$3.746 \left(1.297i_c + \frac{\pi}{57} \right) + 1.69i_c = 0.721 \rightarrow \begin{cases} i_w = 0.157 [rad] = 9^\circ \\ i_c = 0.079 [rad] = 4.5^\circ \end{cases}$$

$$\Rightarrow \boxed{C_L = 0.721 + 6.086 \cdot \alpha}$$

Maximal lift coefficient:

To get the maximal lift coefficient, the wing has to stall:

$$\alpha_w = \alpha_{\substack{stall \\ EPPLER \\ 560}} = 0.367 [rad] = \alpha + i_w - \varepsilon_w$$

$$\Rightarrow \alpha_{stall} = -i_w + \varepsilon_w + 0.367 = -0.157 + 0.232 \cdot 0.079 + 0.367 = 0.228 [rad] = 13.1^\circ$$

$$C_{L_{max}} = 3.746 \cdot 0.157 + 1.69 \cdot 0.079 + 6.086 \cdot 0.228 = \boxed{2.11}$$

Zero lift angle:

$$C_L = 0.721 + 6.086 \cdot \alpha = 0$$

$$\Rightarrow \boxed{\alpha_{C_L=0} = -0.118 [rad] = -6.8^\circ}$$

Final results:

Property	Result
Lift coefficient slope	$C_{L,\alpha} = 6.086 \left[\frac{1}{rad} \right]$
Lift coefficient as a function of angle of attack	$C_L = 0.721 + 6.086 \cdot \alpha$
Minimal lift coefficient at height of 0ft and 5000ft	$C_{L_{min}}_{height=0\ ft} = 0.317$ $C_{L_{min}}_{height=5000\ ft} = 0.395$
Incidence angles	$\begin{cases} i_w = 0.131[rad] = 9^\circ \\ i_c = 0.079[rad] = 4.5^\circ \end{cases}$
Maximal lift coefficient	$C_{L_{max}} = 2.11$
Stall angle	$\alpha_{stall} = 0.228[rad] = 13.1^\circ$
Zero lift angle	$\alpha_{C_L=0} = -0.118[rad] = -6.8^\circ$

TABLE 21 - LIFT CHARACTERISTICS

7.5.2. DRAG COEFFICIENT

The drag is calculated from a superposition of the form and skin drag and the lift-induced drag:

$$C_D = \underbrace{C_{D_0}}_{\text{form\&skin drag}} + \underbrace{KC_L^2}_{\text{induced drag}}$$

In order to calculate the drag, one needs to calculate the constants:

$$C_{D_0}, K = \frac{1}{\pi A e}$$

(e - Oswald efficiency number)

For conventional fixed-wing aircraft with moderate aspect ratio and sweep, Oswald efficiency number is typically between 0.7 and 0.85.

An estimated value of 0.775 was chosen. Therefore:

$$C_{D_i} = K \cdot C_L^2$$

$$\eta_c = \eta_b = 1$$

$$K_w = \frac{1}{\pi \cdot 9 \cdot 0.775} = 0.0456;$$

$$K_c = \frac{1}{\pi \cdot 11 \cdot 0.775} = 0.0373;$$

$$K_b = \frac{1}{\pi \cdot 0.5 \cdot 0.775} = 0.821;$$

$$\Rightarrow \boxed{K_{plane} \approx 0.056}$$

Property	Result
Drag coefficient as a function of lift coefficient	$C_D = 0.02 + 0.056C_L^2$

TABLE 22 - DRAG PROFILE

7.6. PERFORMANCE CALCULATIONS

7.6.1. THRUST CALCULATIONS

Maximal thrust:

For cruise flight:

$$\begin{cases} T = D \\ W = L \end{cases} \rightarrow \frac{T}{W} = \frac{D}{L} = \frac{1}{L/D}$$

$$\frac{L}{D} = \frac{\frac{1}{2}\rho SV^2 C_L}{\frac{1}{2}\rho SV^2 C_D} = \frac{C_L}{C_D}$$

$$T_{\max} \Rightarrow \left(\frac{D}{L} \right)_{\max} = \frac{C_{D_{\max}}}{C_{L_{\max}}}$$

$$\begin{cases} C_{L_{\max}} = 2.11 \\ C_D^* = C_{D_0} + KC_{L_{\max}}^2 = 0.02 + 0.056 \cdot 2.11^2 = 0.269 \end{cases}$$

$$\Rightarrow T_{\max} = W \left(\frac{D}{L} \right)_{\max} = 220 \cdot g \cdot \frac{0.269}{2.11} = 28[lbf] = 902.7[poundal]$$

Minimal thrust:

For cruise flight:

$$\begin{cases} T = D \\ W = L \end{cases} \rightarrow \frac{T}{W} = \frac{D}{L} = \frac{1}{L/D}$$

$$\frac{L}{D} = \frac{\frac{1}{2}\rho SV^2 C_L}{\frac{1}{2}\rho SV^2 C_D} = \frac{C_L}{C_D}$$

$$T_{\min} \Rightarrow \left(\frac{D}{L} \right)_{\min} = \frac{C_D^*}{C_L^*}$$

$$\begin{cases} C_L^* = \sqrt{\frac{C_{D_0}}{K}} = \sqrt{\frac{0.02}{0.056}} = 0.598 \\ C_D^* = 2C_{D_0} = 0.04 \end{cases}$$

$$\Rightarrow T_{\min} = W \left(\frac{D}{L} \right)_{\min} = 220 \cdot g \cdot \frac{0.04}{0.598} = 14.7[lbf] = 473.6[poundal]$$

Thrust for Cruise Flight

$$C_{L_{\alpha=0}} = 0.722 \Rightarrow C_D = 0.02 + 0.056 \cdot 0.722^2 = 0.0492$$

$$\Rightarrow T = W \left(\frac{C_D}{C_L} \right) = 220 \cdot g \cdot \frac{0.0492}{0.722} = 15[lbf] = 489.5[poundal] = 53.5\% T_{\max}$$

Final results:

Property	Result
Maximum thrust	$T_{\max} = 28[lbf] = 902.7[poundal]$
Minimum thrust	$T_{\min} = 14.7[lbf] = 473.6[poundal]$
Thrust for cruise flight	$T = 15[lbf] = 489.5[poundal] = 53.5\% T_{\max}$

TABLE 23 - THRUST PROPERTIES

7.6.2. VELOCITY CALCULATIONS

$$\text{Velocity: } v = \frac{L}{\frac{1}{2} \rho S_{\text{wing}} C_L^2}$$

Assumption:

$$\text{Maximal velocity: } V_{\max} = 110[knots]$$

Stall velocity (minimum):

$$V_{\text{stall}} = \sqrt{\frac{L}{\frac{1}{2} \rho_{\text{height}=0} S C_{L_{\max}}}} = \sqrt{\frac{W}{\frac{1}{2} \rho S C_{L_{\max}}}} \quad L=W$$

$$V_{\text{stall}_{\text{height}=0}} = \sqrt{\frac{W}{\frac{1}{2} \rho_{\text{height}=0} S C_{L_{\max}}}} = \sqrt{\frac{220 \cdot 32.185}{\frac{1}{2} \cdot 0.0765 \cdot 17.586 \cdot 2.11}} = 70.6 \left[\frac{ft}{sec} \right] = 41.8[knot]$$

$$V_{\text{stall}_{\text{height}=5000 ft}} = \sqrt{\frac{W}{\frac{1}{2} \rho_{\text{height}=5000} S_{\text{wing}} C_{L_{\max}}}} = \sqrt{\frac{220 \cdot 32.185}{\frac{1}{2} \cdot 0.0613 \cdot 17.586 \cdot 2.11}} = 78.9 \left[\frac{ft}{sec} \right] = 46.7[knot]$$

Final results:

Property	Result
Minimum velocity (stall) - height of 0ft and 5000ft.	$V_{stall_{height=0}} = 70.6 \left[\frac{ft}{sec} \right] = 41.8[knot]$ $V_{stall_{height=5000\ ft}} = 78.9 \left[\frac{ft}{sec} \right] = 46.7[knot]$
Maximal velocity	$V_{max} = 110[knots]$

TABLE 24 - VELOCITY PROPERTIES

7.6.3. CLIMB & TURN CALCULATIONS

Climb:

To get maximum climb angle, the lift coefficient have to be the lift coefficient for best endurance of flight:

DATA: $T_{max}^{(engine\ properties)} = 121[lbf]$

$$C_L^+ = \sqrt{\frac{3C_{D_0}}{K}} = \sqrt{\frac{3 \cdot 0.02}{0.056}} = 1.035$$

$$C_D^+ = 4C_{D_0} = 4 \cdot 0.02 = 0.08$$

$$\cos(\gamma) = \frac{\frac{1}{2} \rho V^2 S C_L^+}{W} = \frac{\frac{1}{2} \cdot V^2 \cdot 0.0765 \cdot 17.586 \cdot 1.035}{220 \cdot 32.185} = 9.832 \cdot 10^{-5} V^2$$

$$\Rightarrow V = 100.85 \sqrt{\cos(\gamma)}$$

$$\sin(\gamma) = \frac{T_{max} - \frac{1}{2} \rho V^2 S C_D^+}{W} = \frac{121 \cdot 32.185 - \frac{1}{2} \cdot 10170.38 \cos(\gamma) \cdot 0.0765 \cdot 17.586 \cdot 0.08}{220 \cdot 32.185} =$$

$$= 0.55 - 0.0773 \cos(\gamma) \Rightarrow \gamma_{climb\ max} = 0.49[rad] = 28.2^\circ$$

Dive:

To get maximum dive angle, the lift coefficient is the same lift coefficient for maximum climb angle:

$$\cos(\gamma) = \frac{\frac{1}{2} \rho V^2 S C_L^+}{W} = 9.129 \cdot 10^{-5} V^2 \Rightarrow V = 100.85 \sqrt{\cos(\gamma)}$$
$$\sin(\gamma) = \frac{\frac{1}{2} \rho V^2 S C_D^+ - T_{\max}}{W} = \frac{\frac{1}{2} \cdot 10170.38 \cos(\gamma) \cdot 0.0613 \cdot 17.586 \cdot 0.08 - 121 \cdot 32.185}{220 \cdot 32.185} =$$
$$= -0.55 + 0.0619 \cos(\gamma) \Rightarrow \gamma_{\text{dive max}} = -0.51[\text{rad}] = -29.2^\circ$$

Turn:

Minimum turn radius without climbing:

$$\gamma = 0 \Rightarrow n_{\max} = 4 = \frac{1}{\cos(\phi_{\max})} \Rightarrow \phi_{\max} = 1.318[\text{rad}]$$
$$R_{\text{max turn}} = \frac{V_{\min}^2}{g} \frac{1}{\tan(\phi)} = \frac{78.9^2}{32.158} \frac{1}{\tan(1.318)} = 50[\text{ft}]$$
$$n = 2.5 = \frac{1}{\cos(\phi_{n=2.5})} \Rightarrow \phi_{n=2.5} = 1.159[\text{rad}]$$
$$R_{n=2.5} = \frac{V_{\min}^2}{g} \frac{1}{\tan(\phi)} = \frac{78.9^2}{32.158} \frac{1}{\tan(1.159)} = 84.6[\text{ft}]$$

Final results:

Property	Result
Maximum climb angle	$\gamma_{\text{climb max}} = 0.49[\text{rad}] = 28.2^\circ$
Maximum dive angle	$\gamma_{\text{dive max}} = -0.51[\text{rad}] = -29.2^\circ$
Minimum turn radius without climbing (n=4)	$R_{\text{max turn}} = 50[\text{ft}]$
Turn radius at n=2.5	$R_{n=2.5} = 84.6[\text{ft}]$

TABLE 25 - CLIMB AND TURN PROPERTIES

7.6.4. RANGE AND ENDURANCE

Max Range:

$$R = \frac{V}{SFC} \frac{C_L}{C_D} \ln \left(\frac{W_{i-1}}{W_i} \right)$$

$$SFC = 0.75 \left[\frac{lb}{hp \cdot hr} \right] = 3.788 \cdot 10^{-7} \left[\frac{lb}{ft \cdot lbf} \right] (W_i / W_{i-1})$$

Warmup and takeoff: 0.970

Climb: 0.985

Landing: 0.995

The UAV is launched by a rocket missile, so there is not a takeoff stage.

Climb:

$$\begin{cases} W_1 = 220[lbf] \\ W_2 = 220 \cdot 0.985 = 216.7[lbf] \end{cases} \rightarrow W_{mean} = 218.35[lbf]$$

$$\rho_{mean} \approx 0.0689 \left[\frac{lb}{ft^3} \right]$$

$$C_{L_{best\ climb}}^+ = \sqrt{\frac{3C_{D_0}}{K}} = \sqrt{\frac{3 \cdot 0.02}{0.056}} = 1.035$$

$$C_{D_{best\ climb}}^+ = 4C_{D_0} = 0.08$$

$$\rightarrow V_{maximum\ climb} = \sqrt{\frac{2W}{\rho S C_L^+}} = \sqrt{\sqrt{\frac{K}{3C_{D_0}}} \frac{2W}{\rho S}} = \sqrt{\sqrt{\frac{0.056}{3 \cdot 0.02}} \frac{2 \cdot 218.35 \cdot 32.185}{0.0689 \cdot 17.586}} = 105.86 \left[\frac{ft}{sec} \right]$$

$$T_{maximum\ climb} = W \left(\frac{D}{L} \right) = 218.35 \cdot \frac{0.08}{1.035} = 16.88[lbf]$$

$$\eta = \frac{TV}{550hp} = \frac{16.88 \cdot 105.86}{550 \cdot 26} = 0.125$$

$$R_{climb} = \frac{\eta}{SFC} \frac{C_L}{C_D} \ln \left(\frac{W_1}{W_2} \right) = \frac{0.125}{3.788 \cdot 10^{-7}} \left(\frac{1.035}{0.08} \right) \ln \left(\frac{220}{216.7} \right) = 64.5 \cdot 10^3 [ft] = 10.6[NM]$$

Cruise:

$$\begin{cases} W_1 = 216.7[lbf] \\ W_2 = 193.3[lbf] \end{cases} \rightarrow W_{mean} = 205[lbf]$$

$$\rho_{height=5000\ ft} = 0.0613 \left[\frac{lb}{ft^3} \right]$$

$$C_{L_{best\ endurance}}^* = \sqrt{\frac{C_{D_0}}{K}} = \sqrt{\frac{0.02}{0.056}} = 0.598$$

$$C_{D_{best\ endurance}}^* = 2C_{D_0} = 0.04$$

$$\eta_{cruise} = 0.5$$

$$R_{cruise} = \frac{\eta}{SFC} \frac{C_L}{C_D} \ln \left(\frac{W_1}{W_2} \right) = \frac{0.5}{3.788 \cdot 10^{-7}} \left(\frac{0.598}{0.04} \right) \ln \left(\frac{216.7}{193.3} \right) = 2.25 \cdot 10^6 [ft] = 371[NM]$$

Endurance:

Climb:

$$E_{climb} = \frac{\eta}{SFC \cdot V} \frac{C_L}{C_D} \ln \left(\frac{W_{i-1}}{W_i} \right) = \frac{R_{climb}}{V_{climb}} = \frac{10.6}{63} = 10[min]$$

Cruise:

$$E_{cruise} = \frac{R_{cruise}}{V_{cruise}} = \frac{371}{80} = 4.6[hr]$$

Final results:

Property	Result
Maximum range for climb	$R_{climb} = 10.6[NM]$
Maximum endurance for climb	$E_{climb} = 10[min]$
Minimum range for cruise	$R_{cruise} = 371[NM]$
Maximum endurance for cruise	$E_{cruise} = 4.6[hr]$

TABLE 26 - RANGE AND ENDURANCE PROPERTIES

8. WING DETAILED DESIGN

8.1. WING STRUCTURE - INTRODUCTION

The primary function of the wings is to generate enough lift in order to enable the vehicle to fly.

During the flight the wings are subjected to many and varied loads and forces caused by: positive high/low angle of attack, negative high/low angle of attack, taxiing, maneuvers, and more.

We mostly referred them as three main loads and forces: **Drag**, **Lift** and **Gravity**.

Any combination of these three must not cause bending, buckling, shear and/or torque of the wing structure.

Each wing is basically built of two parts:

- The internal structure, which refers to components like spars and ribs
- The skin, which can be made of fabric, metal or composites.

In order to make the wings stronger and stiffer, the structure is composed of the three main elements, as follows:

- **Spars:** The main structural members of the wing.
Most of the load carried by the wing taken by them.
Extend Lengthwise of the wing.
Most wings have two spars. One in the front, where the wing geometry allows it to be. The other is in the back as close to the trailing edge as it can be.

- **Ribs:** The forming elements of the structure of a wing.
Repeated along the wing at frequent intervals.
They support the covering, take loads on their plane and provide the airfoil shape.
Usually perforated in order to reduce weight.

- **Stringers:** Thin strips of material to which the skin of the structure is fastened.
Placed as far as possible from the neutral axis.
Run spanwise and attached to the ribs.
Used to take some of the axial forces and to increase the stiffness for bending.

The skin of the wing provides impenetrable aerodynamic surface.

It spreads the aerodynamic load along the ribs and stringers, and takes some of the Shear and torque loads.

The two farthest spars and an added skin layer create the torsion box which is the internal structure preventing bending and twisting of the wing.

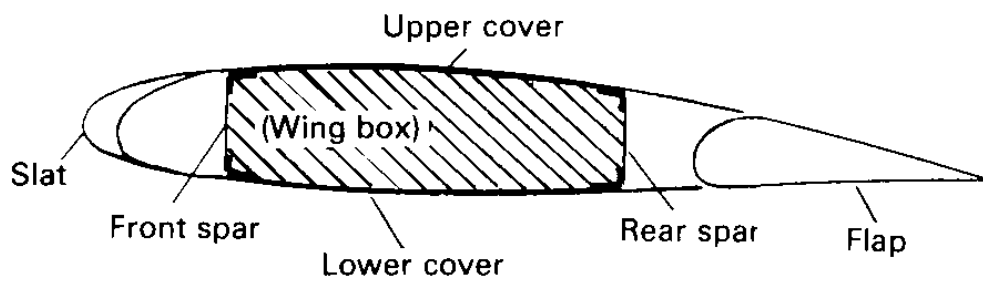
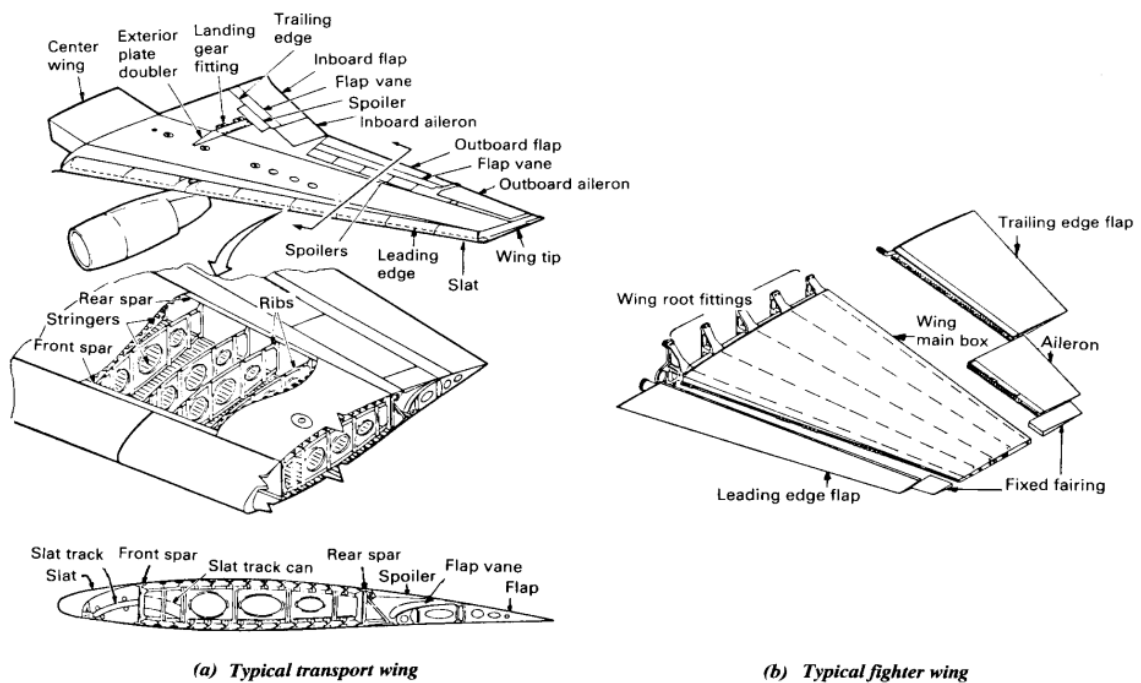


FIGURE 47 - TYPICAL WING TORQUE BOX ENCLOSE AREA



(a) Typical transport wing

(b) Typical fighter wing

Fig. 8.1.1 Typical transport and fighter wing.

FIGURE 48 - TYPICAL TRANSPORT AND FIGHTER WING COMPONENTS

8.2. WING STRUCTURE – DESIGN

As been explained in the introduction, the wing is loaded with several forces, therefore it needs to be well structured and yet be as light as possible.

The lift load distribution on a trapeze wing:

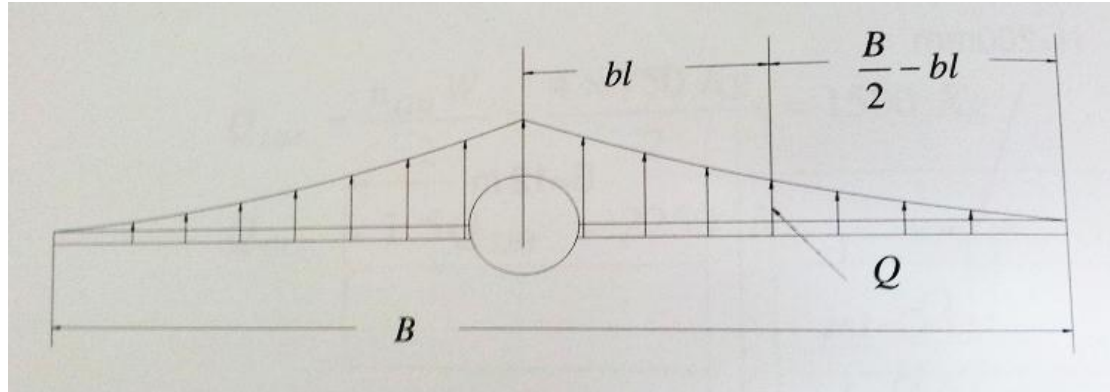


FIGURE 49 - LOAD DISTRIBUTION ON TRAPEZE WING

$$Q = \frac{nW}{S} \left[C_{TIP} \left(\frac{B}{2} - bl \right) + \frac{4(C_{ROOT} - C_{TIP})}{3B} \left(\frac{B}{2} - bl \right)^2 \right]$$

$$M = \frac{nW}{S} \left[\frac{1}{2} C_{TIP} \left(\frac{B}{2} - bl \right)^2 + \frac{2(C_{ROOT} - C_{TIP})}{3B} \left(\frac{B}{2} - bl \right)^3 \right]$$

$$S = \frac{B(C_{TIP} + C_{ROOT})}{2}$$

Q – force magnitude $[kgf]$

M – moment magnitude $[kg \cdot mm]$

n – load factor

W – weight $[kg]$

S – wing area $[mm^2]$

C_{TIP} – tip chord $[mm]$

C_{ROOT} – root chord $[mm]$

B – wing span $[mm]$

bl – distance from the wing root $[mm]$

To simplify the calculation a triangle distribution replaced the original (it provide a greater load on the wing and keep us on the safe side).

Wing's parameters:

$$n = 4$$

$$SF = 1.5$$

$$W = 60[kg]$$

$$S = 955500[mm^2]$$

$$C_{TIP} = 273[mm]$$

$$C_{ROOT} = 364[mm]$$

$$B = 3000[mm]$$

$$\Rightarrow Q_{ROOT} = 125.71[kgf]$$

$$\Rightarrow Q = -\frac{2Q_{ROOT}}{B} \cdot bl + Q_{ROOT}$$

Assuming this lift load distribution the resultant force is:

$$F = SF \cdot \int_x Q = SF \cdot \int_{bl=0}^{B/2} Q = 1.5 \cdot 925 = 1387.5N = 141.4kgf$$

The resultant force is applied on one specific point: $X_C = \frac{\int_{x=0}^{B/2} F \cdot x}{\int_{x=0}^{B/2} F} = 0.5m$

As expected of triangle distribution it resulted at a third distance from the root to the tip of the wing.

Canard's parameters:

$$n = 4$$

$$SF = 1.5$$

$$W = 40[kg]$$

$$S = 649350[mm^2]$$

$$C_{TIP} = 206[mm]$$

$$C_{ROOT} = 275[mm]$$

$$B = 2700[mm]$$

$$\Rightarrow Q_{ROOT} = 83.83[kgf]$$

$$\Rightarrow Q = -\frac{2Q_{ROOT}}{B} \cdot bl + Q_{ROOT}$$

Assuming this lift load distribution the resultant force on the canard is:

$$F = SF \cdot \int_x Q = SF \cdot \int_{x=0}^{B/2} Q = 1.5 \cdot 555 = 832.5N = 84.8kgf$$

The resultant force is applied on one specific point: $X_c = \frac{\int_{x=0}^{B/2} F \cdot x}{\int_{x=0}^{B/2} F} = 0.45m$

8.3. CALCULATIONS OF THE THICKNESS OF THE WEB

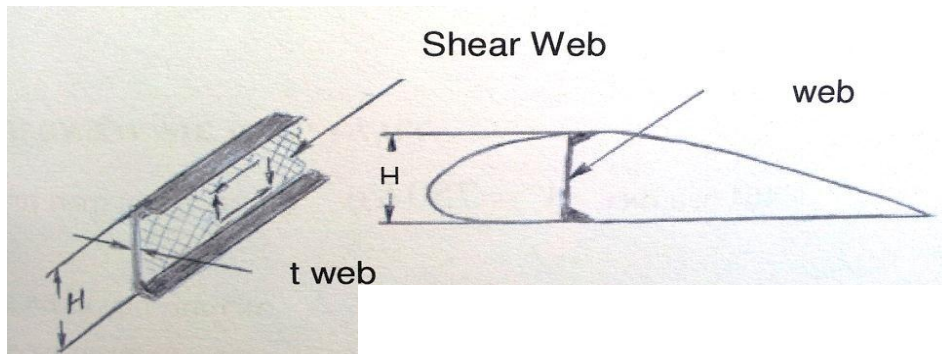


FIGURE 50 - PARAMETERS FOR WEB CALCULATION

Wing's calculations:

$$\tau = \frac{Q_{\max-\text{wing}}}{H \cdot t_{\text{WEB}}}$$

$$\tau_{\text{allow-carbon_fabric}} = 6 \text{ Kg} / \text{mm}^2$$

$$t_{\text{WEB-wing}} = \frac{Q_{\max}}{\tau_{\text{allow}} H} = \frac{1.5 \cdot 125.71}{6 \cdot \frac{16.1}{100} \cdot 364} = 0.54 \text{ mm}$$

Canard's calculations:

$$\tau = \frac{Q_{\max-\text{canard}}}{H \cdot t_{\text{WEB}}}$$

$$\tau_{\text{allow-carbon_fabric}} = 6 \text{ Kg} / \text{mm}^2$$

$$t_{\text{WEB-canard}} = \frac{Q_{\max}}{\tau_{\text{allow}} H} = \frac{1.5 \cdot 83.83}{6 \cdot \frac{16.1}{100} \cdot 275} = 0.47 \text{ mm}$$

Both the wing's web thickness as well as the canard's web thickness are very small in comparison to the industrial use. Therefore, the thickness of both webs is determined to be 1.5mm .

8.4. CALCULATION OF THE HINGES AREA

Flanges

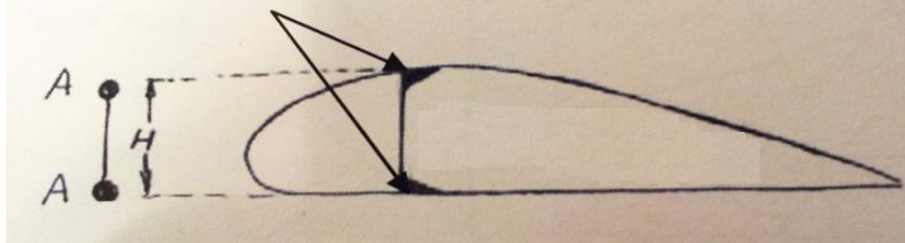


FIGURE 51 - FLANGES PARAMETERS

$$A = \frac{1.5M}{H \cdot \sigma}$$

The area of the flanges is distributed as the moment on the wing, and is displayed in the graphs and tables below.

For the wing:

$$A = \frac{1.5M}{H \cdot \sigma}$$

$$H = \frac{16.1}{100} \cdot 364 = 58.6 \text{ mm}$$

$$\sigma = 120 \text{ Kg} / \text{mm}^2$$

$$\sigma_{allow} = 0.6 \cdot 120 = 72 \text{ Kg} / \text{mm}^2 = 706.3 \text{ N} / \text{mm}^2$$

$$A = \frac{M}{27596}$$

bl [mm]	0	500	1000	1400
M [N · mm ²]	918638	386171	90448	3419
A [mm ²]	33.3	14	3.28	0.12

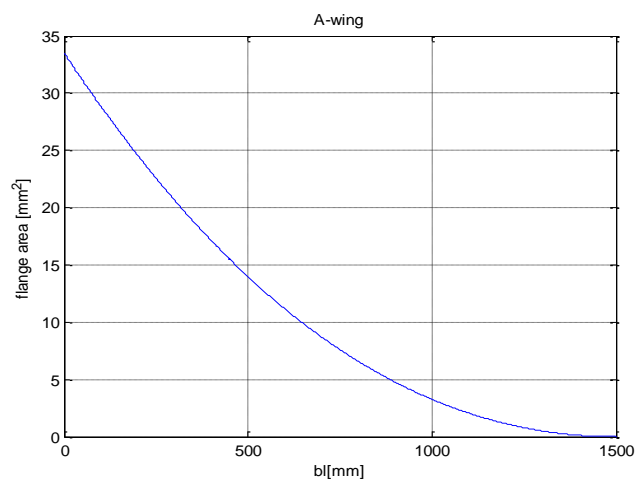


FIGURE 52 - FLANGE AREA ALONG THE WING

For the canard:

$$A = \frac{1.5M}{H \cdot \sigma}$$

$$H = \frac{16.1}{100} \cdot 275 = 44.28 \text{ mm}$$

$$\sigma = 120 \text{ Kg}f / \text{mm}^2$$

$$\sigma_{allow} = 0.6 \cdot 120 = 72 \text{ Kg}f / \text{mm}^2 = 706.3 \text{ N} / \text{mm}^2$$

$$A = \frac{M}{20846.3}$$

bl [mm]	0	450	900	1200
M [N · mm]	555442	232007	54200	5749
A [mm²]	26.65	11.13	2.6	0.28

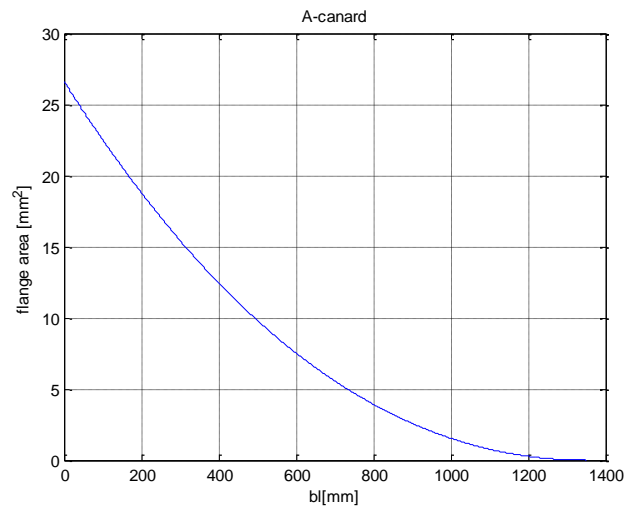


FIGURE 53 - FLANGE AREA ALONG THE CANARD

8.5. CALCULATION OF THE SKIN THICKNESS

The connection between the Maximal stress of a hollow cantilever beam to the skin thickness through Stress Analysis:

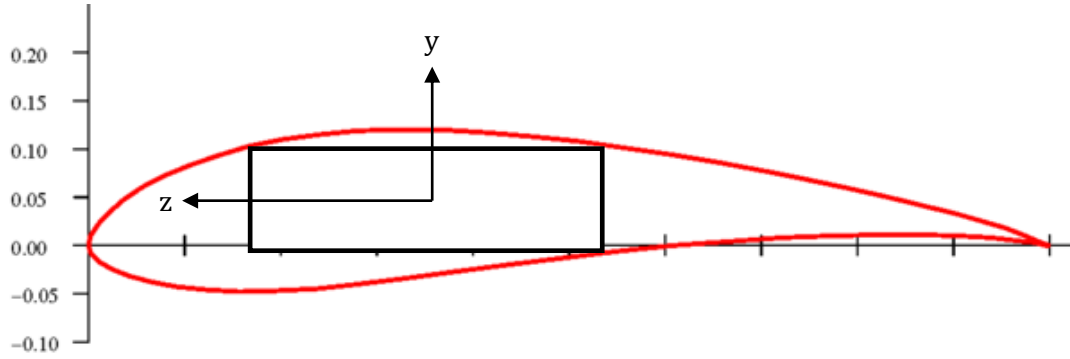


FIGURE 54 - WING AND CANTILIEVER BEAM CROSS-SECTIONS

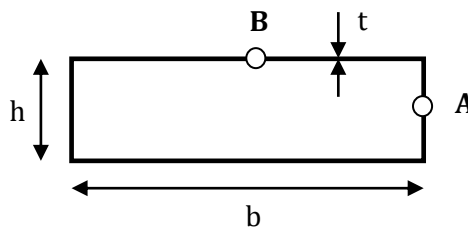
Stress Tensor 2D is given by: $\sigma_{ij} = \begin{pmatrix} \sigma_{xx} & \sigma_{xy} \\ \sigma_{yx} & \sigma_{yy} \end{pmatrix}$

Our only force is the lift in y axis: $\sigma_{yy} = 0$

Bending Stress in x axis is given by: $\sigma_{xx} = -\frac{M_z y}{I_{zz}}$

Shear Stress is given by: $\tau_{xy} = \frac{V_y Q}{I_{zz} b}$; $Q = \int_A y dA$

Analysis of two points on the beam section:



For thin-walled section: $I_{zz} = \frac{1}{6} t h^2 (3b + h)$

In addition: $Q_A = \frac{th}{2} \left(b + \frac{h}{2} \right)$; $Q_B = 0$

$$b = 320\text{mm}(MAC); h = 58\text{mm}$$

From the wing's data:
 $y_A = 0; y_B = \frac{h}{2} = 29\text{mm}$

Thus: $I_{zz} = 5.71t \cdot 10^5 [\text{mm}^4]$
 $Q_A = 10121 \cdot t [\text{mm}^3]$

The wing's principal stresses:

$$A: \begin{cases} \sigma_{xx} = 0 \\ \tau_{xy} = \frac{1387.5 \cdot 10121 \cdot t}{5.71t \cdot 10^5 \cdot 320} = 0.077 [\text{MPa}] \end{cases}$$

$$B: \begin{cases} \sigma_{xx} = -\frac{693.75 \cdot 10^3 \cdot 29}{5.71t \cdot 10^5} = \frac{35.2}{t} \\ \tau_{xy} = 0 \end{cases}$$

From Tresca's Yield Criterion:

$$\sigma_{1,2} = \frac{\sigma_{xx} + \sigma_{yy}}{2} \pm \sqrt{\left(\frac{\sigma_{xx} - \sigma_{yy}}{2}\right)^2 + \sigma_{xy}^2} \Rightarrow \sigma_1 - \sigma_2 < \sigma_{yield}$$

Thus: $A: \sigma_{1,2}^A = \begin{pmatrix} 0 & 0.077 \\ 0.077 & 0 \end{pmatrix} [\text{MPa}]$; $B: \sigma_{1,2}^B = \begin{pmatrix} \frac{35.2}{t} & 0 \\ 0 & 0 \end{pmatrix} [\text{MPa}]$

And the failure occurs when: $(\sigma_1 - \sigma_2)^B < \frac{35.2}{t} [\text{MPa}]$

A comparison between properties of several materials to find a reasonable wing thickness:

Material	Yield Stress – σ_y [MPa] ($FS = 0.6$)
Carbon UD	706.3
Aluminum 2024-T3	290.4
Aluminum 7075-T6	270.8

TABLE 27 - MATERIAL YIELD STRESS

Calculation of Tresca's Yield Criterion for different thicknesses:

<i>Thickness [mm]</i>	$(\sigma_1 - \sigma_2) [MPa]$
0.25	140.8
0.5	70.4
1	35.2
1.5	23.5
2	16.25
2.5	13

TABLE 28 - TRESCA'S YIELD CRITERION AT DIFFERENT THICKNESSES

The structure is safe for all the thicknesses and materials above.

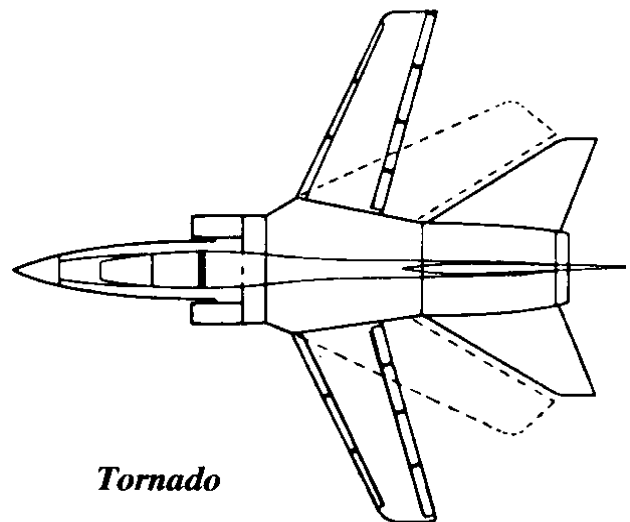
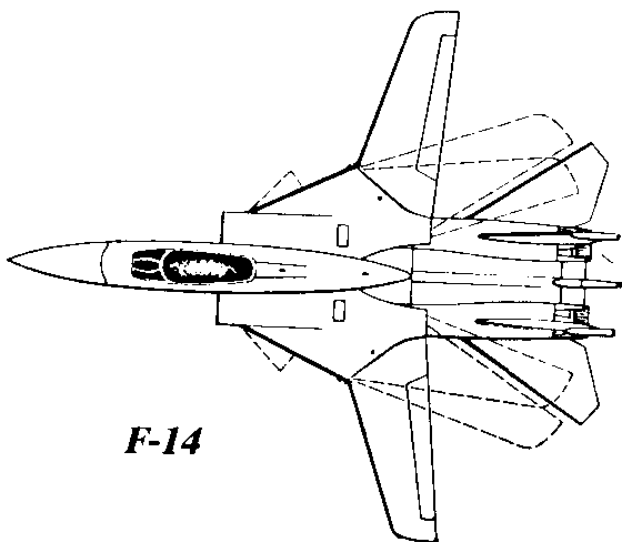
A thickness of $1.5mm$ is the lowest not too expensive to manufacture.

8.6. WING ROOT JOINTS

The wing root joint is one of the most critical areas in aircraft structure (especially for fatigue). It basically has two types of wing joint design: **Fixed** joint, **Rotary** joint.

The second type will be discussed and used in this design.

There are number of variable-swept wing aircraft, such as:



Two main groups of rotary joints:

Joint	Ref. Fig.	Advantages	Disadvantages
Swivelling pivot* (horizontal movement)	8.7.1 — 8.7.8	Required by variable (swivelling) geometry wing design for the best aerodynamic efficiency to accomplish missions required.	Structural weight penalty, high cost, complicate design, close tolerance requirements make manufacturing maintenance, repair, and replacement difficult and expensive
Folding joints	—	Mainly designed for the aircraft to fit on a carrier hangar deck. (with limited space)	Structural weight penalty, complicate joint control mechanism

TABLE 29 - ROTARY JOINTS ADVANTAGES AND DISADVANTAGES

Some more advantages of variable-swept wing:

- Fly throughout a broad regime of speed and altitude efficiently
- Tailored lift and drag
- Improved ride quality
- Lessening of fatigue damage

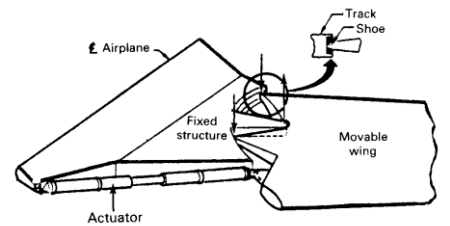
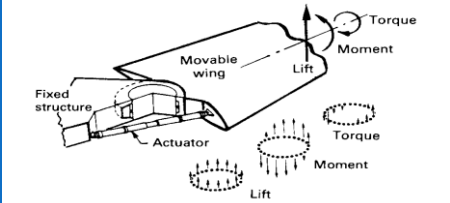
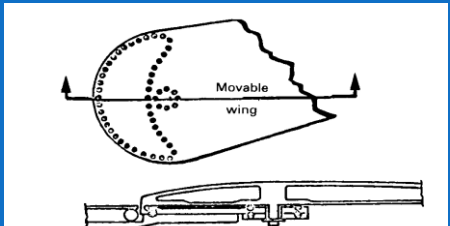
Some more disadvantages of variable-swept wing:

- Many wing positions to investigate and analyze
- New fail-safe criteria
- Many flutter-critical configurations
- Free play in mechanisms
- Dynamic loads
- Requires high reliability materials
- Change in stability, control and structural stiffness during wing sweep

Several principles should be preserved to make the joint most efficient:

- It is important to keep the joint short (a long joint tends to pull load in from adjoining areas).
- Holes sizes should be held as tight as practical.
- Correlation of small component test results with analytical techniques will increase the probability of successful selection.

Common Pivot Mechanisms:

Mechanism	Advantages	Disadvantages
<p>I "Shoe-in-track"</p>  <p>Fig. 8.7.2 Track and shoe design.</p>	<ul style="list-style-type: none"> - Low wing thickness requirements - Efficient load reaction means 	<ul style="list-style-type: none"> - Less rigidity - Little room for route electrical, mechanical and fluid lines - High static loads at many discrete points of the fuselage structure
<p>II Moment bearing</p>  <p>Fig. 8.7.3 Moment bearing design.</p>	<ul style="list-style-type: none"> - Low friction - Nominal depth of wing cross-section 	<ul style="list-style-type: none"> - Same routing problems as I - Large number of parts fitting with close tolerances
<p>III Track with roller</p>  <p>Fig. 8.7.4 Track with roller bearing design.</p>	<ul style="list-style-type: none"> - Workable system - Minimum wing thickness - Distributed reaction loads - Low friction 	<ul style="list-style-type: none"> - Large number of close tolerance parts - Same routing problems as I and II - Many detail features which affects Reliability - Complicated actuation mechanism

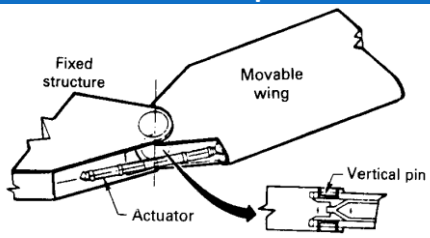
<p style="text-align: center;">IV Vertical pin</p>  <p style="text-align: center;"><i>Fig. 8.7.5 Vertical pin design.</i></p>	<ul style="list-style-type: none"> - Structural simplicity - Load paths determined with Confidence - Minimum volume of hinge - Simple actuator mechanism - Very few moving parts - Minimum weight 	<ul style="list-style-type: none"> - High journal bearing stresses - Great local wing thickness - Great reliance upon the integrity of single-load paths
--	---	---

TABLE 30 - PIVOT MECHANISMS COMPARISON

Most studies made for alternates designs suggests:

→ **Concept IV: Vertical pin design**

For extremely thin wings (thickness-to-chord ratio under 7-8%):

→ **Concepts I or II will offer the best solution**

More about the Vertical pin design:

- Can be modified to provide additional fail-safe features
- Has been applied on modern variable sweep wings
- Provides the lightest structural arrangement
- Provides the least interruption to the wing bending
- Used in many platforms

Wing dynamics:

- Bending moment taken across as a couple of equal and opposite loads acting parallel to and in the plane of the upper and lower skins
- A vertical pin through the pivot axis transfer the couple to the movable outer wing to the fixed center section

There is an influence of pivot location on the weight:

- The optimum spanwise location for minimum weight is not converges with aerodynamic considerations.

A trade-off has to be made according to the next graph:

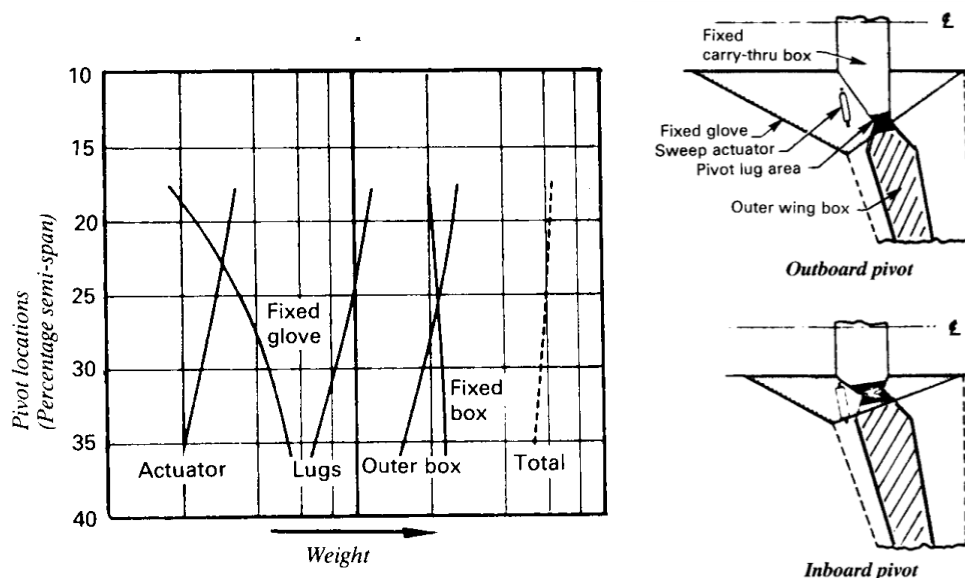


FIGURE 55 - SEMI-SPAN LOCATION TRADE-OFFS

Two basic designs of the joint:

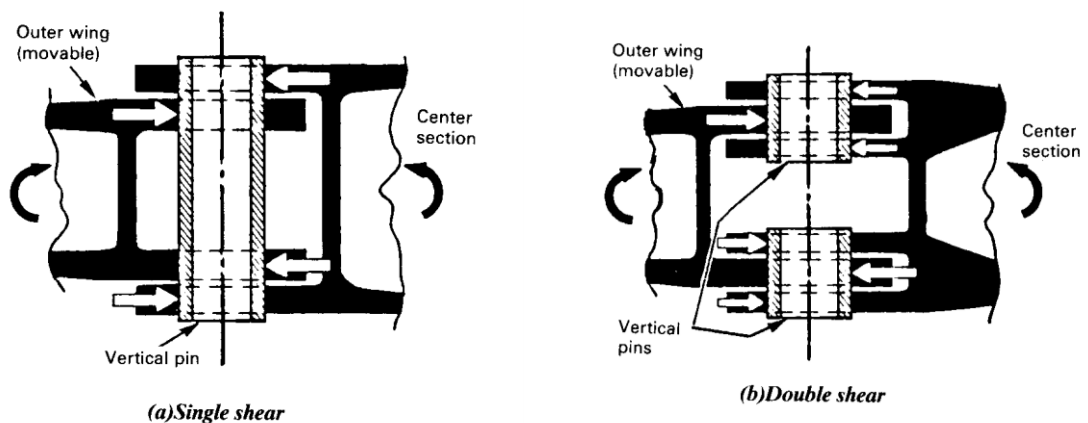


FIGURE 56 - VERTICAL PIN VARIATIONS

8.7. PIVOT MODELING

The spar is made of carbon fiber layers at $\pm 45^\circ$ at the tip of the wing, and gradually changing into unidirectional fibers in order to transfer the load to the hinge.

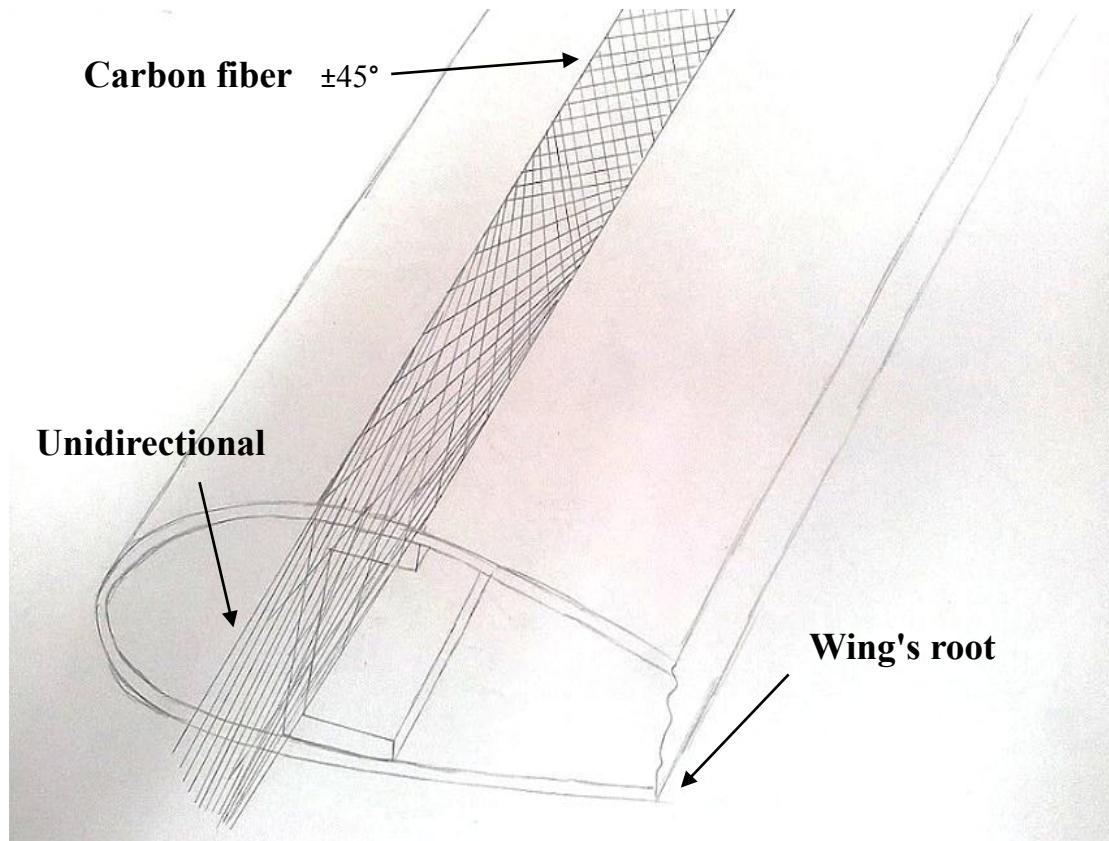


FIGURE 57 - SPAR FIBERS LAYERS ANGLE CHANGING

Modeling of the pivot:

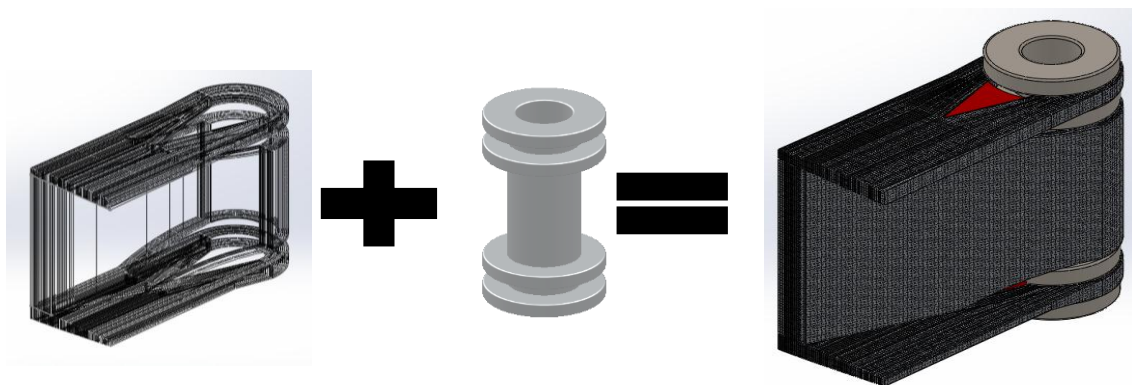


FIGURE 58 - PIVOT CAD MODELING

The unidirectional carbon fibers at the root are wrapped around the hinge, and the red part in the model is epoxy that filling in the gap caused by the spar's shape.

Modeling of the wing-pivot connection:

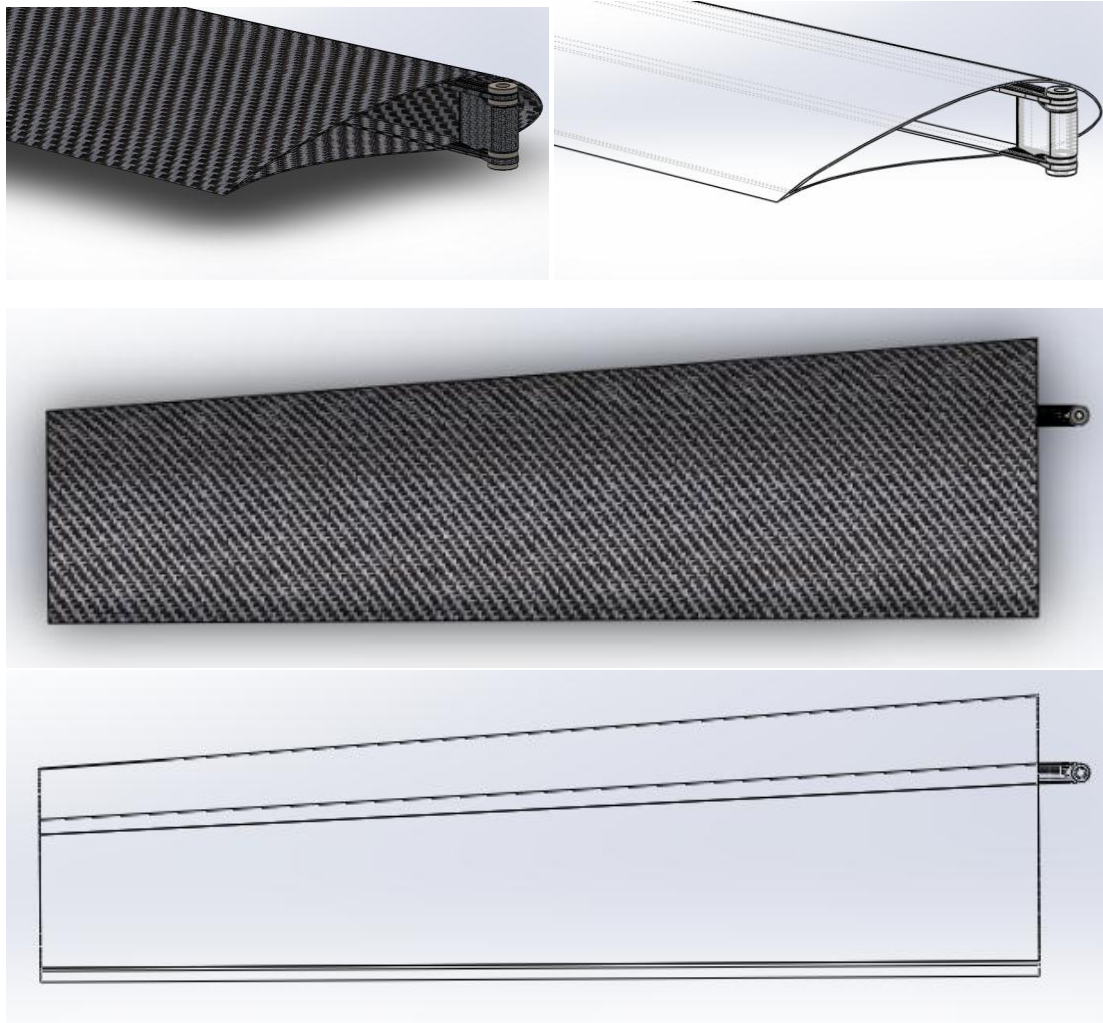


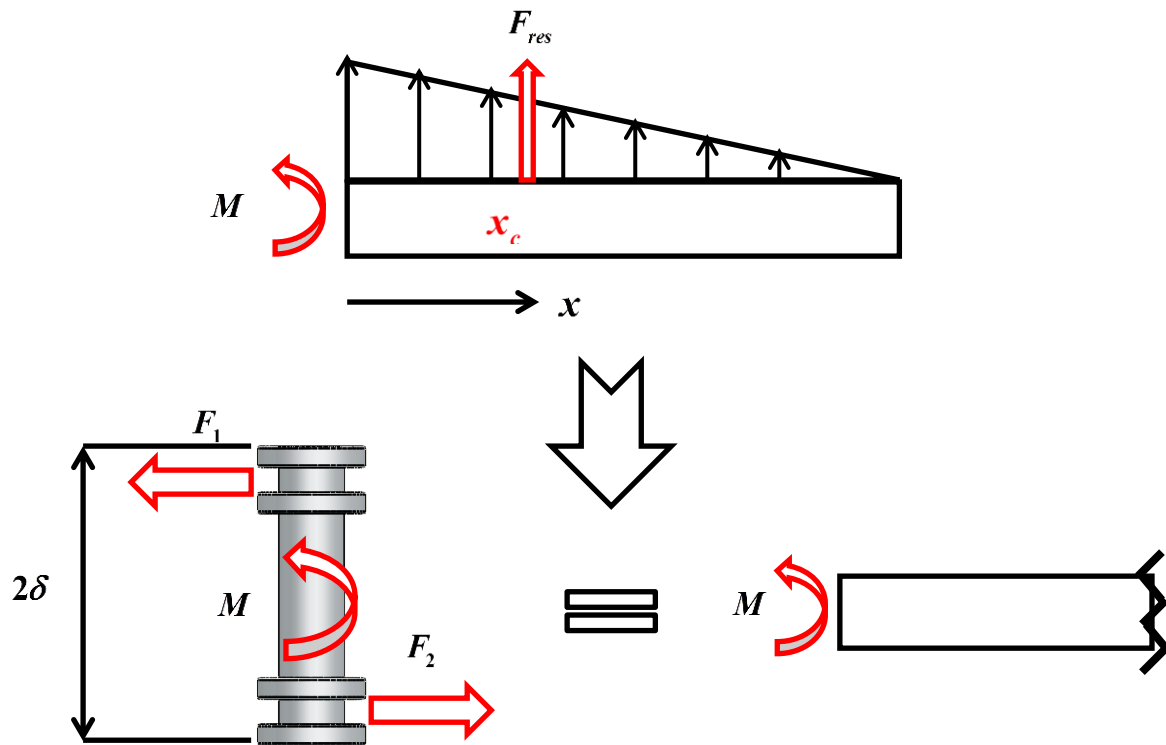
FIGURE 59 - WING-SPAR-PIVOT MODELING

8.8. PIVOT STRESS CALCULATIONS AND ANALYSIS

8.8.1. STRESS CALCULATIONS

According to evaluate the stresses applied on the pivot:

Forces and moments distribution As demonstrated earlier:



Forces cause a bending moment on the wing's root.

The same bending moment referred as a couple of forces on the pivot, which we wish to evaluate for safety of the connection.

Hinge's load calculation:

$$M_{root} = F_{res} \cdot x_c = 1.5 \cdot 925 \cdot 0.5 = 693.75 [N \cdot m]$$

$$F_1 = F_2 = \frac{M_{root}}{2 \cdot \delta} = \frac{693.75}{2 \cdot \left(\frac{55.38 \cdot 10^{-3}}{2} \right)} = 12527 [N]$$

Allowed stresses calculations for the carbon fibers and the aluminum hinge:

$$\sigma_{allowed} \Big|_{Carbon\ fibers} = 72 \left[\frac{kg}{mm^2} \right] = 706.3 \cdot 10^6 \left[\frac{N}{m^2} \right] = 706.3 [MPa]$$

$$\sigma_{allowed} \Big|_{Al. 7075-T6} = 27.6 \left[\frac{kg}{mm^2} \right] = 270.8 \cdot 10^6 \left[\frac{N}{m^2} \right] = 270.8 [MPa]$$

Applied stresses calculations for the carbon fibers and the aluminum hinge:

$$\sigma \Big|_{fibers} = \frac{F_1}{A_{fibers}} = \frac{12527}{102.4 \cdot 10^{-6}} = 122.3 [MPa]$$

$$\sigma \Big|_{hinge} = \frac{F_1}{A_{hinge}} = \frac{12527}{781 \cdot 10^{-6}} = 16 [MPa]$$

The applied stresses are lower than the allowed stresses:

$$122.3 [MPa] = \sigma \Big|_{fibers} < \sigma_{allowed} \Big|_{Carbon\ fibers} = 706.3 [MPa]$$

$$16 [MPa] = \sigma \Big|_{hinge} < \sigma_{allowed} \Big|_{Al. 7075-T6} = 270.8 [MPa]$$

8.8.2. ANALYSIS

A stress analysis was generated by the "ANSYS" software to prove the wing design.

The analysis used an aluminum wing instead of carbon wing due to the software limitations.

Shear stresses:

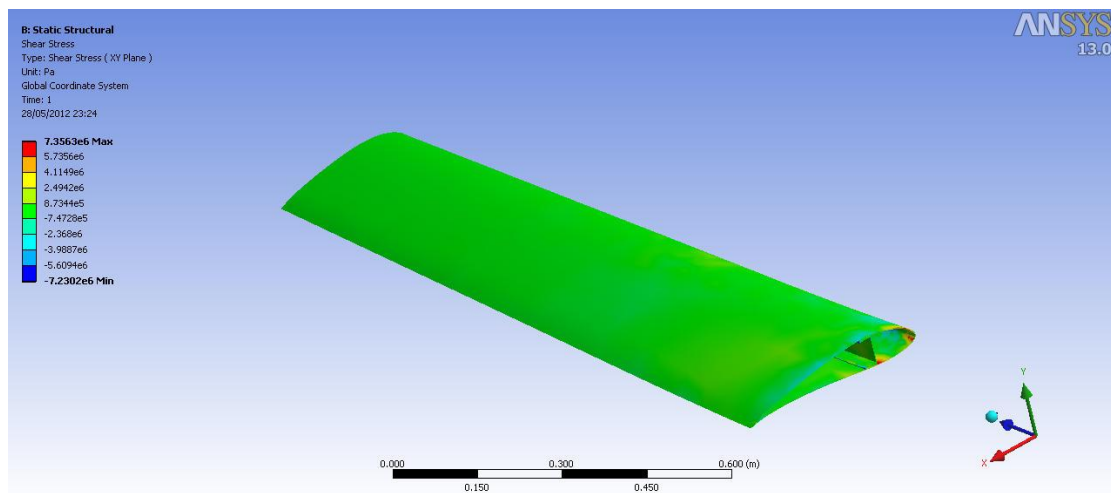


FIGURE60 - SHEAR STRESS ANALYSIS, ISOMETRIC VIEW

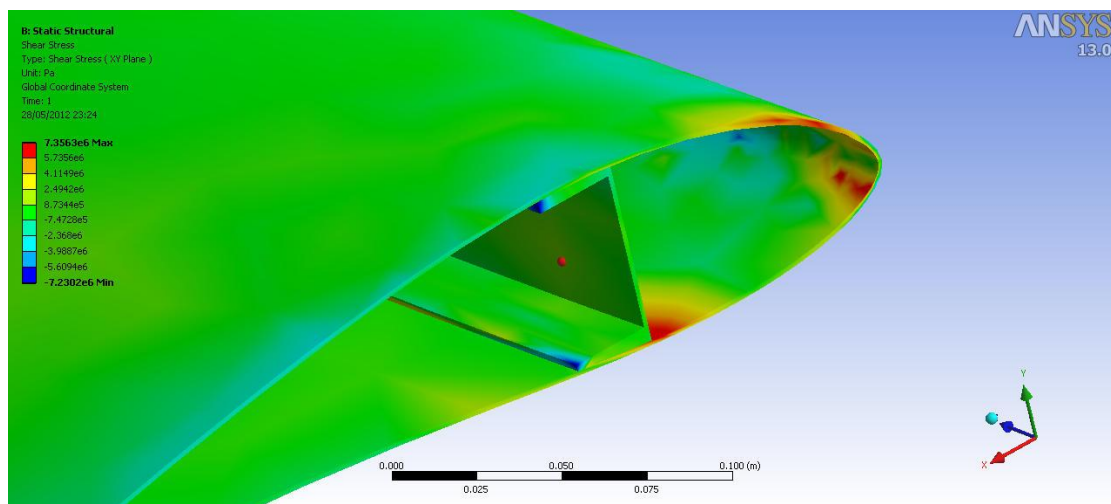


FIGURE61 - SHEAR STRESS ANALYSIS, CLOSER VIEW

Maximal stresses - Von Mises:

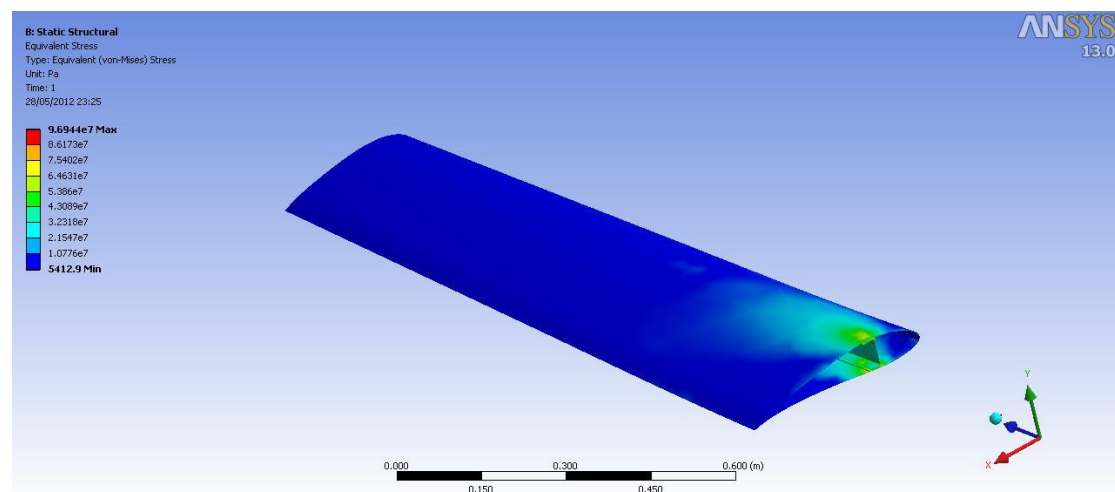


FIGURE62 - VON-MISES STRESSES, ISOMETRIC VIEW

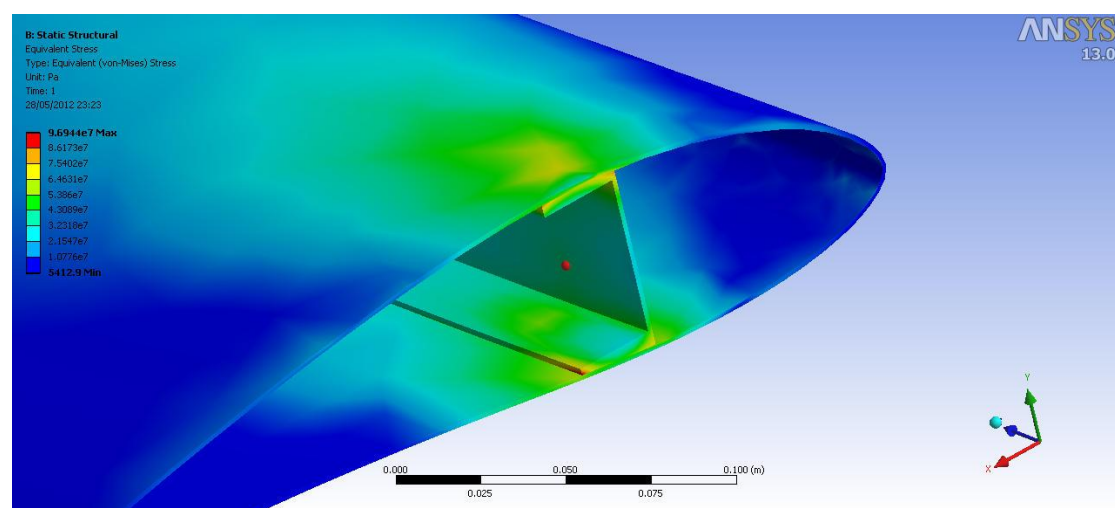


FIGURE63 - VON-MISES STRESSES, CLOSER VIEW

Deflection:

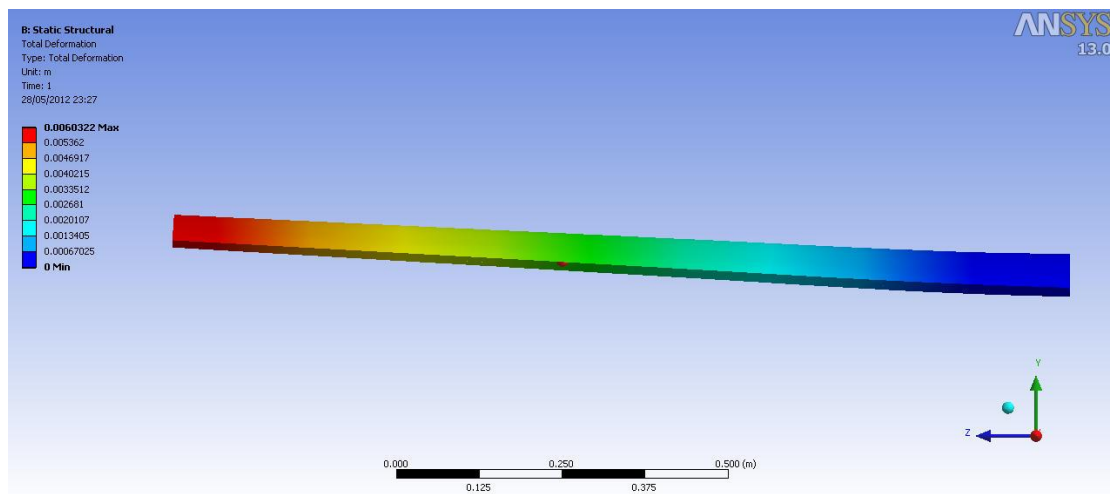


FIGURE 64 - WING DEFLECTION ANALYSIS

To evaluate the results for the carbon wing, a stress factor was calculated as followed:

$$\frac{\sigma_{allowed-carbon\ fiber}}{\sigma_{allowed-aluminum}} = \frac{706.3}{270.8} = 2.6$$

Material	Max. Deflection [mm]
Aluminum	6
Carbon	2.3

TABLE31 - MAXIMAL WING DEFLECTION

9. WING'S FOLDING MECHANISM

The opening-wing and canard system:

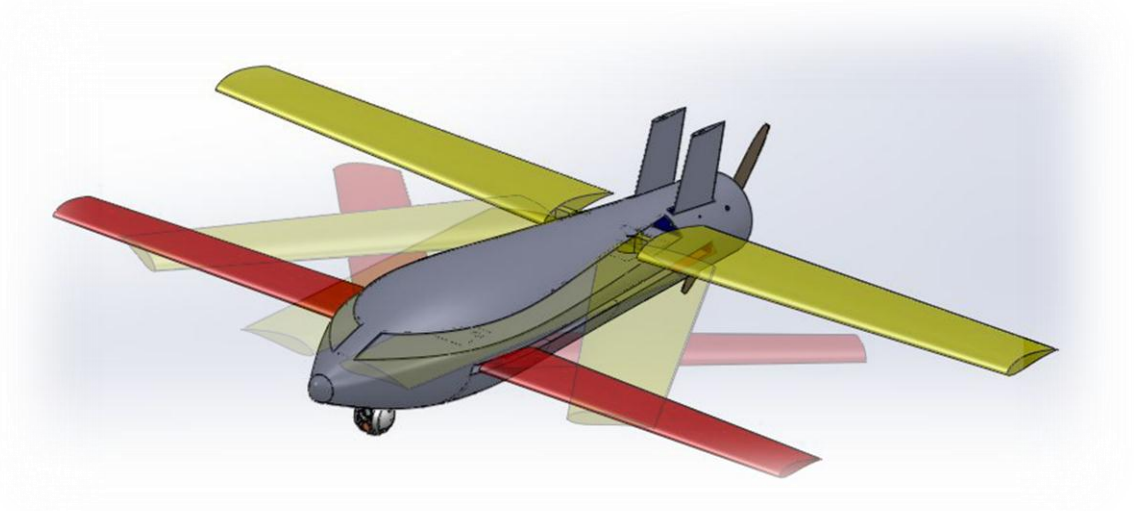


FIGURE 65 - WING AND CANARD CONFIGURATION ILLUSTRATION

Diamond-back:

This set of opening is cheap and easy to use. It is produced in several sizes and suitable for using over small bombs.



9.1. DESCRIPTION OF THE DISPLAYED SOLUTION

1. The purpose is to design an opening set like the "Long Shot" by "Lockheed Martin" with a combination of the popular "diamond back".
2. The mechanism of the wing's opening is a stretched spring that has been placed between the two wings. This slit is leaded by a conducted one.
3. The process of opening the wing is fully automated during launch time.

The tracks move along with the wings until the UAV leaves the canister. At that moment, the tracks fall and the wing opening system starts working automatically.

4. During launch preparations, the wings are kept closed.

9.2. CALCULATIONS

$$\rho = \rho_{SL-std} = 1.225 \left[\frac{kg}{m^3} \right]$$

$$b_{wing} = 9.843[ft], b_{canard} = 8.858[ft]$$

$$C_{D_0} = 0.02, K_{plane} = K_w = K_c = 0.065$$

$$C_{L_w, \alpha} = 3.62 \left[\frac{1}{rad} \right]$$

$$C_{L_c, \alpha} = 3.72 \left[\frac{1}{rad} \right]$$

The average velocity of the UAV during launch time is:

$$V_{launch} = \mathbf{50 \text{ knots}} = \mathbf{25.7 [m / sec]}$$

Lift areas:

$$S_{wing} = 10.471 [ft^2] = \mathbf{0.972 [m^2]}$$

$$S_{canard} = 7.116 [ft^2] = \mathbf{0.665 [m^2]}$$

The wing's lift during launch time:

$$\left. \begin{aligned} C_{L_w, \alpha} &= 3.62(i_w - 0.232i_c) \\ C_{L_c, \alpha} &= 3.72 \cdot 1 \cdot 0.68(i_c + 0.05i_w) \end{aligned} \right\} \begin{aligned} i_w &= 0.157[rad] = 9^\circ \\ i_c &= 0.079[rad] = 4.5^\circ \end{aligned}$$

$$L_{wing} = \frac{1}{2} \rho_{sl} V_{launch}^2 S_{wing} C_L = \frac{1}{2} 1.225 \cdot 25.7^2 \cdot 0.972 \cdot 0.502 = 197 [N]$$

$$L_{canard} = \frac{1}{2} \rho_{sl} V_{launch}^2 S_{canard} C_L = \frac{1}{2} 1.225 \cdot 25.7^2 \cdot 0.665 \cdot 0.323 = 87 [N]$$

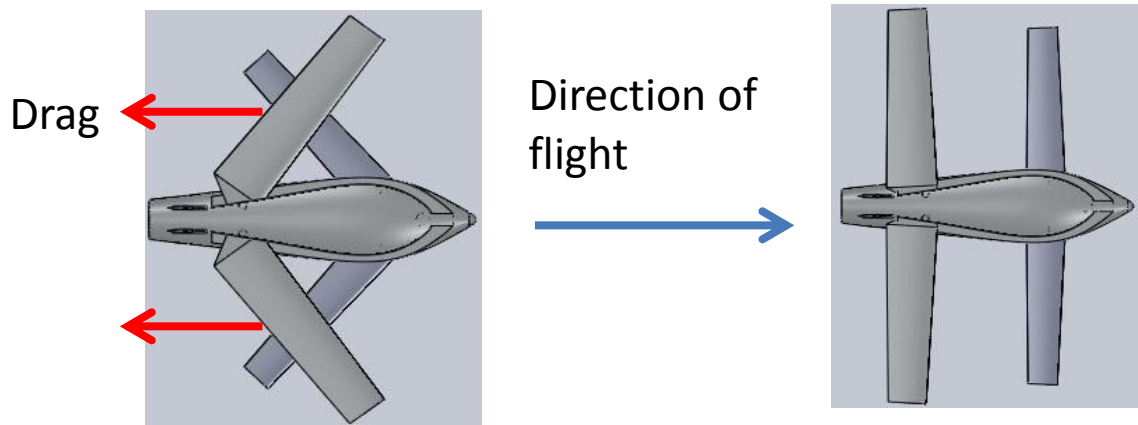
The wing's drag during launch time:

$$C_{L_0} = 0.721$$

$$C_{D_{\alpha=0}} = 0.02 + 0.056 \cdot C_{L_0}^2$$

$$D_{wing} = \frac{1}{2} \rho V^2 S_{ref} C_D = \frac{1}{2} 1.225 \cdot 25.7^2 \cdot 0.972 \cdot 0.049 = 19.26 [N]$$

$$D_{canard} = \frac{1}{2} \rho V^2 S_{ref} C_D = \frac{1}{2} 1.225 \cdot 25.7^2 \cdot 0.665 \cdot 0.049 = 13.18 [N]$$



The weight of the wing was not considered in the calculations, but the lift that its producing was considered. By this consideration we have increased the safety factor of both the hinge and the bearing together.

The length of the connecting rods and the angles were determined in a way that the wings will be on the same line in the opened configuration.

In order to choose the spring and to perform the calculations, we used the sizes of the rods and their angle's position.

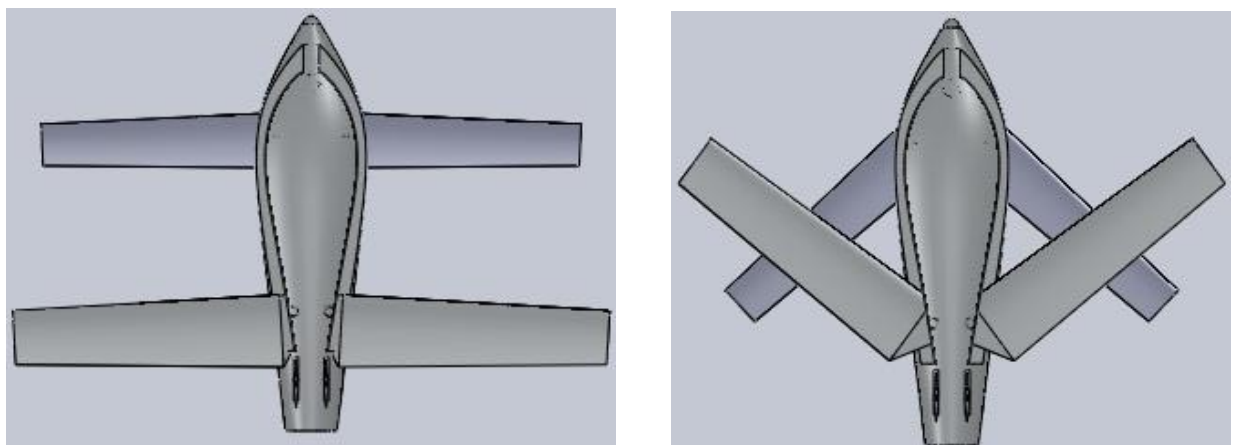


FIGURE 66 - FINAL IMPROVED CONFIGURATION, OPENED(LEFT) AND SEMI-CLOSED(RIGHT)

9.3. MECHANISM COMPONENTS

9.3.1. THE CALCULATION OF BEARING AND HINGE DIAMETERS

We designed the wing's hinges in a way that they will not suffer shear stress due to lift force.

We've assumed triangular, linear like, lift distribution. By this assumption, the centralized equal force attacks at the first third of the wing (in a way that resembles elliptic distribution lift):

$$b_{wing} = 9.843[ft] = 3[m]$$

$$b_{canard} = 8.858[ft] = 2.615[m]$$

$$r_{lift-wing} = \frac{1.5}{3} = 0.5[m]$$

$$r_{lift-canard} = \frac{1.3}{3} = 0.433[m]$$

The distance from the center of hinge to the beginning of the wing is negligible (because it's really small comparing to with wing).

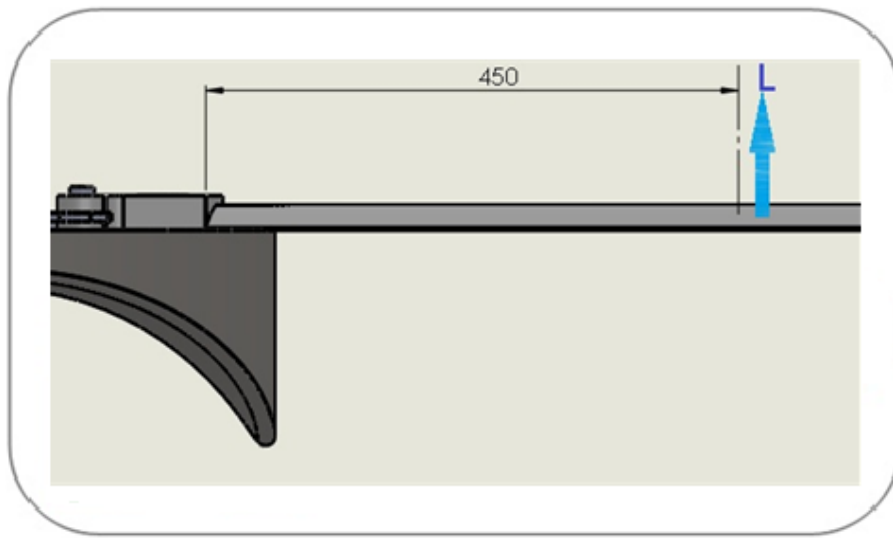


FIGURE 67 - RESAULTANT FORCE ILUSTRATION

The required moment:

$$M = l \cdot L_{wing} = 0.5 \cdot 1423 = 711.5[N \cdot m]$$

$$M = l \cdot L_{wing} = 0.433 \cdot 1000 = 433[N \cdot m]$$

The effective area that the moment applied on is:

$$A = \frac{\pi d^2}{4}$$

$$\left. \begin{aligned} I_{\text{pivot}} &= \frac{\pi d^4}{64} \\ y_{\text{max}} &= \frac{d}{2} \end{aligned} \right\} \Rightarrow \sigma_{\text{wing}} = \frac{My}{I} = \frac{7247}{d^3} < 0.577S_y$$

$$\sigma_{\text{canard}} = \frac{My}{I} = \frac{4410}{d^3} < 0.577S_y$$

$$S_y = 400 [MPa]$$

So we'll choose:

$$d_{\text{wing}} > 31 [mm]$$

$$d_{\text{canard}} > 27 [mm]$$

In our case we've chosen: $d_{\text{wing}} = 35 [mm]$ steel *ASTM A36*
 $d_{\text{canard}} = 30 [mm]$

The internal diameter of the bearing was chosen according to the rotating hinge diameter of the wings. The external diameter was chosen according to the type of bearing - considering the applied forces.

After performing market survey the chosen bearing was a 35 mm FYH spherical Bearing. Its price is 20 \$. (www.vxb.com)

The chosen bearing for the canard was a 30 mm ID Single row taper roller bearing by SKF Company.

The bearings:

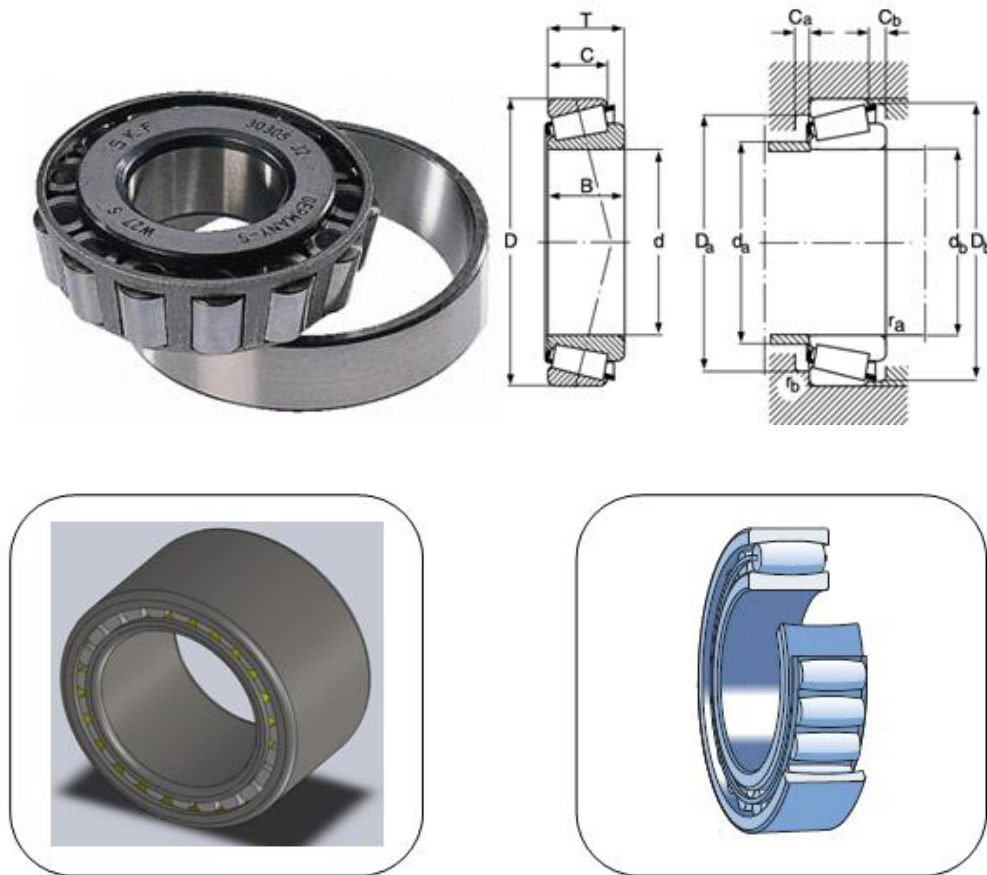


FIGURE 68 - DIFFERNTTYPES OF BEARINGS

9.3.2. CHOOSING OF THE MAIN SPRING

The spring's mechanism is made up of: a spring, a rod which on top of it the spring is placed and a pin which leads the spring on top of the rod and attached to the connecting rods. The whole mechanism is placed in track on a coordinating surface.

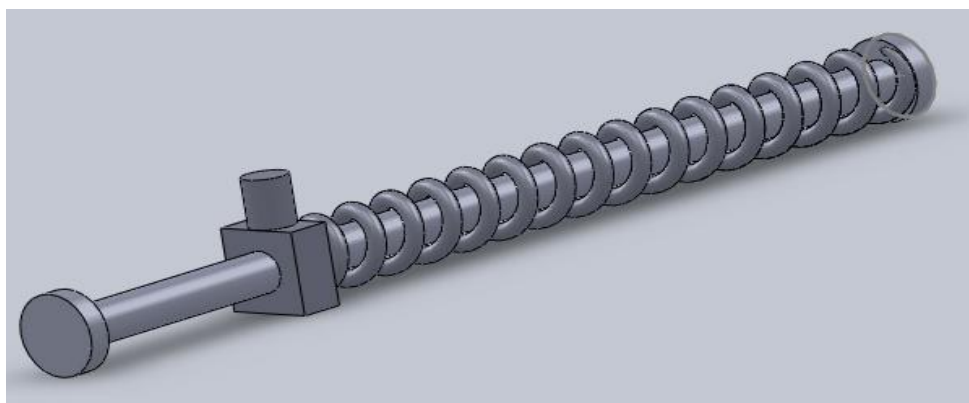


FIGURE 69 - SPRING MECHANISM

The spring is stretched while the wings are folded. While launching the UAV, the spring is also released and opens the wings.

Assuming that the bearings are ideals (they are not transferring moment), the only force on the spring is the drag force of the wing.

The drag force attacks at l_1 . The centralized equal force attacks at the effective distance from the base of the wing- the mean cord of the wing.

The drag moment on the rotating hinge:

$$D_{wing} = 7.89 [N]$$

$$D_{canard} = 5.38 [N]$$

$$b_{wing} = 9.843 [ft] = 3 [m]$$

$$b_{canard} = 8.858 [ft] = 2.615 [m]$$

$$C_{average} = 0.32 [m]$$

$$l_{Drag-wing} = \frac{1.5}{2} = 0.75 [m]$$

$$l_{Drag-canard} = \frac{1.3}{2} = 0.65 [m]$$

$$M_{Dwing} = l \cdot D_{wing} = 0.75 \cdot 7.89 = 5.917 [N \cdot m]$$

$$M_{Dcanard} = l \cdot D_{canard} = 0.65 \cdot 5.38 = 3.497 [N \cdot m]$$

The drag force is applied at a half wing span. The hinge is placed at a fourth wing cord and while assuming that the wings are tangent to one another when they are closed we can find the distance from the symmetric line:

$$(c_{wing})_{root} = 0.364 [m]$$

$$(c_{canard})_{root} = 0.273 [m]$$

$$l_{2wing} = \frac{0.364}{4} = 0.091 [m]$$

$$l_{2canard} = \frac{0.273}{4} = 0.06825 [m]$$

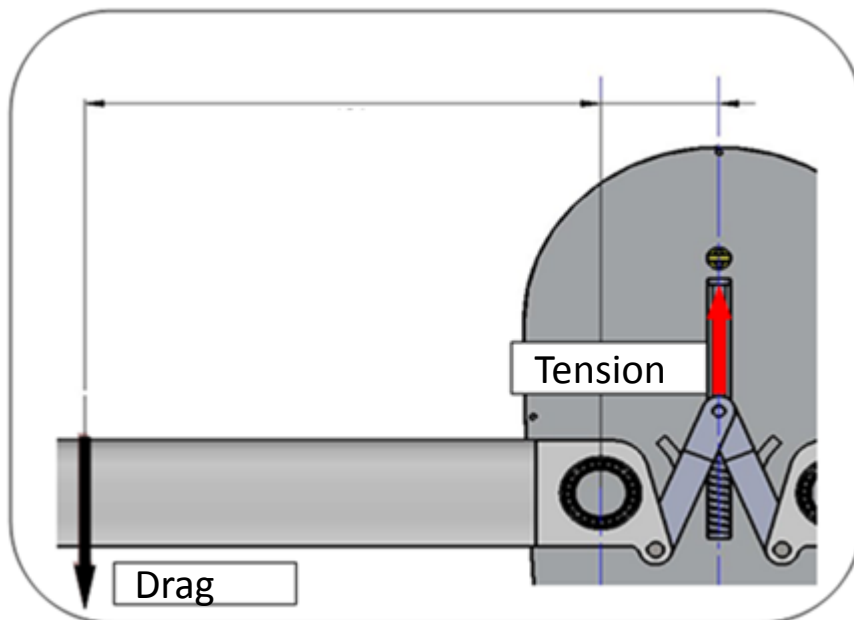


FIGURE 70 - MECHANISM TENSION AND DRAG ILLUSTRATION

The moment that applied on the spring:

$$M_{D2wing} = l_2 \cdot F_{spring} \Rightarrow F_{spring} = \frac{2M}{l_2} \Rightarrow \begin{matrix} F_{spring-wing} = 130 [N] \\ F_{spring-canard} = 102 [N] \end{matrix}$$

The above calculated forces are the tension forces that applied on the spring during opening of the wing/canard .The spring have to overcome those forces and to open the wings.

The chosen spring equals the moment to the one that creates the drag force .The spring's specifications:

$$F = K\Delta x = K \cdot R \cdot \frac{\pi}{2} \rightarrow R = 5 \text{ mm}$$

R stands for the distance of the second rotating pin, this due to geometric considerations.

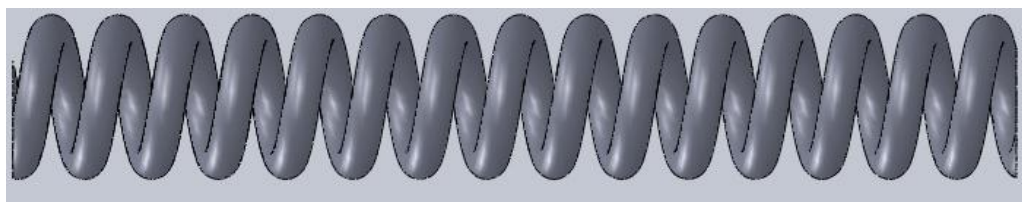


FIGURE 71 - SPRING MODEL

9.3.3. CONNECTING RODS BETWEEN THE SPRING AND THE WINGS

The connecting rods have the following form so that they will not disturb each one during the opening of the wings. The length was determined also due to geometric considerations.

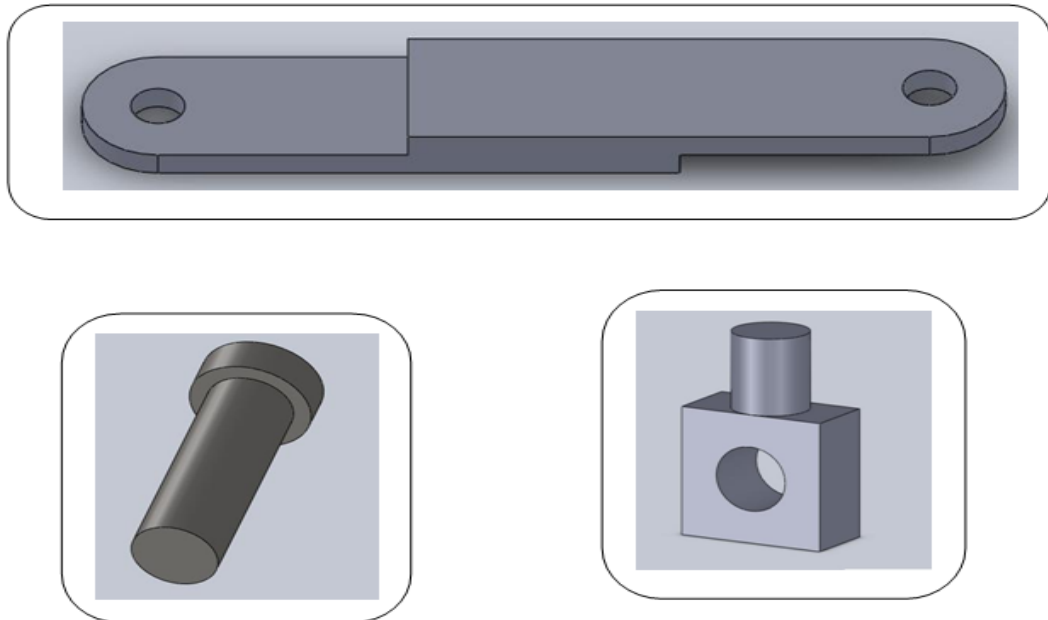


FIGURE 72 - CONNECTING RODS AND PINS

9.3.4. MOVEMENT LIMITERS DESIGN

The Limiters of the wings are designed in order to lock the wings at the opened state. When the wings are open, the spring is released and the limiters lock and stop the wings. The limiters are placed in the coordinating surface. While the wing is closed it holds the limiter pressed inside. While the wing is opened there is a hole above the limiter. The limiter enters this hole and locks the wing according to the coordinating surface.

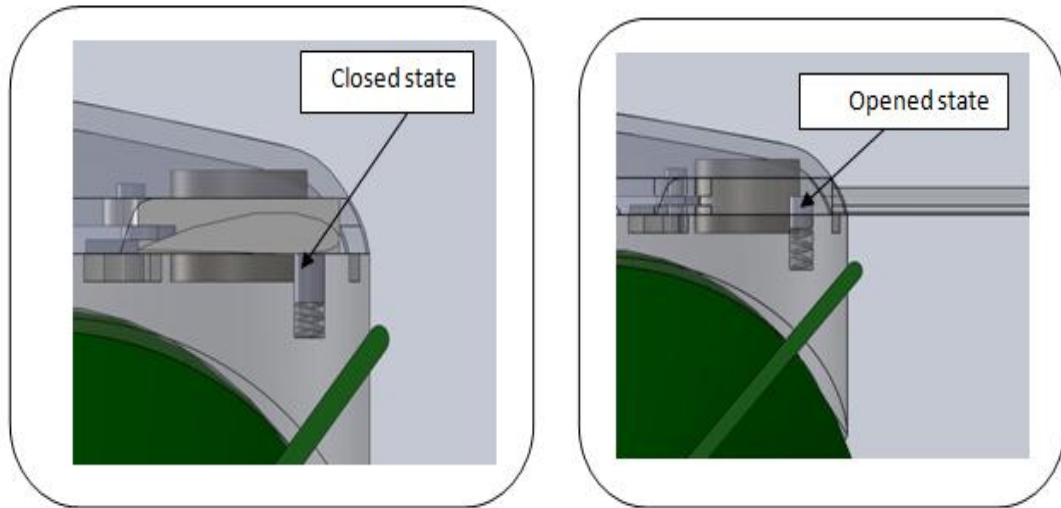


FIGURE 73 - LIMITERS OPERATIONAL STATES

The limiters are close to the rotating hinge so they are not suffering shear forces. For that reason we will choose such diameter that will stop the wing and lock it stable. The spring that lifts the limiter doesn't suffer significant forces as well, so we need a spring which overcomes the limiter weight.

The limiter's material is: 1020 Standard Steel, $S_y = 350$ [GPa]

The limiter's diameter: $d=1\text{mm}$

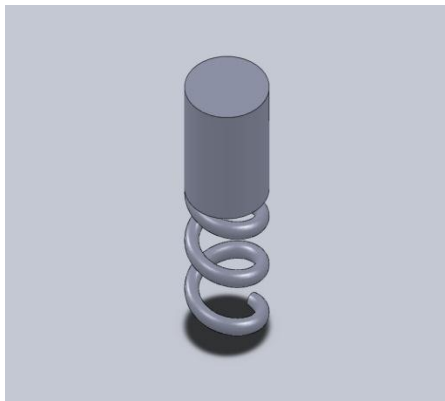
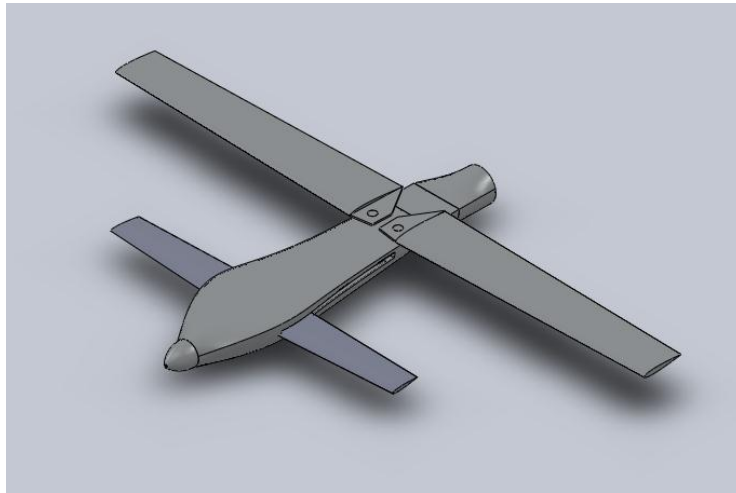


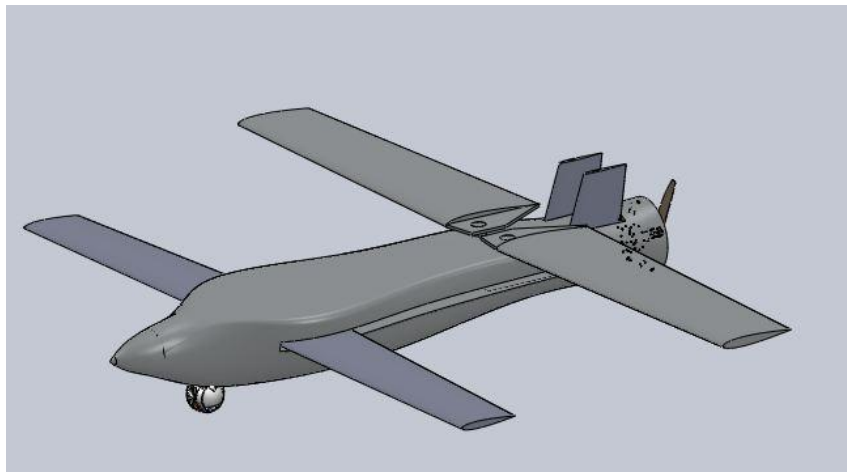
FIGURE 74 - LIMITER MODEL

10. FINAL CONFIGURATION

After a professional debate we had to choose one configuration, we chose to merge configuration A and B, when we took more from configuration A than B. Configuration A brought the canard and the doubled horizontal tail, while configuration B brought the round and simple body shape. At our PDR, the Plane geometry design was shown as below:



Most of the aerodynamic drag was cost due to wrong body geometry design. That drag is caused mainly from the "come and back" geometry – meaning that the body becomes thinner in the middle of it and then expands until it reaches the engine diameter. To resolve that issue, we made the guideline of the body as much as monotonic as possible, because of the limitation of the root of the canard at the front of the plane. The first iteration in this process is in the pictures below:



In order to improve more the aerodynamic of the plane, we redesign the nose and cover the wings axis. That was the second and last iteration, and it is shown in the pictures below:

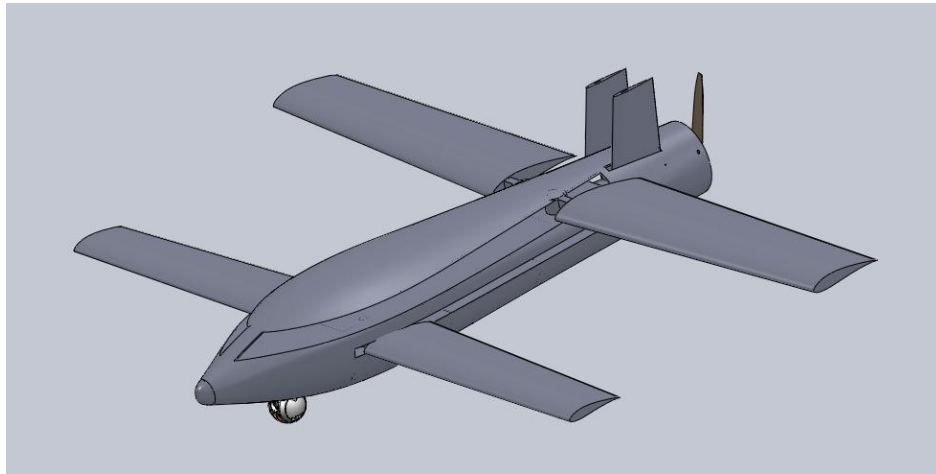


FIGURE 75 - FINAL IMPROVED CONFIGURATION, ISOMETRIC VIEW

As for the wings and canards slots we designed a concept to close them after they open, because of aerodynamic considerations. The solution is some kind of a "curtain" as following:

This is a draw of a section from the middle of our plane. The plane itself is painted in black. The smashed line indicates the space to the wing/canard. In red is the "curtain" itself, made of plastic, with a $2[mm]$ thick and in blue is a aluminum 2024 strip that connect the curtain to the plane body.

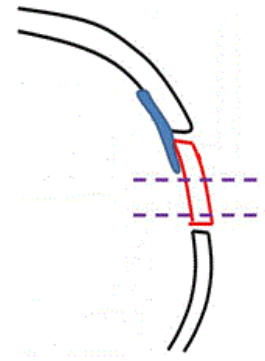


FIGURE 76 - SLOTS "CURTAIN"

Wing dimensions:

$$L = 2.9m$$

$$C_r = 36.4cm$$

$$C_t = 27.3cm$$

Canard dimensions:

$$L = 2.8m$$

$$C_r = 27.5cm$$

$$C_t = 21cm$$

Body dimensions:

$$L = 2.1m$$

$$W = 53cm$$

10.1. INTERNAL LAYOUT OF THE COMPONENTS

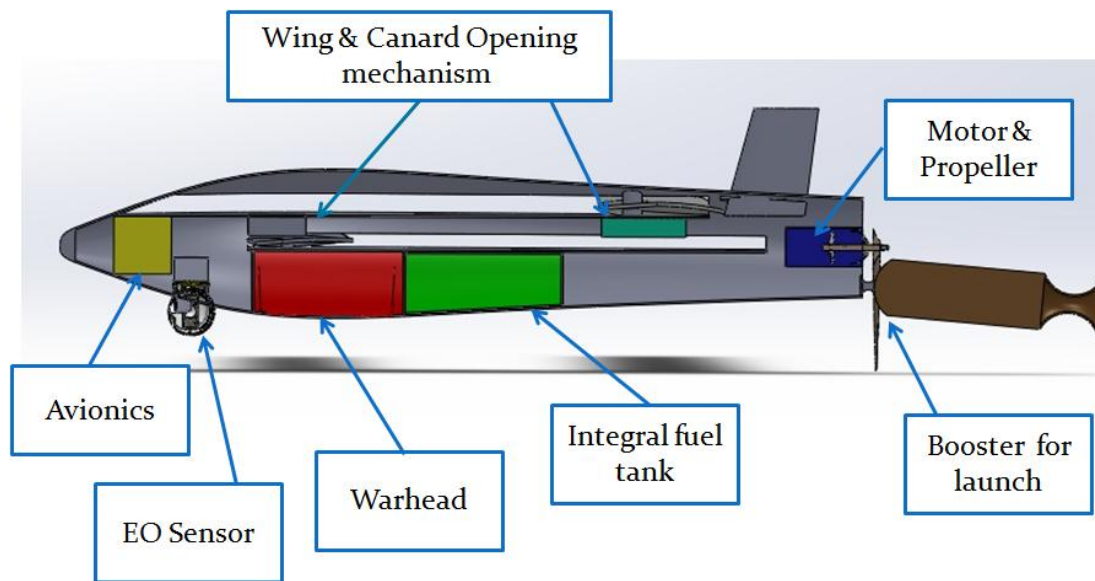


FIGURE 77 - INTERNAL LAYOUT OF THE IMPROVED FINAL CONFIGURATION

In this draw it can be the main components of the plane; the avionics and the EO sensor in the front, the motor and the booster in the back and the integral warhead and fuel tank in middle.

The components positions decide in iterative way, according to the weight table described next (Wishing the fuel tank to be positioned in the center of gravity area).

10.2. WEIGHTS TABLE

The table below describes the center of mass as calculated by Excel:

S/N		Part name	Mass[gr]	X[cm]	My[N*cm]
1	Structure	Fuselage	15000	115	16922
2		Wings	6740	145	9587
3		Mechanics -wing	3500	145	4978
4		Reinforcements- wing	2000	145	2845
5		Canard wings	4060	55.5	2211
6		Mechanics-canard	2000	55.5	1089
7		Reinforcements- canard	1000	55.5	544
8		Tail	2000	185	3630
9		Fuel injection system	3000	130	3826
10	Engine	Engine	6800	195	13008
11		Fuel	15000	107.48	15314
12		Fuel tank	1000	107.48	1021
13		Oil	1000	110	1079
14	Warhead	Warhead	20000	78	12557
15	Payload	Sensor	8000	30.2	2370
16		Battery	5000	180	8829
17	Avionics	Computer+Control system	2000	17.5	343
		Total Mass :	98100		
		CGx[cm]:	107.48		

FIGURE 78 - WEIGHTS TABLE

The table above is displaying the position of the center of gravity when the wings and the canard are closed. As it can be seen in the table, the center of gravity in closed position is distanced 107.5 cm from the reference point (the front of the UAV).

10.3. AERODYNAMIC CALCULATIONS

10.3.1. CENTER OF GRAVITY

The first estimation of the mass of each part and the center of gravity of the UAV was taken from the book "Aircraft Design: a Conceptual Approach" by Daniel P. Raymer. The estimation system is based on statistics from other planes or UAVs. In order to calculate the mass, the geometric dimensions of the UAV were calculated. The total mass of the UAV is calculated in the "initial sizing" part of the report.

One must remember that this method is only first estimation method. This method was chosen, because it is based on real UAV's and it is very accurate for a first estimation method.

In the market survey for the UAV, the properties of the needed subsystems and parts were founded. After finding all the properties, the all the mass was added to make sure the mass of the UAV is not bigger than the demand – 200 lb.

Each part or system in the UAV was measured. The position of the center of gravity of each part was measured from the reference point, which was placed in the front of the UAV.

The equation below used us to calculate the position of the center of gravity. The center of gravity is equal to the sum of the partial mass duplicate by the distances of the parts from the reference point, divided by the total mass:

$$X_{C.G} = \frac{\sum X_{C.G_i} \cdot M_i}{M_{total}}$$

While:

$X_{C.G_i}$ - The distance of the center of gravity of each part or system from the reference point (the nose of the UAV).

M_i - The mass of each part or system.

M_{total} - The total mass of the UAV.

$X_{C.G}$ - The distance of the center of gravity of the UAV from the reference point.

In order to prevent the movement of the center of gravity during flight, iterations have been made in order to place the fuel and its tank in the center of gravity.

Other parts of the UAV that can change the center of gravity are the wings and canard. While launching the UAV, the wings and canard are opening. That means the center of gravity is depends on the opening wing.

10.3.2. AERODYNAMIC CENTER

In order to find the position of the aerodynamic center of the UAV, the positions of the aerodynamic centers were normalized after multiplying them by the lift of each area. One can assume that the wing and canard are the only lift areas on the UAV.

For the wings and the canard, the aerodynamic center is positioned in the quarter of the mean chord. While opening them, the position of the quarter mean chord is changed with the opening angle, which means that the aerodynamic center is changed as a function of the opening angle as well.

The chosen wing and canard have a shape of a trapeze. Therefore, the following equations are applied:

$$* \quad \bar{C}_{\text{mean chord}} = \frac{2}{3} \cdot C_{\text{root}} \cdot \frac{(1 + \lambda + \lambda^2)}{1 + \lambda}$$

$$** \quad \alpha_{\text{leading_edge}} = a \tan \left(\frac{C_{\text{root}} - C_{\text{tip}}}{b / 2} \right)$$

$$*** \quad \bar{y} = \frac{b / 2 \cdot (C_{\text{root}} - \bar{C})}{C_{\text{root}} - C_{\text{tip}}}$$

$$(\text{Thales' theorem: } \frac{b / 2}{C_{\text{root}} - C_{\text{tip}}} = \frac{\bar{y}}{C_{\text{root}} - \bar{C}})$$

The equation below uses to calculate the aerodynamic center of the UAV:

$$X_n = \frac{X_{n_{\text{wing}}} \cdot L_{\text{wing}} + X_{n_{\text{canard}}} \cdot L_{\text{canard}}}{L_{\text{total}}}$$

While:

- $X_{n_{\text{wing}}}$, $X_{n_{\text{canard}}}$ - The position of the aerodynamic center of the wing and canard from the reference point.
- L_{wing} , L_{canard} - The lift force of the wing and canard.
- $L_{\text{total}} = L_{\text{wing}} + L_{\text{canard}}$ - The total lift force of the UAV.

FIGURE 79 - WING'S ARODYNAMIC CENTER CALCULATION

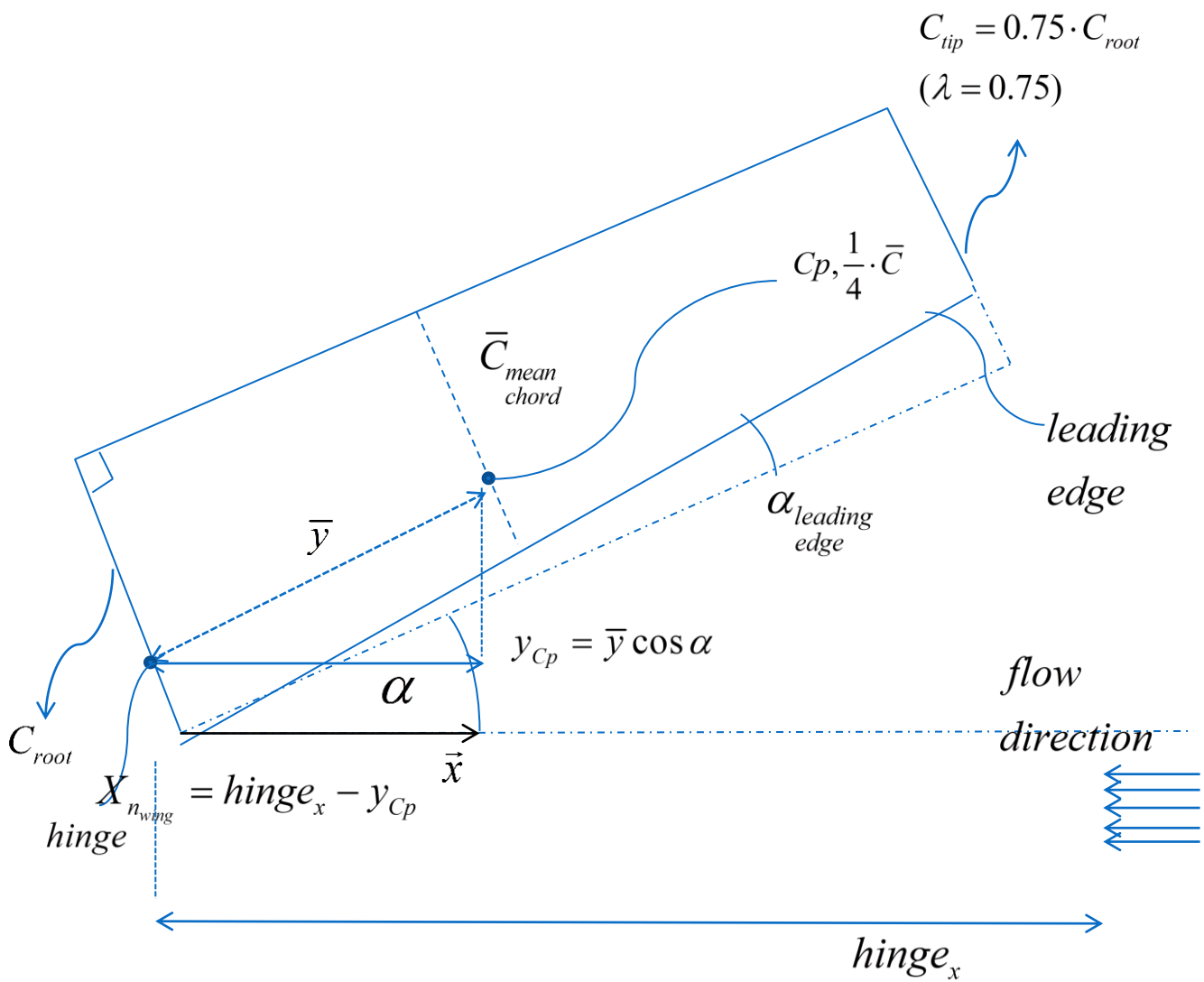
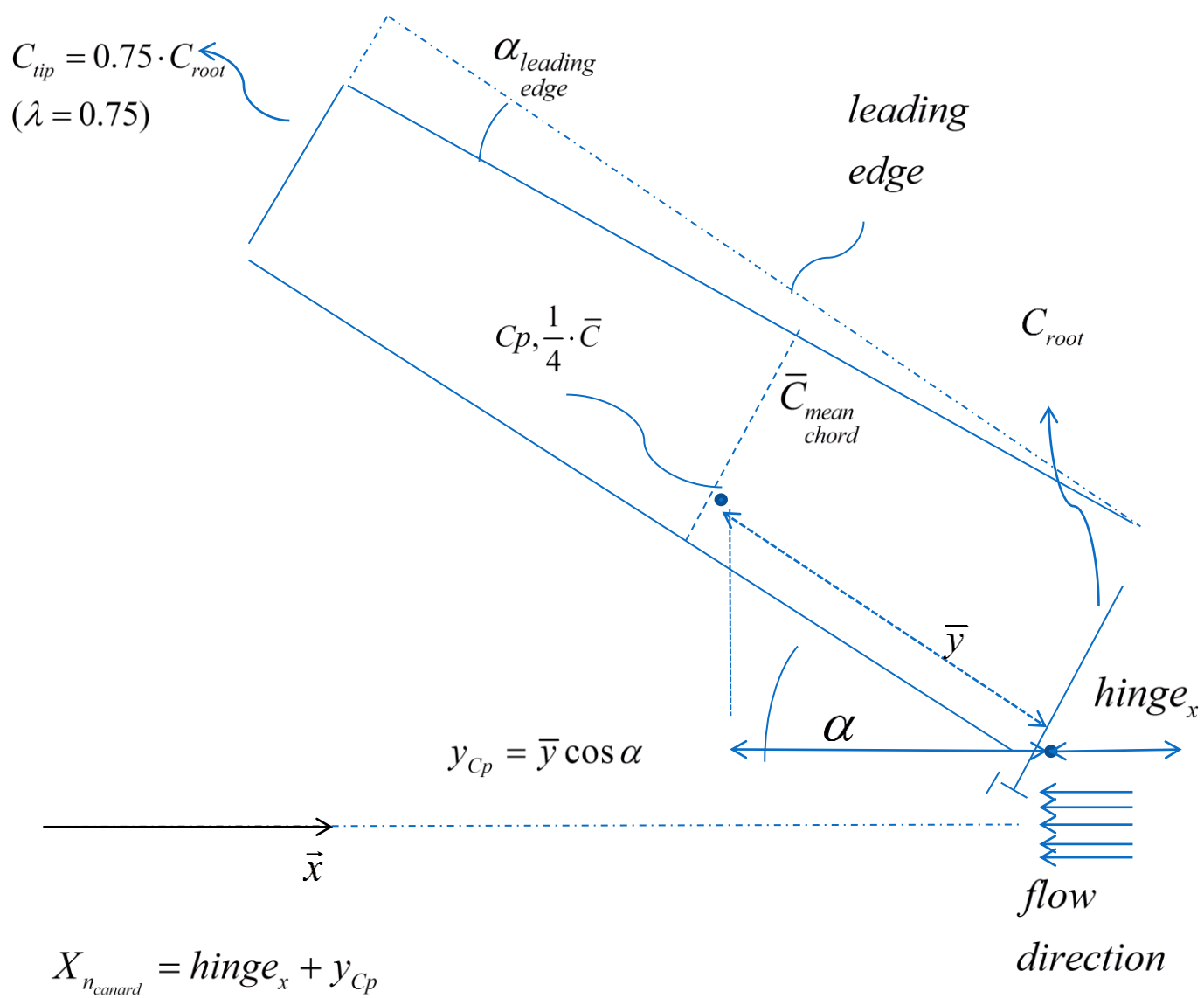


FIGURE 80 - CANARD'S AERODYNAMIC CENTER CALCULATION



As it can be seen in the equations, the position of the aerodynamic center depends on the lift forces of the wings the canard. The lift forces depend on the lift area. While opening the wing and canard, a certain amount of area doesn't participate in the total lift area because it is placed over the body. The graph below displays the change of the lift areas of the wing and the canard as a function of the opening angle (for the new configuration, 40%-60% lift areas ratio between the canard and wing, which will be demonstrated in the following section of "aerodynamic stability"):

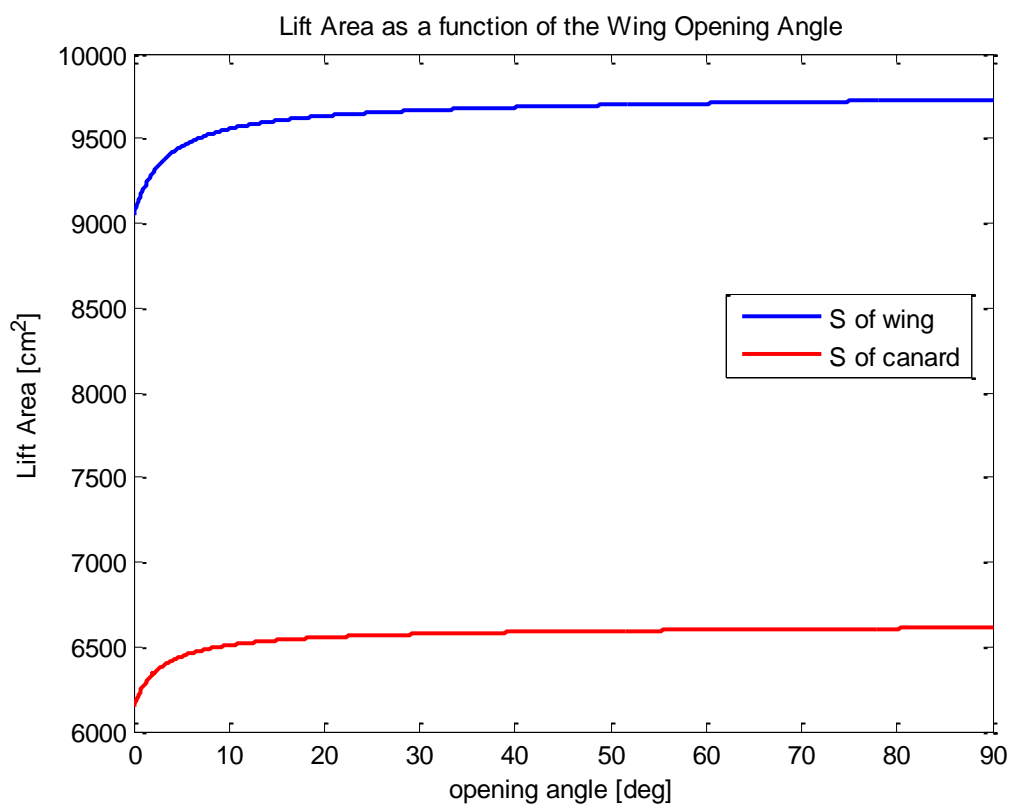


FIGURE 81 - LIFT AREA AS FUNCTION OF THE WING SWEEP ANGLE

10.3.3. STABILITY MARGIN

In order to have a stable UAV (stability is when the moment gets smaller while the angle of attack of the UAV is getting bigger), the center of gravity must be in front of the aerodynamic center (that means that the distance of the center of gravity from the reference point, the nose of the UAV, must be smaller than the distance of the aerodynamic point).

The equation below shows the calculation methods of the stability margin:

$$\text{stability margin[cm]} = X_n - X_{C.G.}$$
$$\text{stability margin[\%]} = 100 \cdot \frac{X_n - X_{C.G.}}{C_{wing\ root}}$$

As one can see, in the calculations of the center of gravity, the aerodynamic center, and the mean chord, all of them depend on the opening angle of the wing (α).

The aerodynamic center is closer to the aerodynamic center of the biggest lift area (in this case, the wing). If the wing is larger, the aerodynamic center will be closer to the aerodynamic center of the wing and less close to the aerodynamic center of the canard. Therefore, while the wing and canard are unfolding (in small unfolding angles), the aerodynamic center is positioned in front to the gravity center – the stability margin is negative. A negative stability margin creates a pitch-up. Two solutions were suggested:

- In the PDR, the configuration had a lift area ratio between the canard and the wing of 25%-75%. Creating more tandem-like configuration was supposed to solve the problem – 40%-70% ratio of canard-wing (the canard opens from the back of the plane, and affects the aerodynamic center towards the engine).
- If the change of the configuration will not be enough, there is a need for placing the booster in an angle.

After beginning with the first solution, a comparison between the stability of the configuration has been made. The characteristics which were compared: aerodynamic center, gravity center, and stability margin [%] as a function of the opening angle.

10.3.4. CALCULATIONS RESULTS

25%-75% configuration:

Opening Angle	Cp [cm]	C.G [cm]	% chord stability
$\alpha = 5^\circ$	66.9	124.9	-165.8%
$\alpha = 7.5^\circ$	67.2	125.0	-165.0%
$\alpha = 10^\circ$	67.7	125.0	-163.8%
$\alpha = 20^\circ$	70.8	125.4	-155.9%
$\alpha = 35^\circ$	79.1	126.2	-134.7%
$\alpha = 50^\circ$	91.1	127.3	-103.4%
$\alpha = 65^\circ$	106.2	128.7	-64.4%
$\alpha = 80^\circ$	123.3	130.3	-20.1%
$\alpha = 90^\circ$	135.2	131.4	10.8%

TABLE 32 - 25%/75% AERODYNAMIC CALCULATIONS

40%-60% configuration:

Opening Angle	Cp [cm]	C.G [cm]	% chord stability
$\alpha = 5^\circ$	81.2	105.6	-67.0%
$\alpha = 7.5^\circ$	81.4	105.6	-66.6%
$\alpha = 10^\circ$	81.6	105.6	-66.2%
$\alpha = 20^\circ$	82.9	105.8	-62.8%
$\alpha = 35^\circ$	86.5	106.0	-53.6%
$\alpha = 50^\circ$	91.9	106.4	-40.0%
$\alpha = 65^\circ$	98.5	106.8	-22.9%
$\alpha = 80^\circ$	106.0	107.2	-3.5%
$\alpha = 90^\circ$	111.2	107.5	10.1%

TABLE 33 - 40%/60% AERODYNAMIC CALCULATIONS

From the table above it is easy to see that the 25%-75% configuration is a lot more unstable for small opening angles of wing and canard.

Notice that the new configuration was able to maintain, and even improve in a few, the stability margin of the UAV in flight conditions ($\alpha = 90^\circ$), as required – about 10%.

The changes of the center of gravity and aerodynamic center as a function of the opening angle:

25%-75% configuration:

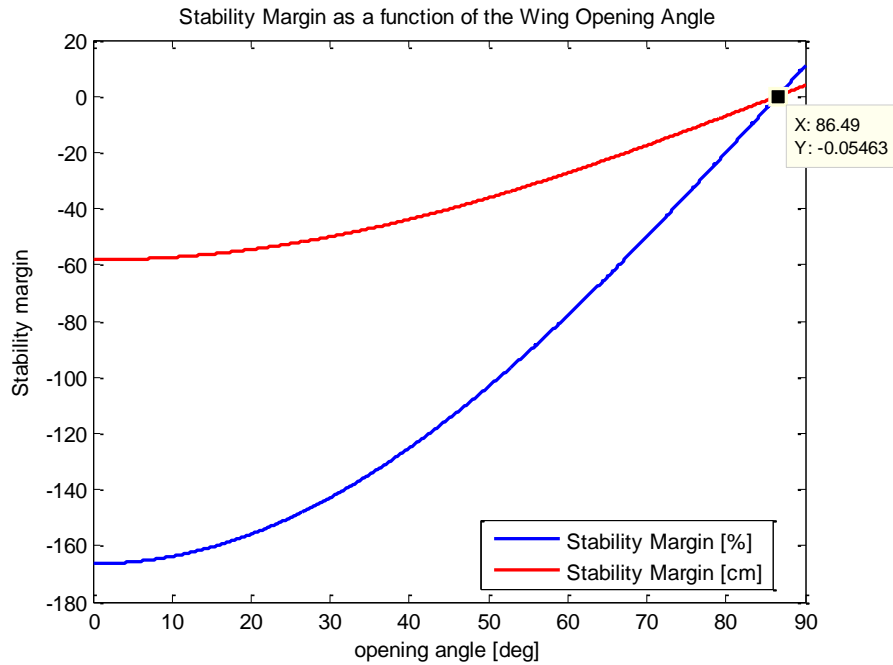


FIGURE 82 - 25%/75% STABILITY MARGIN

40%-60% configuration:

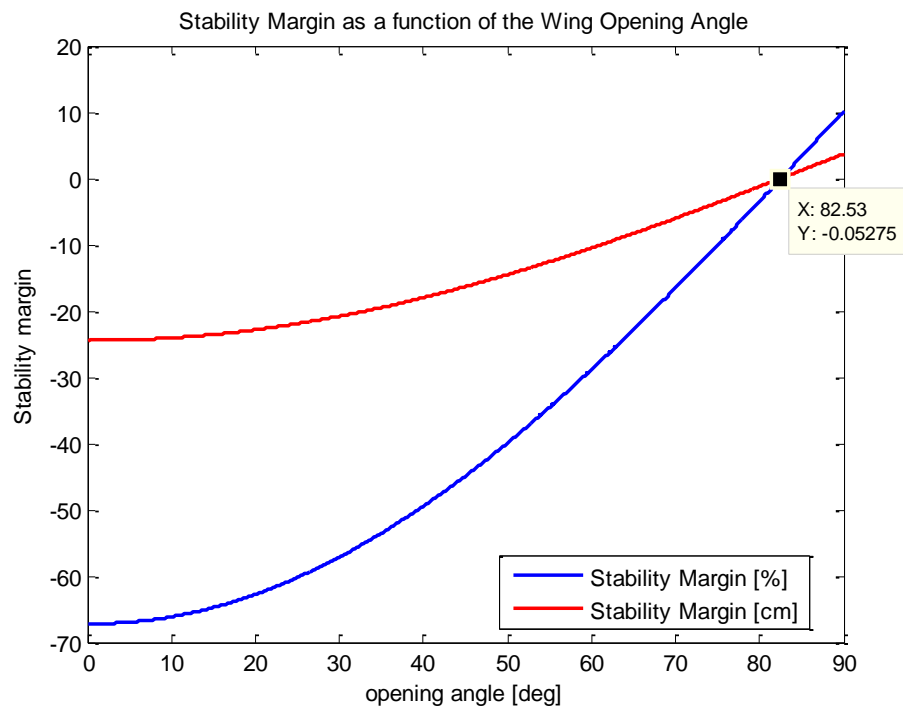


FIGURE 83 - 40%/60% STABILITY MARGIN

The graphs demonstrate that the 25%-75% configuration is stable only from bigger opening angles than the 40%-60% configuration (from 86.5 degrees instead of 82.5 degrees). Therefore, from now on, the configuration will be 40%-60% lift areas ratio between the canard and wing.

For bigger opening angles than 82.5, the UAV is stable. For smaller opening angles, it is still needed to find a solution for the lack of stability while opening the wings and the canard – placing the booster in an angle.

Description of the experiment cell:

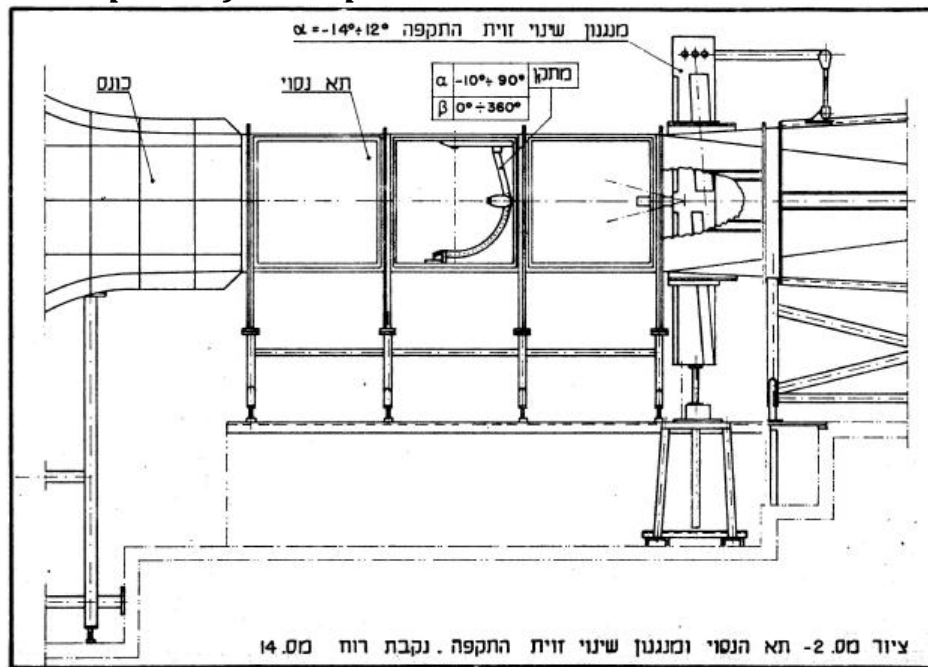


FIGURE 85 - EXPERIMENT CELL DISCRIPTION

11.2. MODEL SIZING

General instructions:

1. Max. Length: 100 cm – As a result of balance rod length, stability and sensitivity limitations.
2. Max. Section area: 2-4% of cell's section area.
3. Model should be as light as possible – In order to minimize the non-aerodynamic loads on the balance rod and keep results as accurate as possible.
4. Rear mount for balance rod should be bigger by about 6 mm than the balance rod's diameter in order to prevent any contact between the internal surface of the model and the balance rod.
5. Model shouldn't be too small in order to get accurate results.
6. Wing tips should be away from the cell's walls - In order to prevent any flow disruptions near the cell walls.

According to the UCAV real flight conditions we have done the experiment in the sub-sonic wind tunnel, and due to the tunnel proportions the max width of our UCAV model could be 50 cm so we created a scale replica of 1:7 scale from the 3m wing span UCAV using the method of Rapid Prototyping (3D printing).

Rapid Prototyping:

Using a CAD program we designed the part we wanted to be created. The printer software is able to read STL files. Those files take the shape of the model and translate it in to thousands of triangles according to its location in space. The model is built from two materials the actual material of the model and another material used for supporting the layers of the model while the model is being built. The printer knows where and what material to put in each layer after each layer it is hardened so the next layer can be built over it. After the model is done we rinse the support material off the model and get holes where they were according to our computer model. Each layer is 0.01mm thick there for it's the tolerance of the model you can get.

The printer we used has a limit of 25x25x25cm size for each part and the density of the material that comes out of the printer

is about: $1.1 \frac{gr}{cm^3}$.

So we divided the model in to six parts: the main body, the nose, a pair of wings and a pair of canards. In addition a few metal parts were created such as wings support and the Morse cone adapter.

11.2.1. THE FULL ASSEMBLY OF THE MODEL

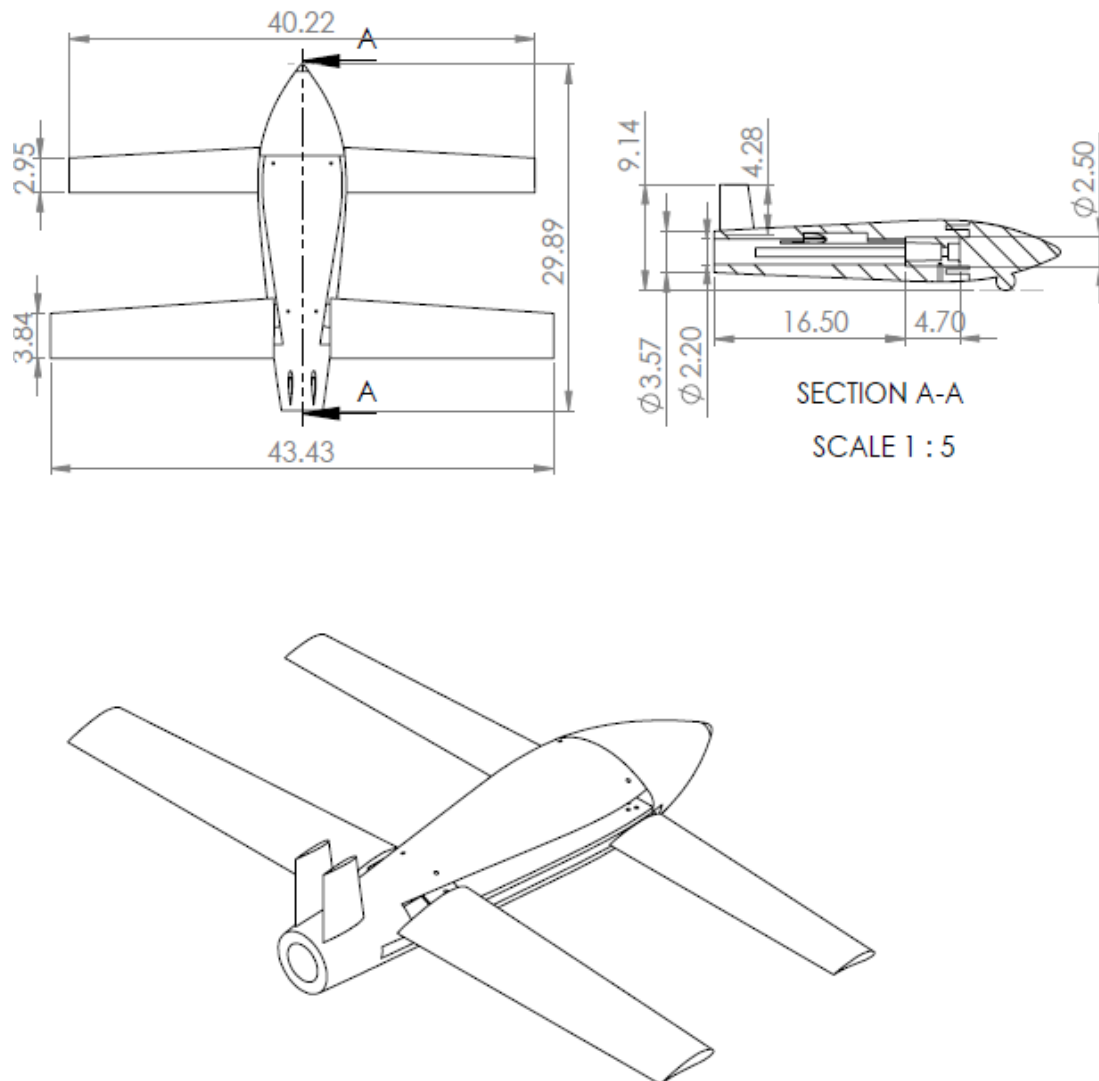


FIGURE 86 - MODEL ASSEMBLY SKETCH

As it can be seen the wind tunnel model is about 30cm long and has a wing span of 44cm.

11.2.2. BALANCE ROD'S ADAPTER DESIGN

Here is the drawing of the balance rod's adapter that we designed for our wind tunnel model:

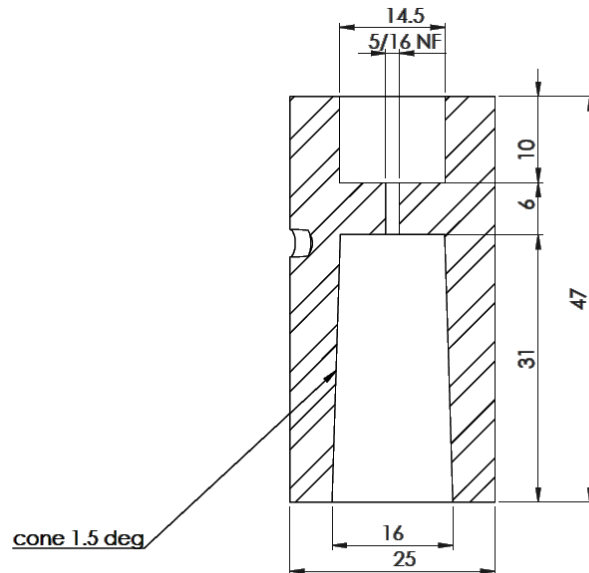


FIGURE 87 - ROD ADAPTER'S SKETCH

General instructions:

1. The rear entrance of the model (for the balance rod) should be bigger than 26 mm.
2. The electric center of the rod should be in the area of the pressure center of the model (which, in our UAV, is moving as a function of the wings and canards opening angle). So, In order to get accurate calculations in the experiment – the adapter should be movable also. One common way to attach the adapter to the model with an option to move it along the body is using bolts, at a few “stations” along the body.
3. The adapter has to be made of aluminum.

Eventually, it was decided to make the adapter stationary, and its location will be at the mean location of the pressure centers that we'll get, even though it will cause some errors.

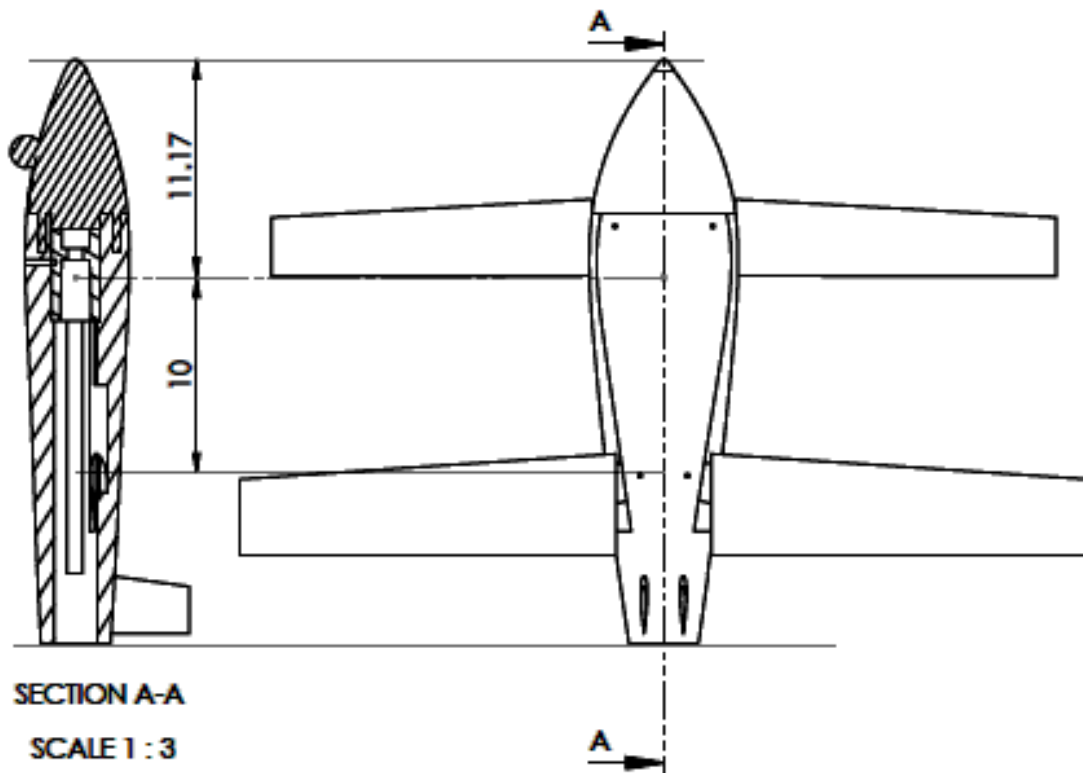


FIGURE 88 - ADAPTER'S LOCATION

11.2.3. PRINTING THE MODEL – THE RESULT OF THE PROCESS



FIGURE 89 - PRINTED MODEL, SEMI-CLOSE 1

After fulfilling the instruction about the maximum size of a part, which led us “breaking” the model into parts (nose, body and tails, wings, canards) here is the result:



FIGURE 90 - PRINTED MODEL, SEMI-CLOSE 2

Nose is being held by pressure, wings and canards are being held by steel spacers and hinges. Also, steel reinforcements were inserted to the wings and canards

12. WIND TUNNEL TEST

12.1. EXPERIMENT PLAN

In order to keep similarity rules:

The Re of the real UAV is approximately: $Re = \frac{\rho v L}{\mu} = \frac{1.225 \cdot 40 \cdot 0.36}{2 \cdot 10^{-5}} \cong 8.8 \cdot 10^5$

Model's Re has to be at the same Re range as the original's ($Re > 2 \cdot 10^5$).

Here is a plot showing the Re/m as a function of true air speed for different air temperatures in the Technion's wind tunnel:

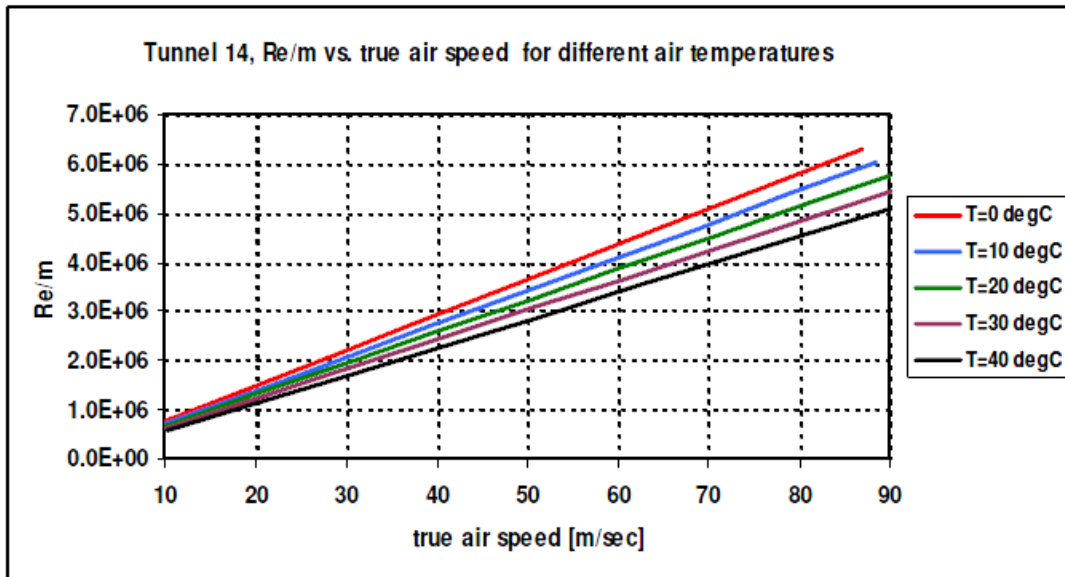


FIGURE 91 - TRUE AIRSPEED AT DIFFERENT TEMPERATURES

In order to stay at the same Re range ($Re > 2 \cdot 10^5$), we'll use an air speed that is greater than $80 \frac{m}{sec}$ for the experiment:

$$Re = \frac{\rho v L}{\mu} = \frac{1.225 \cdot 80 \cdot \frac{0.36}{7}}{2 \cdot 10^{-5}} \cong 2.5 \cdot 10^5$$

But we wanted to avoid the situation in which model's wings can't handle the lift loads, so we lowered the air speed to $45 \frac{m}{sec}$, which led us

$$\text{to: } Re = \frac{\rho v L}{\mu} = \frac{1.225 \cdot 45 \cdot \frac{0.36}{7}}{2 \cdot 10^{-5}} \cong 1.41 \cdot 10^5$$

As of Goals - we would like to:

1. Find the 2D lift coefficient slope, stall angle, pitch and yaw moments coefficients and lift coefficient through the different flight stages (cruise and launch).
2. Learn about UAV's stability status (and find the location of the neutral point) through the different flight stages (cruise and launch).
3. Learn about situations where a flow separation may occur.

While AOA will be changed between -20 to 20 degrees and the slip angle will be changed also between -20 to 20 degrees, the wings and canards folding angle will vary between 2 positions:

1. A transient position of 45 degrees (called "closed").
2. A fully opened position of 90 degrees.

The actual experiments table:






No.	Experiment Code	Configuration		Plane	AOA Range [Degrees]	Air Speed
1	7369	Open		Longitudinal	-16-16	45
2	7373	Open		Lateral	-20-20	45
3	7376	Close		Longitudinal	-20-20	45
4	7377	Close		Lateral	-20-20	45
5	7381	Open		Longitudinal	-20-20	45
6	7383	Open wing only - With tufts		Longitudinal	-20-20	45
7	7385	Body only		Longitudinal	-20-20	45

TABLE 34 - EXPERIMENT TABLE

The different configurations:

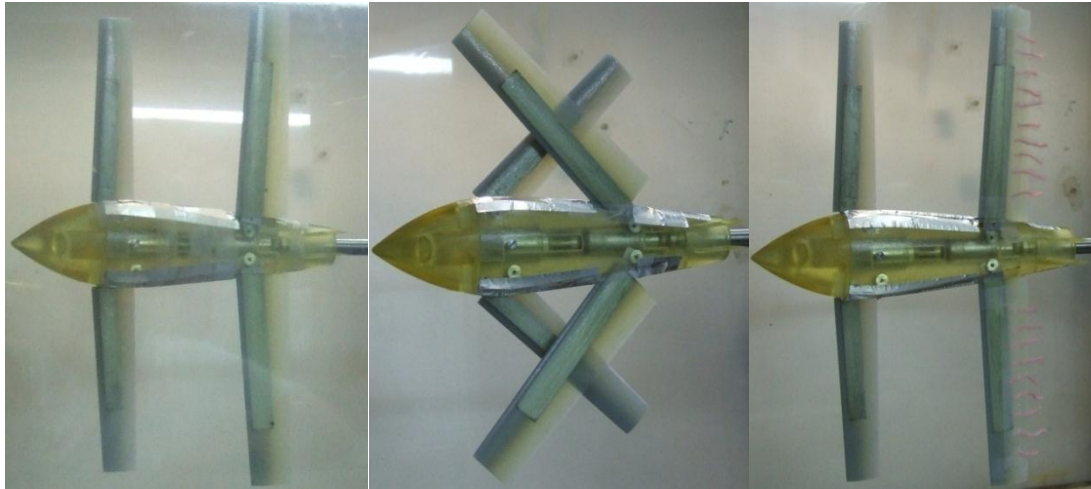


FIGURE 92 - OPENED, CLOSED AND OPEN WITH TUFTS TEST MODEL

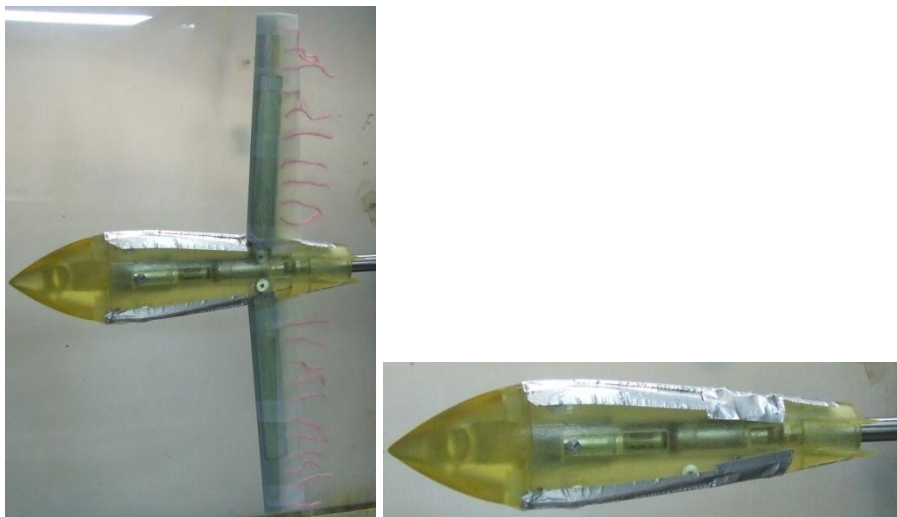


FIGURE 93 - OPEN WING ONLY WITH TUFTS, BODY ONLY TEST MODEL

Conclusions:

1. Additional strengthening of the wind tunnel model is needed so it can be able to carry the lift loads of 80 m/s air speed, and by that to get the necessary Re number and get more accurate results.
2. Additional experiments have to be performed on the wings and canards in order to evaluate their mutual effect on each other.

12.2. WIND TUNNEL'S RESULTS

12.2.1. OPENED CONFIGURATION

Lift coefficient as a function of attack angle:

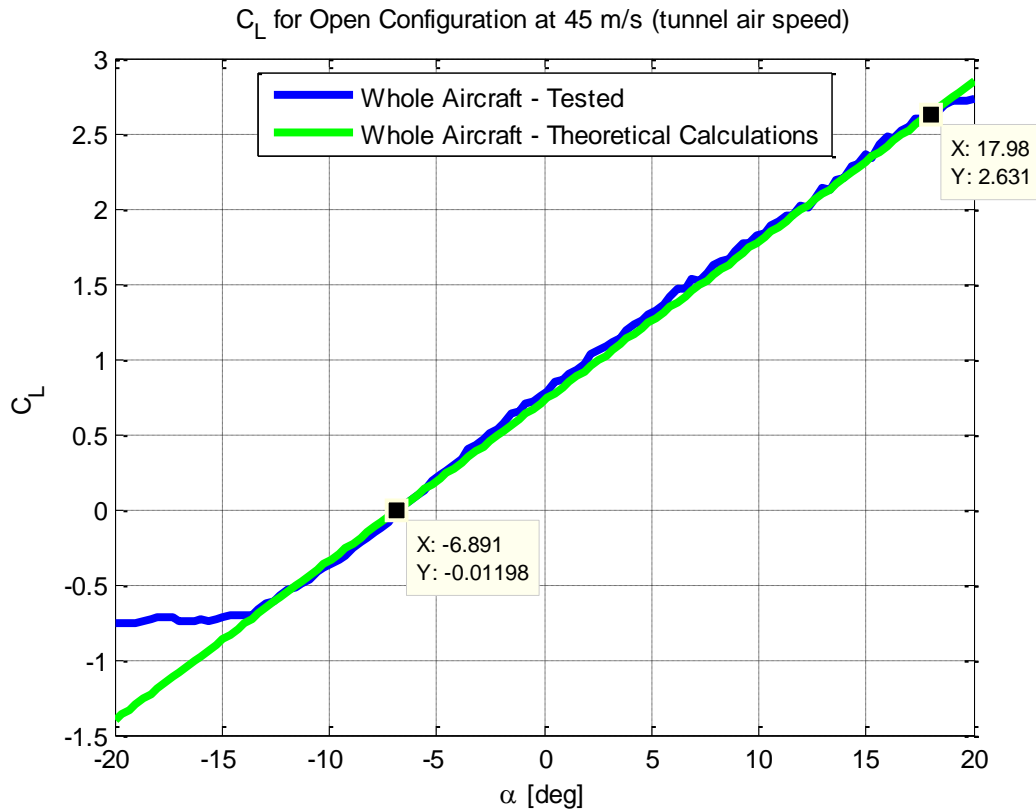


FIGURE 94 - LIFT COEFFICIENT, OPENED, 45 [M/S] - TEST VS. THEORY

The green line is the theoretical lift results, and the blue line is the wind tunnel results. The results are very close to each other and in general speaking, the theoretical results are very accurate. The wind tunnel zero lift angle from the wind tunnel is -6.89 degrees, while the theoretical zero lift angle is -6.8 degrees – the results are very close. The only big difference between the results is between the stall angles – the wind tunnel stall angle is 18 degrees and the theoretical stall angle is 13.1 degrees. This difference can occur because the wings are not the endless. In the tunnel, vortexes are created on the tips of the wings which create a smaller effective angle on the wings.

Lift coefficient as a function of attack angle for each lift generator component:

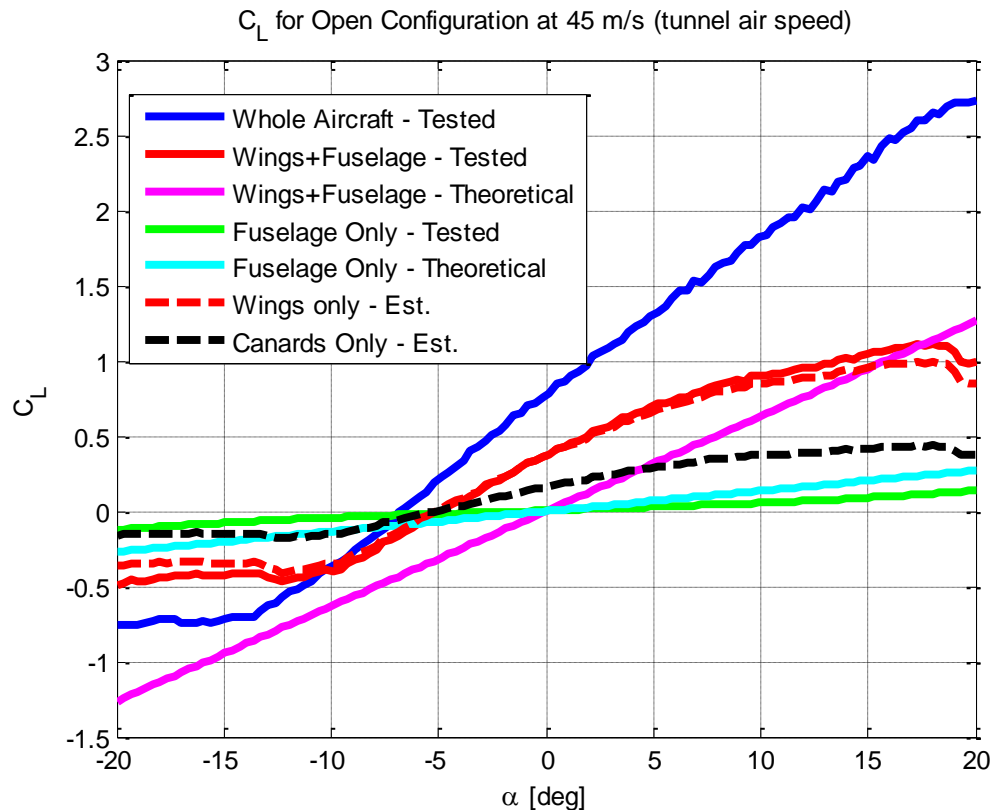


FIGURE 95 - LIFT COEFFICIENT, OPENED, 45[M/S] - TEST VS. THEORY IN DIFFERENT STAGES OF THE WIND TUNNEL TEST

For the comparison between the wind tunnel and the theoretical results for each lift component, the results are not so close:

- For the fuselage, there is a difference between the slopes of the lift line
 - the theoretical slope of the lift line is quite higher. The explanation for the phenomenon is a wrong choice of the 2D slope lift line -

$$2\pi \left[\frac{1}{rad} \right].$$

- For the wing's lift coefficient, the slope lift line is quite suitable to the wind tunnel results, but there is an offset – the lift coefficient from the wind tunnel is higher than the theoretical lift coefficient. The explanation for this phenomenon can be the lack of consideration of the body-wing effects on each other that can enlarge the lift.

The canard's lift coefficient isn't compares because these results were not tested in the wind tunnel and was estimated for the theoretical calculations.

Moment coefficient as a function of lift coefficient:

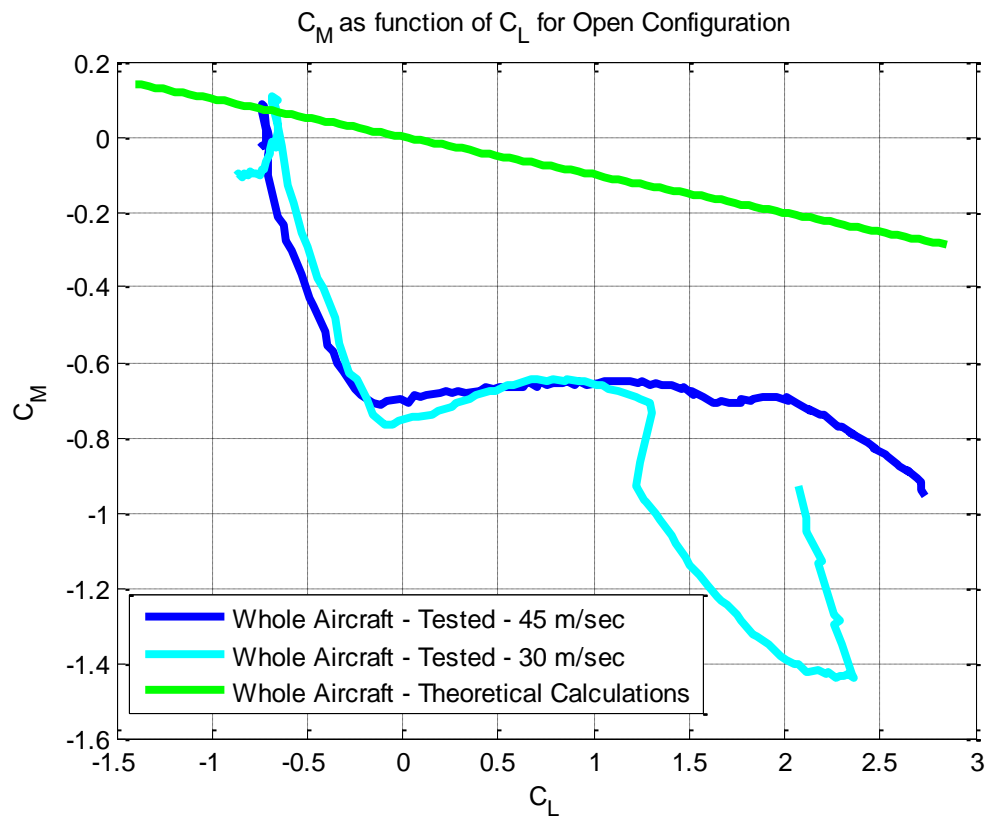


FIGURE 96 - MOMENT COEFFICIENT VS. LIFT COEFFICIENT, OPENED

There is a big difference between the results. An explanation for this phenomenon can be the smaller speed than needed. A proof for this explanation is the enlargement of the divergence in smaller speeds (for 30 m/sec). The model is trimming only on deep stall (very negative lift coefficient). There is a need to consider this phenomenon on the control section.

Moment coefficient as a function of attack angle for each lift generator component:

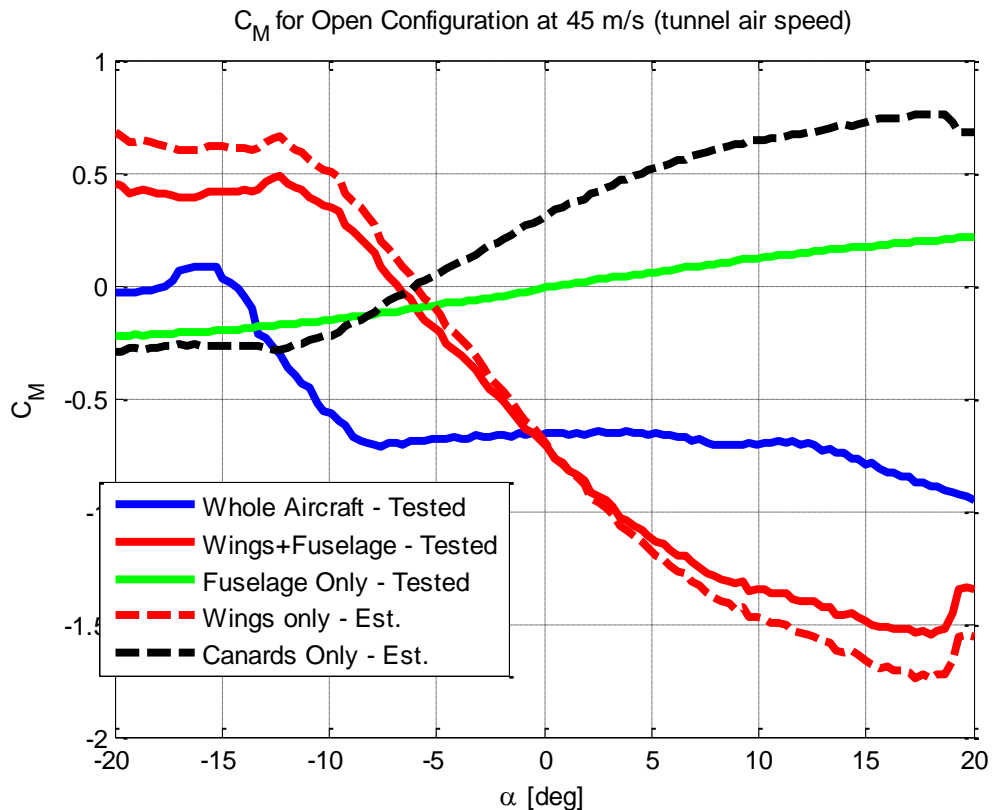


FIGURE 97 - MOMENT COEFFICIENT VS. LIFT ANGLE, OPENEND, 45[M/S]

The moment coefficient for each lift generator component is linear for most of the angles. The changes in the slopes occur on logical angle (changing in slopes shows a stall of a lift generator component). The whole moment of the model have earlier changes in the slop. The explanation for this phenomenon is the wing-canard effects that create an early stall of the canard (because of the upwash). There is a need to consider this phenomenon on the control section.

Drag coefficient as a function of angle of attack:

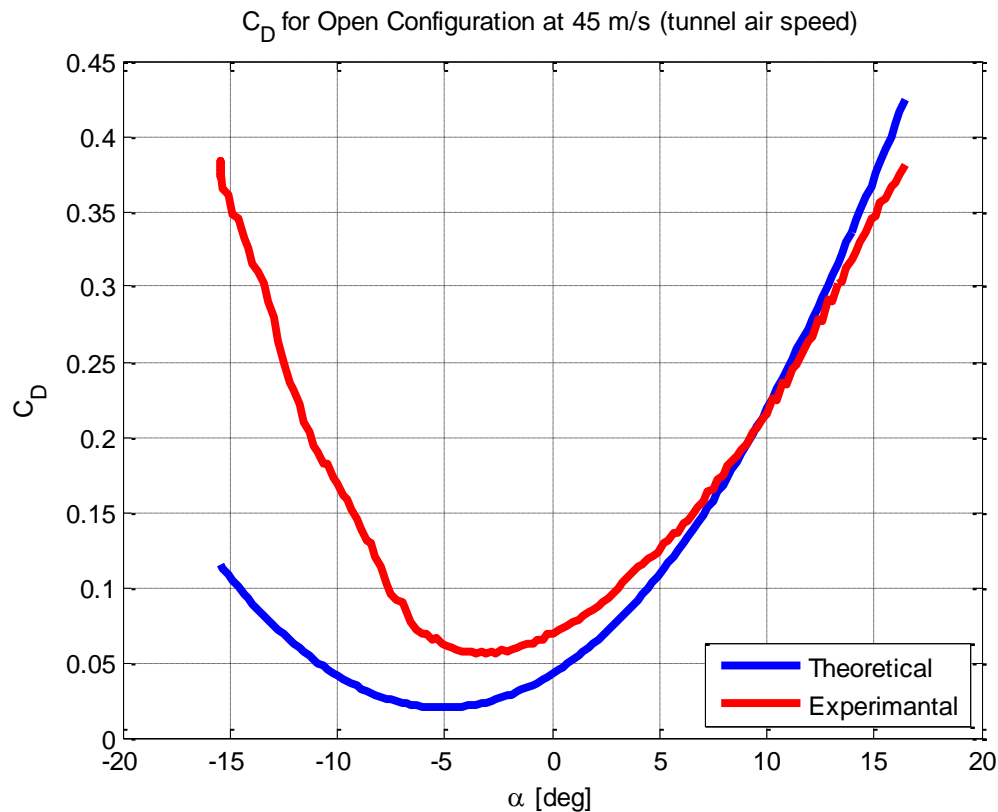


FIGURE 98 - DRAG COEFFICIENT, OPENED, 45[M/S]

We expect to see a difference between the results because of the duct-tape that was on the model in the wind tunnel test, because the longitudinal gauge is the most inaccurate gauge and the drag results are very small (the error will be the biggest for the drag) and because of the base drag of the model. The results are quite close (in the shape of the graph and for some angles of attack). The biggest difference is between the form drag coefficients – the theoretical guess is 0.02 and the wind tunnel results shows 0.056. The form drag coefficient results cannot be compared because of the duct-tape.

12.2.2. SEMI-CLOSED CONFIGURATION (45° OPEN)

Lift coefficient as a function of attack angle:

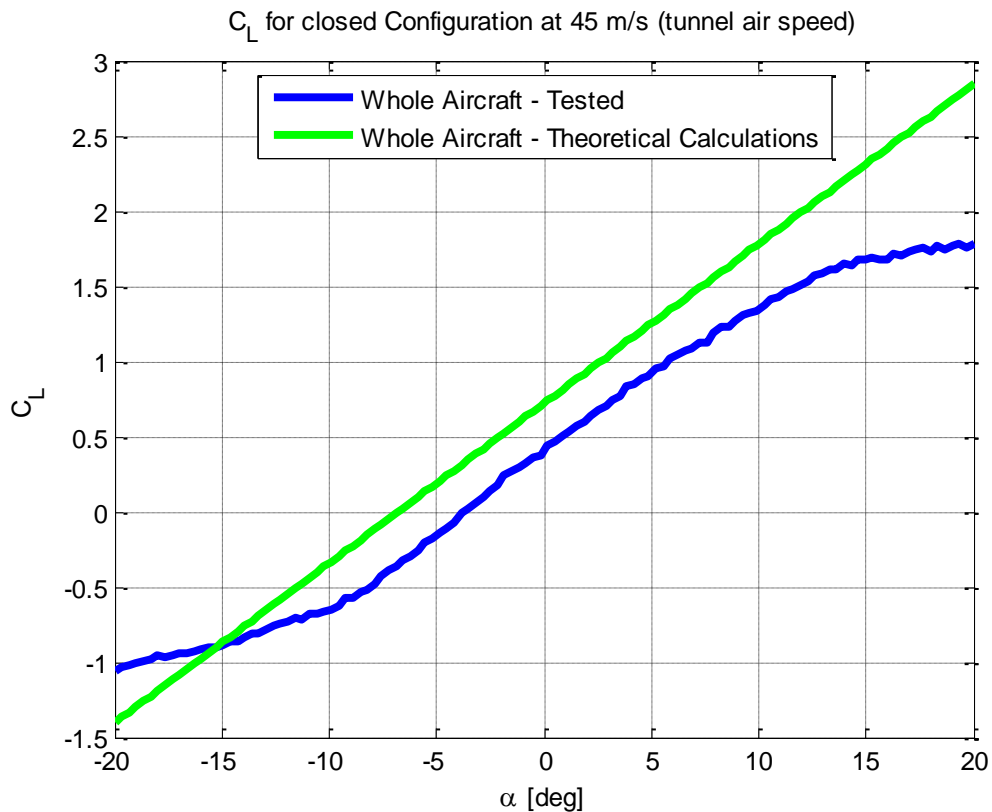


FIGURE 99 - LIFT COEFFICIENT, CLOSED, 45 [M/S]

With compare to the opened configuration, there is less matching between the theoretical and the wind tunnel results. This phenomenon occurred because of the smaller distance between the aerodynamic centers of the wing and canard which enlarge the wing-canard effects. The downwash on the wing is bigger than the up-wash of the canard and therefore, the lift is smaller. In addition, some of the lift area of the wing and canard is covered in the body.

Moment coefficient as a function of Lift Coefficient:

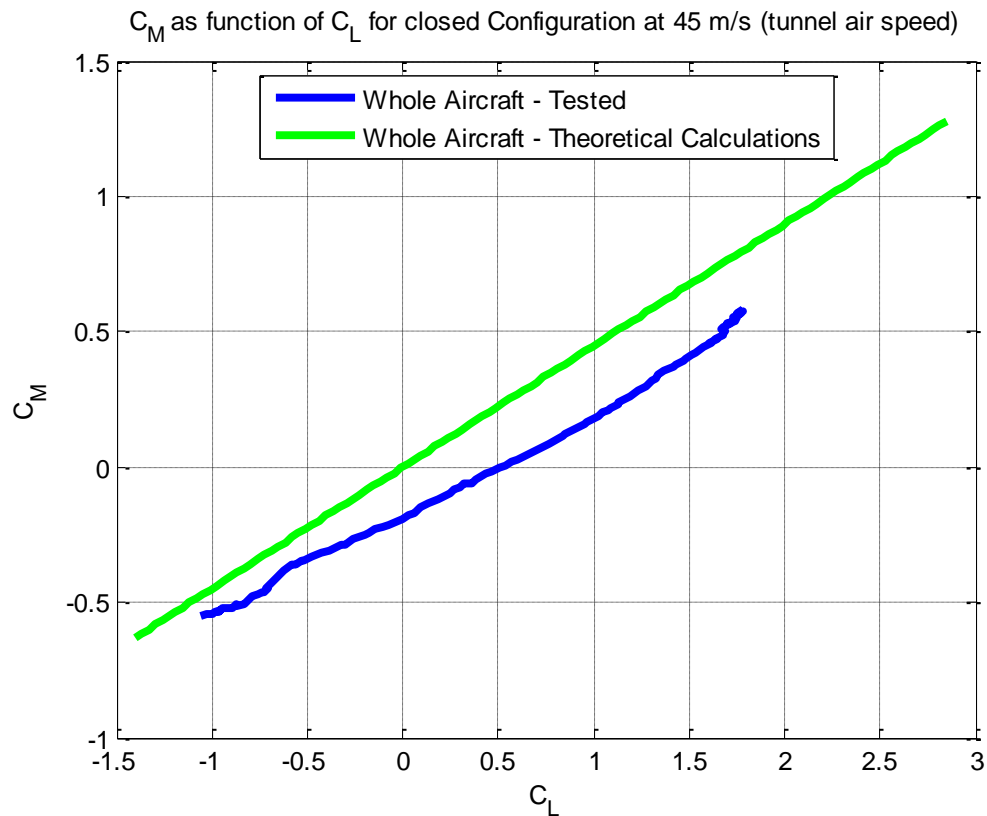


FIGURE 100 - MOMENT COEFFICIENT VS. LIFT COEFFICIENT, CLOSED, 45 [M/S]

The wing tunnel moment coefficient is linear. The offset between the graphs occurs because of the offset in the lift coefficients graphs and because in the theory there is not a consideration of the moment coefficient in the aerodynamic center.

13. GNC - GUIDANCE, NAVIGATION AND CONTROL SYSTEM

13.1. GNC SYSTEMS

The main objective of "iCLEAN" is to eliminate enemies, and do it autonomously. Enemies are defined as static and dynamic object as well. In order to do so, maintaining flight in performance envelopes, or to follow the flight path in the homing phase as calculated in the guidance and navigation units, a good control system (i.e. sufficient GM and PM to the relevant loops) is crucial. This chapter first describes the aerodynamic model of a canard configuration. Linearization and small angles assumption have made. Afterwards, the control system will be defined using state space parameters. Using classic control theory methods such Root Locus, Roth – Horowitz, Nyquist stability criterion, Gibson criterion and more, we have managed to find out specific gain to our controllers so the UAV will be controlled with sufficient margins (due to uncertainty regarding assumptions made, delays of the autopilot etc'). The next step shown is building and comparing two mainstream's guidance laws (PN and APN) and choose the better one to "iCLEAN" UAV.

13.1.1. BACKGROUND

The need to define and use appropriate coordinate systems arises from two main considerations: First, there is a particular coordinate system in which the position and velocity of the UAV “make sense”. For example, for navigation calculations we are concerned with position (which is obtained after two integrations of the accelerometers) and velocity with respect to the Earth, whereas for UAV performance (i.e. rates, angles) we need position and velocity with respect to the atmosphere. The second consideration way using different coordinate systems is that in some coordinates system, the phenomena of interest are most naturally expressed. For example, the direction of "iCLEAN" engine’s thrust force may often be considered fixed with respect to the body of the UAV (unlike the Booster in the launch phase).

Notice that all of our physical parameters are invariants (position, velocity, rates, accelerations etc.), and each selection regarding coordinate systems made is one of many possible selections.

All coordinate systems used are right-handed and orthogonal. Coordinate Systems are designated by the Latin letter F with a subscript intended to be a mnemonic for the name of the system, such as F_I for the inertial reference frame, or F_B for the body reference frame. The origin of the system will be denoted by O and a subscript (e.g. O_I). When describing the place of a coordinate system it means where its origin is. Axes of the system are labeled x, y, and z with the appropriate subscript. Unit vectors along x, y, and z will be denoted i, j, and k respectively and subscripted appropriately.

The definition of a coordinate system must state the location of its origin and the means of determining at least two of its axes, while the third axis being determined by using the right-hand rule. The location of the origin and orientation of the axes may be arbitrary within certain restrictions, but once selected may not be changed. Following are the main coordinate systems of interest used.

13.1.2. COORDINATE SYSTEMS

13.1.2.1. INERTIAL REFERENCE FRAME

The Inertial coordinate system is a fixed coordinate system and is defined arbitrary. Its origin and axes are given and donated by the following:

1. The origin (O_I) is located at arbitrary reference point.
2. The X-axis (donated by x_I) points arbitrarily as well.
3. The Y-axis (donated by y_I) points orthogonal to x_I .
4. The Z-axis (donated by z_I) points to comply with the right-hand rule.

Coordinate vectors expressed in the body frame are appended with a subscript 'I'. Next, we define $V_I = (V_{Ix}, V_{Iy}, V_{Iz})'$ inertial velocity vector, and defined $a_I = (a_{Ix}, a_{Iy}, a_{Iz})'$ to be the projection of acceleration vector along body frame axes.

13.1.2.2. BODY COORDINATE SYSTEM

The body coordinate system is UAV-carried and is directly defined on the body of the UAV. Its origin and axes (see Fig. 99) are given by the following:

1. The origin (O_b) is located at the center of gravity (C.G) of the UAV.
2. The X-axis (x_b) points forward, lying in symmetric plane y-z of the UAV.
3. The Y-axis (y_b) is starboard (points to the right wing).
4. The Z-axis (z_b) points downward to comply with the right-hand rule.

Coordinate vectors expressed in the body frame are appended with a subscript 'b'. Next, we define $V_b = (u, v, w)'$ where u, v and w are the projection of physical velocity vector along body frame axes x_b, y_b, z_b accordingly. Also we defined $a_b = (a_x, a_y, a_z)'$ to be the projection of acceleration vector along body frame axes.

Also defined the angular velocity and rates: $\omega_b = (p, q, r)'$ $\dot{\omega}_b = (\dot{p}, \dot{q}, \dot{r})'$, where p, q, r are the rates around x, y, z axes accordingly. (p for roll, q for pitch and r for yaw). Last vector defined is moments $M_b = (L, M, N)'$ where L is the roll moment (around x axes). M is the pitch moment (around y axes) and N is yaw moment (around z axes).

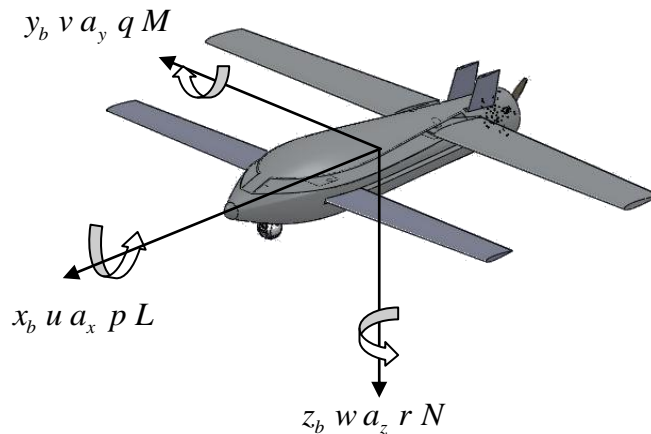


FIGURE 101 - BODY REFERENCE FRAME AND ITS VECTORS

13.1.2.3. WIND COORDINATE SYSTEM

Shown in fig. 100, F_w is a UAV-carried (origin fixed to the body, normally the C.G) coordinate system in which the X_w axis is in the direction of the velocity vector of the UAV relative to the air mass. The Z_w axis is chosen to lie in the plane of symmetry of the UAV and the Y_w axis to starboard. Note that if the relative wind changes, the orientation of the wind-axes changes too but Z_w always lies in the plane of symmetry as defined. An extensive use is made with α (A.O.A) while transforming from Wind to Body frame as shown in sub-section 13.1.4.1.

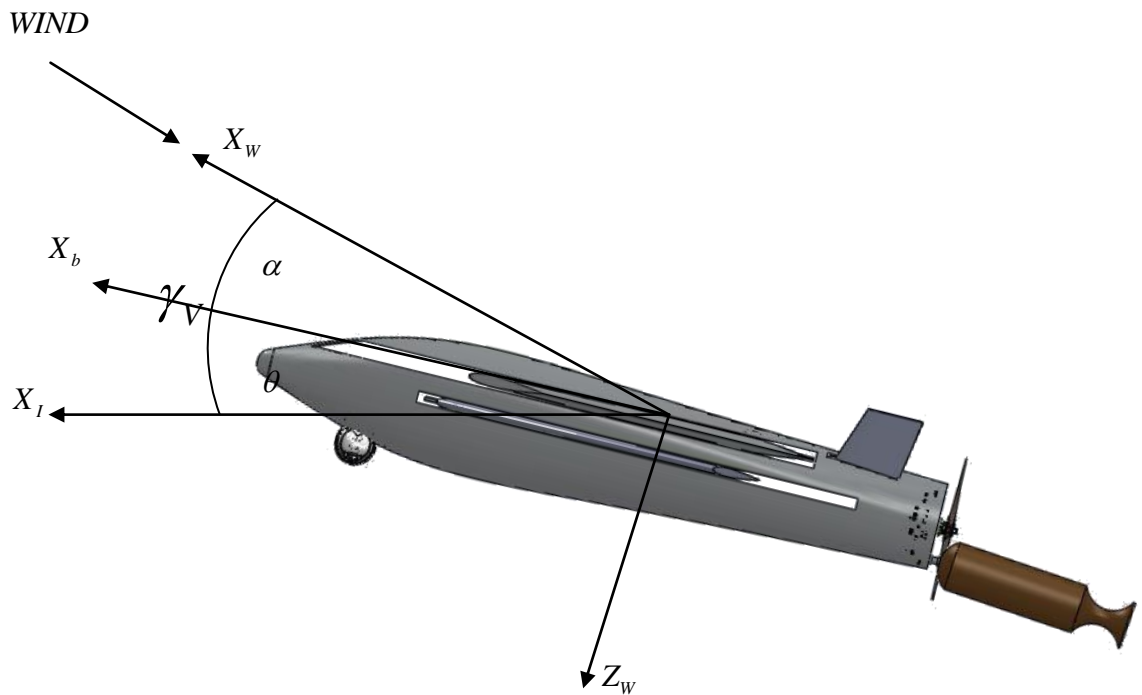


FIGURE 102 - ANGLES DEFINITION IN THE XZ PLANE

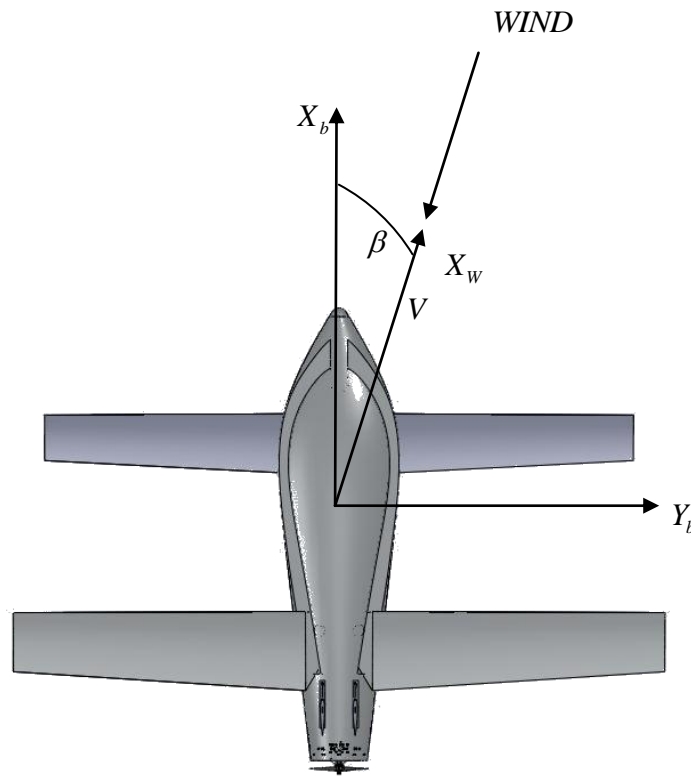


FIGURE 103 - DEFINITION OF SLIDE ANGLE β

13.1.3. PARAMETERIZATION

13.1.3.1. EULER ANGLES

The Euler angles are three angles introduced by Leonhard Euler to describe the orientation of a rigid body. To describe such an orientation three parameters are required. They can be given in several ways, Euler angles being one of them.

Euler angles also represent three composed rotations that move a reference frame to a given referred frame. This is equivalent to saying that any orientation can be achieved by composing three elemental rotations (rotations around a single axis), and also equivalent to saying that any rotation matrix can be decomposed as a product of three elemental rotation matrices. The three angles are (ψ, θ, ϕ) where ψ is the yaw angle, θ is pitch angle and ϕ is roll angle. This order of angles is arbitrary, but this configuration is the most used and often called 321. (Each number for its own axes: z,y,x accordingly). An extensive use of Euler angles is made during flight control dynamics simulation as they

used for transformation from one frame to other as will be shown in sub section 13.1.4.1.

Although it sounds pretty simple, it has some disadvantages like singularity around $\pi/2$ but the assumption is that "iCLEAN" won't meet these angles or even close to it. Therefore, Euler angles parameterization was chosen (instead of quaternion).

13.1.4. TRANSFORMATION

13.1.4.1. ROTATION MATRIX

Using Euler parameters, it is possible to convert a vector from one frame to other. This is done by 3 sequenced rotations around one (temporary) axes, or at once (by multiplying the 3 matrixes).

The transformation matrix from wind to body is given by:

$$D_w^B = \begin{bmatrix} \cos \alpha \cdot \cos \beta & \sin \beta & \sin \alpha \cdot \cos \beta \\ -\cos \alpha \cdot \sin \beta & \cos \beta & -\sin \alpha \cdot \sin \beta \\ -\sin \alpha & 0 & \cos \alpha \end{bmatrix}$$

The transpose matrix of D_w^B realizes $(D_w^B)^T = D_B^W$.

There are many more ways to go from one frame to the other such DCM (Direction Cosine Matrix), Piogram, etc.

13.1.5. EQUATION OF MOTIONS

13.1.5.1. GENERAL

The rigid body equations of motion are the differential equations that describe the evolution of the twelve basic states of "iCLEAN" UAV: the scalar components of V_B, ω_B , and R , plus the three Euler angles as defined. The usual coordinate systems in which we represent the equations of motion are the wind and body axis systems as shown in sub-sections 13.1.5.2 and 13.1.5.3. Mixed systems using both coordinate systems are common. Any such set of equations of motion must be complete. This means that in every expression $\frac{d(state)}{dt} = \dots$ everything on the right-hand side must be given by either an algebraic equation (including variable = constant), by another differential equation, or by some external input to the system.

13.1.5.2. BODY AXIS EQUATIONS

Body Axis Force Equations:

The body axis force can be derived simply using fundamental Newtonian physics. No simple derivations are shown on this paper, but will be discussed when needed.

$$\{F\}_B = m\{\dot{V}_B\}_B + m\{\omega_B\}_B\{V\}_B$$

In terms of the rates (of the inertial components of velocity), as seen in the body-axes:

$$\{\dot{V}_B\}_B = \frac{1}{m}\{F\}_B - \{\omega_B\}_B\{V\}_B$$

All of the terms in this equation have been defined previously, so all we have to do is make the necessary substitutions and expand the equations to solve for \dot{u} , \dot{v} , and \dot{w} . On the right-hand side, the net applied force is comprised of aerodynamic forces (as will be defined in the aerodynamic modeling of "iCLEAN" canard configuration), "iCLEAN" weight, and the force due to thrust:

$$\{F\}_B = \{F_{Aero}\}_B + \{F_{Weight}\}_B + \{F_{Thrust}\}_B = \begin{Bmatrix} F_x \\ F_y \\ F_z \end{Bmatrix} + \begin{Bmatrix} -mg \cdot \sin \theta \\ mg \cdot \sin \phi \cdot \cos \theta \\ mg \cdot \cos \phi \cdot \cos \theta \end{Bmatrix} + \begin{Bmatrix} T \cdot \cos \varepsilon \\ 0 \\ T \cdot \sin \varepsilon \end{Bmatrix}$$

Where F_x, F_y, F_z are the aerodynamic forces, due to drag and lift. T is the thrust, and ε is the misalignment of the engine placement. (If thrust vector direction lies exactly on x_B , $\varepsilon = 0$ and $T = T_x$ (thrust is only in x_B direction)).

As defined previously,

$$\{V\}_B = \begin{Bmatrix} u \\ v \\ w \end{Bmatrix} \quad \{V\}_B = \begin{Bmatrix} \dot{u} \\ \dot{v} \\ \dot{w} \end{Bmatrix} \quad \{\omega\}_B = \begin{bmatrix} 0 & -r & q \\ r & 0 & -p \\ -q & p & 0 \end{bmatrix}$$

↓

$$\{\omega\}_B \{V\}_B = \begin{bmatrix} qw - rv \\ ru - pw \\ pv - qu \end{bmatrix}$$

And as a result the body axis force equations can be easily written:

$$\begin{aligned} \dot{u} &= \frac{1}{m} (F_x + T \cdot \cos \varepsilon) - g \cdot \sin \theta + rv - qw \\ \dot{v} &= \frac{1}{m} (F_y) - g \cdot \sin \phi \cdot \cos \theta + pw - ru \\ \dot{w} &= \frac{1}{m} (F_z + T \cdot \sin \varepsilon) + g \cdot \cos \phi \cdot \cos \theta + qu - pv \end{aligned}$$

Body Axis Moment Equations:

The moment equations are given by

$$\{M_B\}_B = I_B \{\dot{\omega}_B\}_B + \{\omega_B\}_B I_B \{\omega_B\}_B$$

In terms of rates of the inertial component of angular rotation, as seen in body axes,

$$\{\dot{\omega}_B\}_B = -I_B^{-1} [\{M_B\}_B - \{\omega_B\}_B I_B \{\omega_B\}_B]$$

Where M_B are the moments due to aerodynamic and thrust. Our assumption is that thrust doesn't contribute to roll and yaw moment (as ε goes to zero, and $T_y, T_z \rightarrow 0$, although that because "iCLEAN" uses a rotary engine, it has an induced roll moment, but it is minuscule)

$$\{M_B\}_B = \begin{Bmatrix} L \\ M + M_T \\ N \end{Bmatrix}$$

Where M_T is the pitch moment applied by the thrust.

By Solidworks modeling we have found the moments of inertia. The cross products moments involving y are small compared to the main ones (because its symmetry). In this paper all cross products have been neglected. Therefore:

$$I_B = \begin{bmatrix} I_{xx} & 0 & -I_{xz} \\ 0 & I_{yy} & 0 \\ -I_{xz} & 0 & I_{zz} \end{bmatrix}$$

$$I_B^{-1} = \frac{1}{I_D} \cdot \begin{bmatrix} I_{zz} & 0 & I_{xz} \\ 0 & I_D & 0 \\ I_{xz} & 0 & I_{xx} \end{bmatrix}$$

$$\text{Where } I_D = I_{xx} I_{zz} - I_{xz}^2$$

The rest is substitutions and expansions:

$$\begin{aligned}\dot{p} &= \frac{I_{xz}}{I_D} [L + I_{xx}pq - (I_{zz} - I_{yy})qr] + \frac{I_{xz}}{I_D} [N + I_{xz}qr - (I_{yy} - I_{xx})pq] \\ \dot{q} &= \frac{1}{I_{yy}} [M + M_T - (I_{xx} - I_{zz})pr - I_{xz}(p^2 - r^2)] \\ \dot{r} &= \frac{I_{xz}}{I_D} [L + I_{xz}pq - (I_{zz} - I_{yy})qr] + \frac{I_{xx}}{I_D} [N - I_{xz}qr - (I_{yy} - I_{xx})pq]\end{aligned}$$

Body Axis Kinematic Equations:

We use the Euler angles relationships from the transformation for Inertial Frame to Body Frame. The resulting matrix the relate body rates to Euler angles rates are given by:

$$\begin{Bmatrix} \dot{\phi} \\ \dot{\theta} \\ \dot{\psi} \end{Bmatrix} = \begin{bmatrix} 1 & \sin \phi \cdot \tan \theta & \cos \phi \cdot \tan \theta \\ 0 & \cos \phi & -\sin \phi \\ 0 & \sin \phi \sec \theta & \cos \phi \sec \theta \end{bmatrix} \begin{Bmatrix} p \\ q \\ r \end{Bmatrix}$$

↓

$$\begin{aligned}\dot{\phi} &= p + (q \sin \phi + r \cos \phi) \cdot \tan \theta \\ \dot{\theta} &= q \cdot \cos \phi - r \cdot \sin \phi \\ \dot{\psi} &= (q \sin \phi + r \cdot \cos \phi) \cdot \sec \theta\end{aligned}$$

Body Axis Navigation Equations:

The position of the UAV relative to the Earth (Earth Frame) is found by integrating the UAV velocity along its path, or by representing the velocity in Earth-fixed coordinates and integrating each component. The latter is easier, and is given by

$$\begin{Bmatrix} \dot{X}_E \\ \dot{Y}_E \\ \dot{h} \end{Bmatrix} = \begin{bmatrix} \cos \theta \cdot \cos \psi & \sin \phi \cdot \sin \theta \cdot \cos \psi - \cos \phi \cdot \sin \psi & \cos \phi \cdot \sin \theta \cdot \cos \psi + \sin \phi \cdot \sin \psi \\ \cos \theta \cdot \sin \psi & \sin \phi \cdot \sin \theta \cdot \sin \psi + \cos \phi \cdot \cos \psi & \cos \phi \cdot \sin \theta \cdot \sin \psi - \sin \phi \cdot \cos \psi \\ \sin \theta & \sin \phi \cdot \cos \theta & \cos \phi \cdot \cos \theta \end{bmatrix} \begin{Bmatrix} u \\ v \\ w \end{Bmatrix}$$

↓

$$\begin{aligned}\dot{X}_E &= u(\cos \theta \cdot \cos \psi) + v(\sin \phi \cdot \sin \theta \cdot \cos \psi - \cos \phi \cdot \sin \psi) + w(\cos \phi \cdot \sin \theta \cdot \cos \psi + \sin \phi \cdot \sin \psi) \\ \dot{Y}_E &= u(\cos \theta \cdot \sin \psi) + v(\sin \phi \cdot \sin \theta \cdot \sin \psi + \cos \phi \cdot \cos \psi) + w(\cos \phi \cdot \sin \theta \cdot \sin \psi - \sin \phi \cdot \cos \psi) \\ \dot{h} &= -\dot{Z}_E = u \cdot \sin \theta - v \cdot \sin \phi \cdot \cos \theta - w \cdot \cos \phi \cdot \cos \theta\end{aligned}$$

13.1.5.3. WIND AXIS EQUATIONS

Wind Axis Equations:

$$\alpha \equiv \tan^{-1}\left(\frac{w}{u}\right) \Rightarrow \dot{\alpha} = \frac{u\dot{w} - w\dot{u}}{u^2 + w^2}$$

$$V = \sqrt{u^2 + v^2 + w^2} \Rightarrow \dot{V} = \frac{u\dot{u} + v\dot{v} + w\dot{w}}{\sqrt{u^2 + v^2 + w^2}} = \frac{u\dot{u} + v\dot{v} + w\dot{w}}{V}$$

$$\beta = \sin^{-1}\left(\frac{v}{V}\right) \Rightarrow \dot{\beta} = \frac{V\dot{v} - v\dot{V}}{V\sqrt{u^2 + w^2}}$$

13.1.5.4. STEADY STATE SOLUTIONS

We may get some insight into the equations of motion by examining steady-state solutions, which then are algebraic equations. Thus, Body axis rates states:

$$\dot{u} = \dot{v} = \dot{w} = \dot{p} = \dot{q} = \dot{r} = 0$$

And also, Wind axis rates states:

$$\dot{V} = \dot{\alpha} = \dot{\beta} = \frac{pw}{dt} = \frac{qw}{dt} = \frac{rw}{dt} = 0$$

In addition, all of the controllers must be constant:

$$\delta_T = \delta_e = \delta_a = \delta_t = \text{const}$$

13.1.6. CONTROL SYSTEM

13.1.6.1. BASIC FLIGHT CONTROL CONCEPTS

Introduction:

The system that controls the flight is called FCS - Flight Control System. In the early days of flying, the FCS was entirely mechanical. (By means of cables and pulleys) The control surfaces of the aircraft such elevator, ailerons, rudders, were given the necessary deflections to control the aircraft. However, nowadays systems are mainly fly-by-wire FCS. In this system electrical signals are sent to the control surfaces. The signals are sent by the flight (control) computer (FC/FCC). But what is the advantage of automatic flight control? Why would we use an FC instead of a pilot?

There are several reasons doing it. First of all, a computer has a much higher reaction velocity than a pilot. Also, it isn't subject to concentration losses and fatigue. Finally, a computer can more accurately know the state the aircraft is in. "iCLEAN" is an UAV, therefore an automatic FCS is needed to be implemented.

13.1.6.2. THE EQUATIONS OF MOTION

Equation of motion has been already derived, we quickly go through it:
Longitude model –

$$\begin{bmatrix} C_{X_u} - 2\mu_c D_c & C_{X_\alpha} & C_{Z_0} & C_{X_q} \\ C_{Z_u} & C_{Z_\alpha} + (C_{Z_{\dot{\alpha}}} - 2\mu_c) D_c & -C_{X_0} & 2\mu_c + C_{Z_q} \\ 0 & 0 & -D_c & 1 \\ C_{m_u} & C_{m_\alpha} + C_{m_{\dot{\alpha}}} D_c & 0 & C_{m_q} - 2\mu_c K_Y^2 D_c \end{bmatrix} \begin{bmatrix} \dot{u} \\ \alpha \\ \theta \\ \frac{q\bar{c}}{V} \end{bmatrix} = \begin{bmatrix} -C_{X_{\delta_e}} & -C_{X_{\delta_t}} \\ -C_{Z_{\delta_e}} & -C_{Z_{\delta_t}} \\ 0 & 0 \\ -C_{m_{\delta_e}} & -C_{m_{\delta_t}} \end{bmatrix} \begin{bmatrix} \delta_e \\ \delta_t \end{bmatrix}$$

Latitude model –

$$\begin{bmatrix} C_{Y_\beta} + (C_{Y_{\dot{\beta}}} - 2\mu_b) D_b & C_L & C_{Y_p} & C_{Y_r} - 4\mu_b \\ 0 & -\frac{1}{2} D_b & 1 & 0 \\ C_{l_\beta} & 0 & C_{l_p} - 4\mu_b K_X^2 D_b & C_{l_r} + 4\mu_b K_{XZ} D_b \\ C_{n_\beta} + C_{n_{\dot{\beta}}} D_b & 0 & C_{n_p} + 4\mu_b K_{XZ} D_b & C_{n_r} - 4\mu_b K_Z^2 D_b \end{bmatrix} \begin{bmatrix} \beta \\ \varphi \\ \frac{pb}{2V} \\ \frac{rb}{2V} \end{bmatrix} = \begin{bmatrix} -C_{Y_{\delta_a}} & -C_{Y_{\delta_r}} \\ 0 & 0 \\ -C_{l_{\delta_a}} & -C_{l_{\delta_r}} \\ -C_{n_{\delta_a}} & -C_{n_{\delta_r}} \end{bmatrix} \begin{bmatrix} \delta_a \\ \delta_r \end{bmatrix}$$

To use these equations for computations, we often have to transform them into state space form. To put an equation in state space form, we first have to isolate all terms with one of the differential operators D_c and D_B on one side of the equation.

Roll Mode:

The roll mode of "iCLEAN" UAV is approximated by

$$I_{xx}\dot{p} = L_p P + L_{\delta_e} \delta_e$$

$$(L_p < 0, L_{\delta_e} < 0)$$

↓

$$\dot{p} = \frac{L_p}{I_{xx}} P + \frac{L_{\delta_e}}{I_{xx}} \delta_e$$

With substitutions:

$$x = p \quad u = \delta_e \quad a = L_p / I_{xx} \quad b = L_{\delta_e} / I_{xx}$$

$$\dot{x} = \dot{p}$$

We get the system $\dot{x} = ax + bu$,
where u is the controller, and x is the state.

Hence, the transfer function from u to x is:
(By inverse Laplace transform and zero initial conditions)

$$\dot{x} = ax + bu \xrightarrow{L^{-1}}$$

$$sx = ax + bu$$

$$x(s - a) = bu$$

$$\frac{x}{u}(s) = \frac{b}{s - a}$$

The roll mode time constant is $\tau_{roll} = -\frac{1}{a} = -\frac{I_{xx}}{L_p}$

The steady state roll rate is given by $p_{ss} = \frac{-b}{-a} = \frac{L_{\delta_e}}{L_p}$.

Now we wish to decrease τ_{roll} . Since I_{xx}, L_p are constant, it is enabled using roll-rate (\dot{p}) feedback:

$$\delta_e = -k_p p + \delta_{se}$$

$$u = -k_p x + r$$

Therefore, the close loop from r to x is:

$$\frac{x}{r}(s) = \frac{b}{s - (a - bk_p)}$$

And now, the augmented roll-rate time constant is

$$\tau_{roll_new} = -\frac{1}{a - bk_p} = -\frac{I_{xx}}{L_p - k_p L_{\delta_e}}$$

We of course desire $\tau_{roll_new} < \tau_{roll}$

$$\frac{1}{L_p - k_p L_{\delta_e}} > \frac{1}{L_p}$$

$$|L_p| < |L_p - k_p L_{\delta_e}|$$

Sp that $k_p < 0$.

Now, when examining the new and old roll-rate to a step-response, with the values of "iCLEAN" mass and dynamic properties, we can see that the new (feedback) response reach steady state more quickly, but with larger steady state error in comparison the OL roll rate.

Short Period:

The short period approximation is based on the consideration of just the states of angle of attack - α and pitch rate - q , and the pitching moment control δ_e .

$$\bar{X}_{sp} = \begin{Bmatrix} \alpha \\ q \end{Bmatrix} \quad u_{sp} = \{\delta_e\}$$

In terms of dimensional, as derived in the aerodynamic chapter, and by neglecting alpha rate- $\dot{\alpha}$, the system matrices are:

$$A_{sp} = \begin{bmatrix} \frac{Z_w}{m} & \frac{z_q + mV}{mV} \\ \frac{m_w V}{I_{yy}} & \frac{M_q}{I_{yy}} \end{bmatrix} = \begin{bmatrix} a_{11} & a_{12} \\ a_{21} & a_{22} \end{bmatrix}$$

$$B_{sp} = \begin{bmatrix} 0 \\ \frac{M_{\delta m}}{I_{yy}} \end{bmatrix} = \begin{bmatrix} 0 \\ b \end{bmatrix}$$

$$\dot{X} = AX + Bu$$

The state transition matrix is easily derived:

$$[sI - A_{sp}]^{-1} = \frac{\begin{bmatrix} s - a_{22} & a_{12} \\ a_{21} & s - a_{11} \end{bmatrix}}{s^2 - (a_{11} + a_{22})s + (a_{11}a_{22} - a_{12}a_{21})}$$

The OL matrix of tf is therefore:

$$G(s) = \begin{bmatrix} \alpha / \delta_e \\ q / \delta_e \end{bmatrix}$$

And the root locus graph for pitch- rate feedback

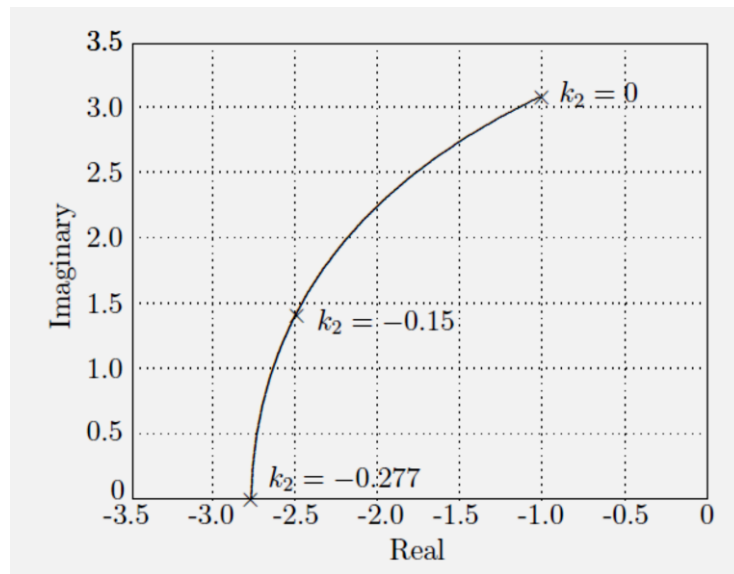


FIGURE 104 - ROOT-LOCUS FOR \dot{q}

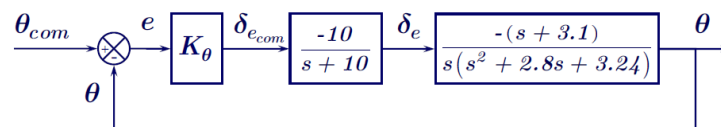


FIGURE 105 - CONTROLLER FOR θ_{com}

13.1.6.3. SIMULINK MODEL

We have modeled the entire control system, using standard atmospheric (ISA). We also modeled all of the control loops for the body axis states and wind axis states.

The Simulink model for pitch- rate and speed controller can be shown in fig. 104.

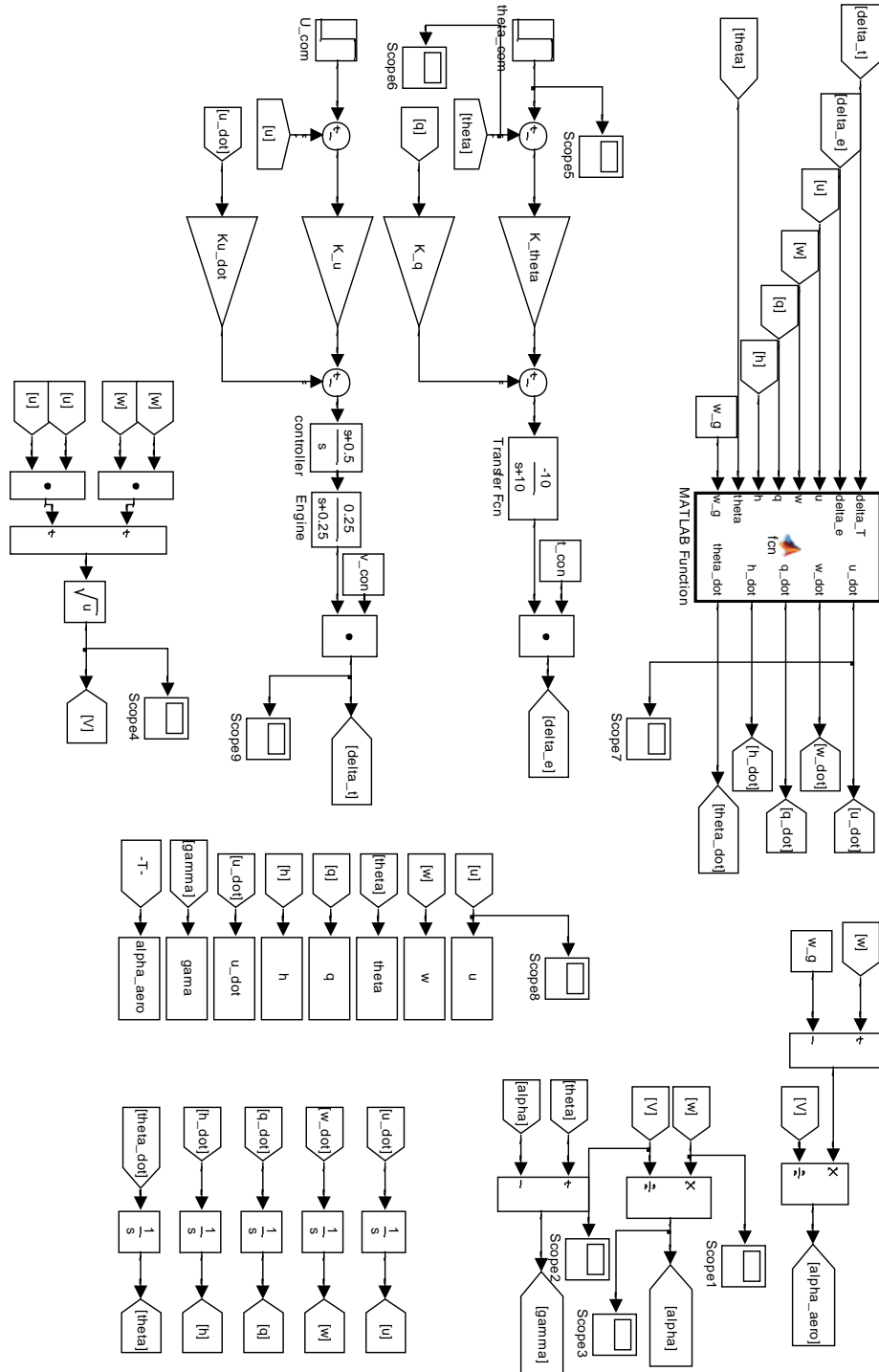


FIGURE 106 - θ AND u LOOPS

13.1.6.4. ANALYSES TOOL

We have developed a Matlab tool for guidance and control design, and also for nominal simulation scenarios.

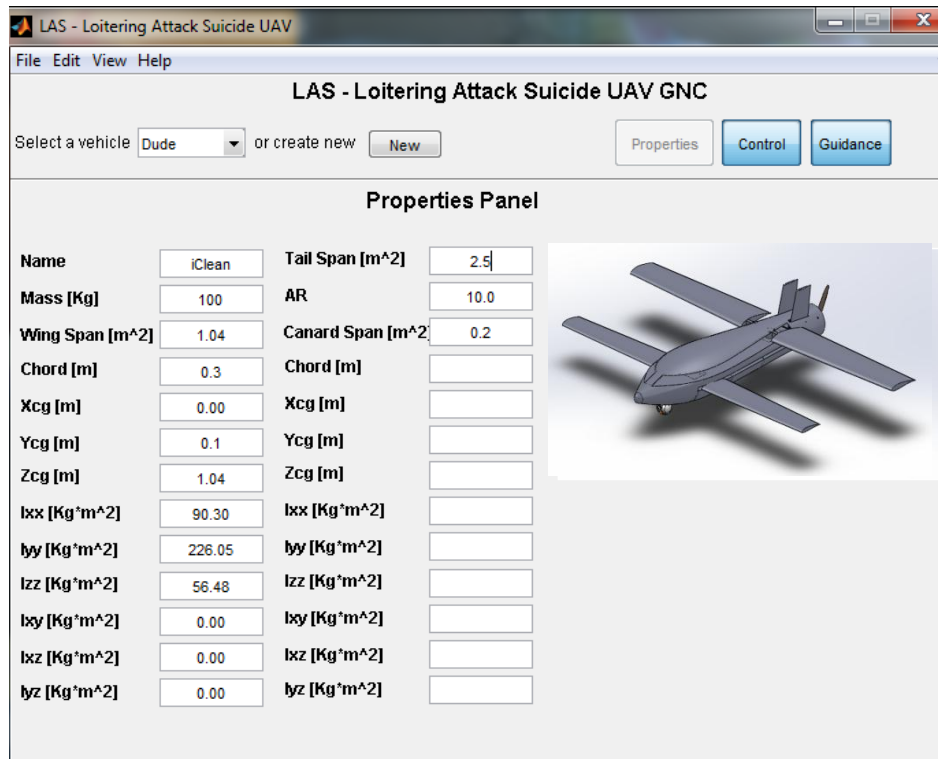


FIGURE 107 - LAS - LOITERING ATTACK SUICIDE UAV, GNC TOOL

As can be seen, the tool is divided into 3 main screens:

1. Properties screen, as can be seen in fig 105 above.
2. Control screen.
3. Guidance screen.

In the first screen the user is asked to fill in the UAV properties. These properties are mainly mass and inertia properties. Properties screen input will feed the Simulink model (described in sub-section 13.1.6.3)

The second screen describes and show graphically all the controllers architecture and it is split to longitude and latitude surfaces, as derived previously. The user can also plot the Bode of each control loop, set up a desired GM and PM and also required damping values. Using RLTOOL generic GUI of Matlab, the control design could be approved.

The last screen is Guidance Screen. In this screen the user inputs initial conditions of "iCLEAN" that represent his 6 DOF state in space (position and orientation) and it's velocity and acceleration vectors: $X_{UAV}, Z_{UAV}, Y_{UAV}, V_{X_UAV}, V_{Y_UAV}, V_{z_UAV}, a_{X_UAV}, a_{Y_UAV}, a_{z_UAV}, \psi, \theta, \phi$, initial conditions of the Target (on earth plane only) such as $X_T, Z_T, Y_T, V_{XT}, V_{YT}, a_{XT}, a_{YT}$ are also required. Another input is the guidance law to be simulated: TPN, APN, PPN or PN.

When clicking Start button, the Simulink model will run and plot the paths of both Target and "iCLEAN".

13.1.6.5. RESULTS

By entering the coefficient values as an assumption or by derived from the wind tunnel test, the simulation was running for a local level runs. We analyzed the control design by checking the step-response, on looking the bode graphs to get the PM and GM:

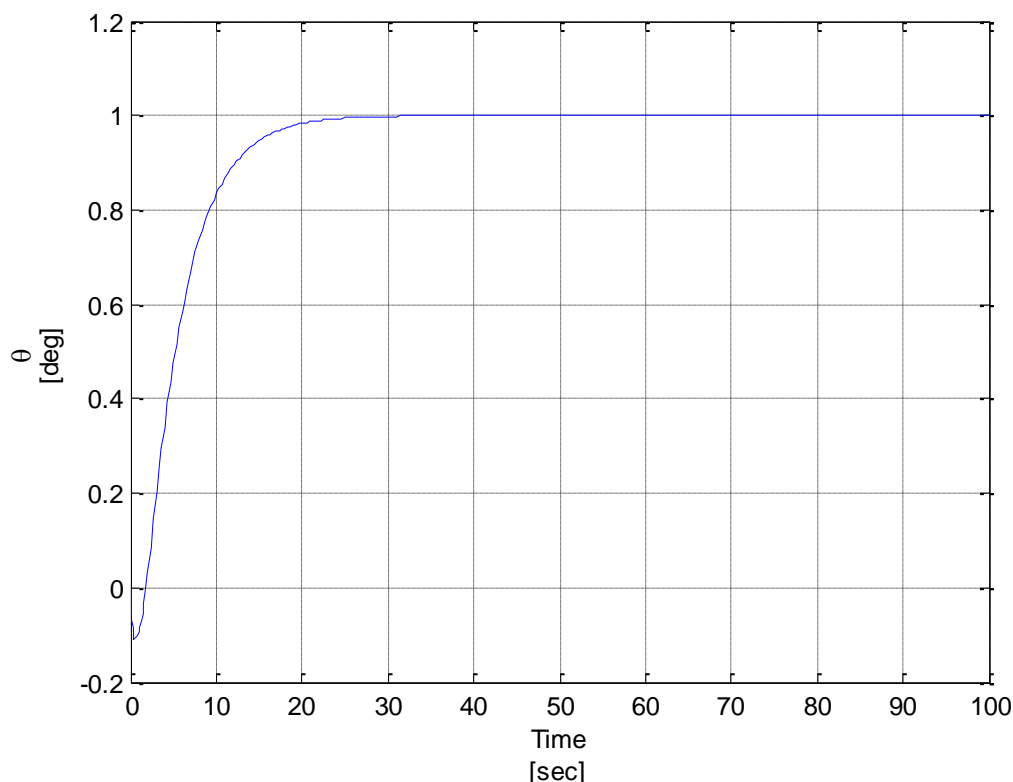


FIGURE 108 - STEP INPUT FOR θ

As can be seen, in the sp, there is no steady state error for θ command.

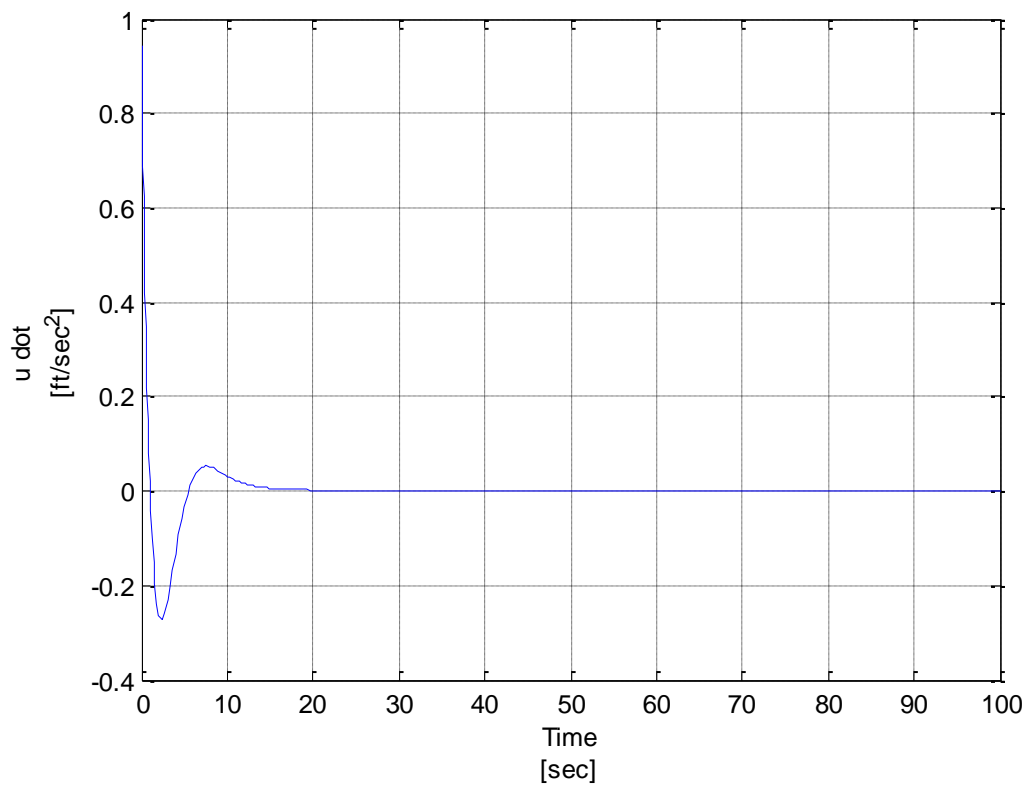


FIGURE 109 - STEP INPUT FOR \dot{u}

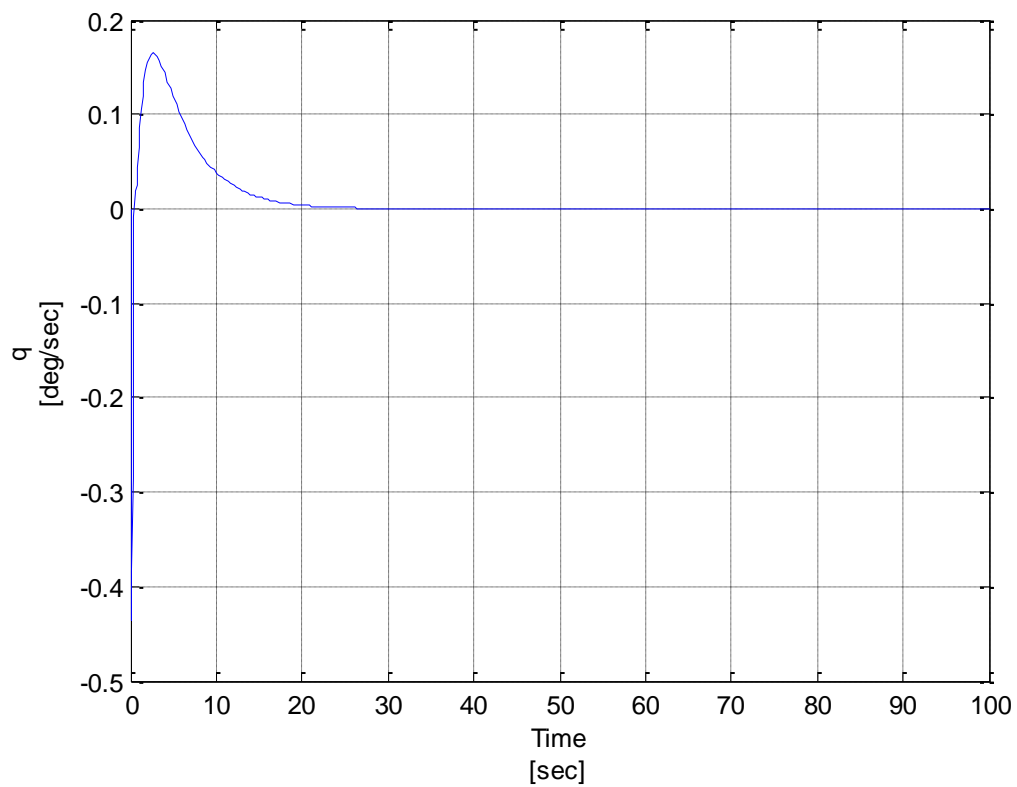


FIGURE 110 - PITCH-RATE RESPONSE

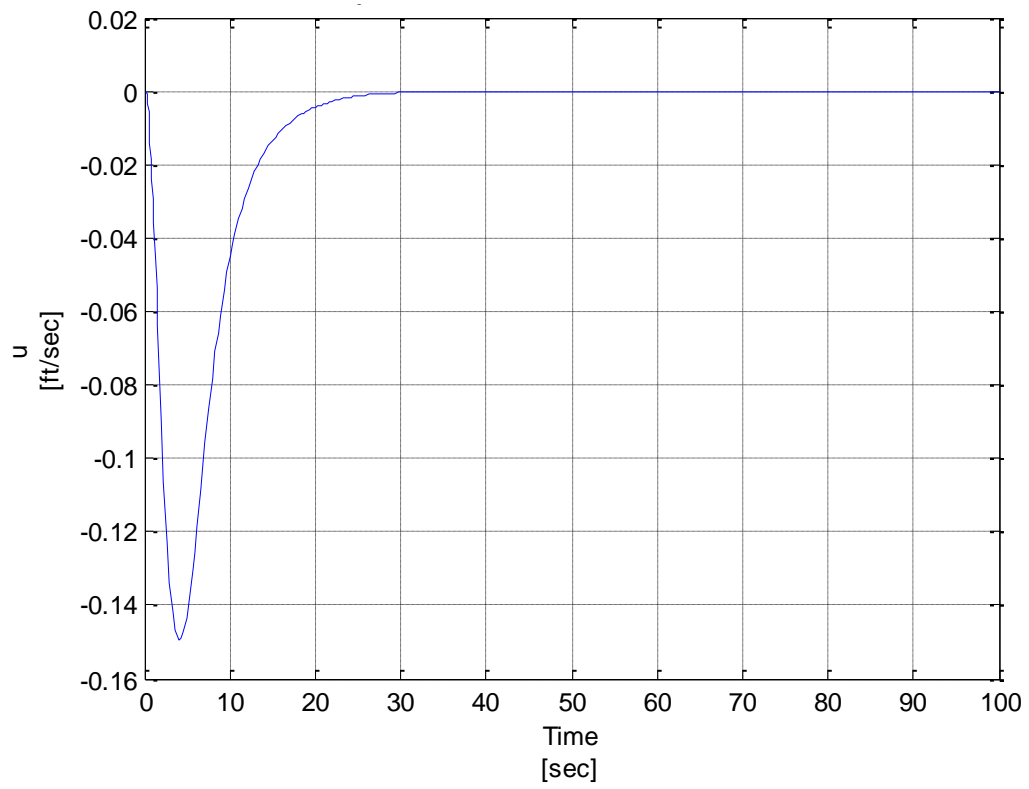


FIGURE 111 - u RESPONSE

13.1.7. GUIDANCE

13.1.7.1. INTRODUCTION

A guidance system is a used to navigate "iCLEAN" UAV. Typically, guidance system refers to a system that navigates without direct or continuous human control. One of the earliest examples of a true guidance system is that used in the German V-1 during World War II.

A guidance system has three major sub-sections: Inputs, Processing, and Outputs. The input section includes sensors, course data, radio and satellite links, and other information sources. The processing section, composed of one or more CPUs, integrates this data and determines what actions, if any, are necessary to maintain or achieve a proper heading. This is then fed to the outputs as means of acceleration commands in X,Y,Z directions. Then, the autopilot need to generate control surface movement and thrust commands to fulfill the guidance acceleration command. Because the dynamic of the UAV is not perfect (probably second or higher order tf), the measured acceleration (in each axis) is never the same as the command. Therefore a closed loop on the acceleration command is needed, and this is exactly the guidance loop.

SUMMARY

This final report unites all the hard work done during the last semesters as part of a student's final project.

In order to satisfy the demand for a loitering suicide UCAV, we had to gather and to implement all the knowledge and abilities obtained through our studies at the faculty of Aerospace Engineering at the Technion Institute of technology, and even more. Moreover, during the process we had been exposed to the complexity of the UAV's systems, sub-systems and the demanding nature of work in the industry. We experienced work in small and large groups, focusing on several areas and systems, both required vast market and literature surveys. Under our supervisor supervision we manage to integrate all the pieces together into a whole new system, UAV.

From this point we had to deal with all the limitations of this kind of vehicle, find solutions to different problems and even to accept that not everything come to place as we want.

Some stresses analysis had been done, we try to overcome some difficulties of stability during launch, which we weren't manage to solve completely.

A detailed design has been made and accordingly a test model created. The same model that afterwards been put to the test inside a wind tunnel, generate some results and help us to get a closer look to the real-life of an engineer, let us realize the connection between the works done earlier to the final product. We had to cope with real-life test results that doesn't always match to the theory, explain the phenomenon, and suggest ways to overcome these obstacles.

Eventually, we were able to design a new Loitering Suicide UCAV which met most of the original costumer requirements; almost satisfy the demanding range and endurance requirements, maximize the number of units on an ordinary launcher vehicle, able to withstand different conditions and situations.

There is still a need to verify the launch problem solutions and optimize the wings and canards according to their effects on one another.

According all the above, this project manage to fulfill its most important and fundamental goal – to make us a lot better engineers before we get out from graduation to the real world!

BIBLIOGRAPHY

1. Analysis and Design of Flight Vehicle Structures, E.F. Bruhn, 1973.
2. Aircraft Design- A Conceptual Approach – Daniel P. Raymer 1992.
3. Aircraft Design, Ajoy Kumar Kundu 2010.
4. The Design of the Aeroplane, Darrol Stinton 1983.
5. Airframe Structural Design, Michael Chun Yung Niu, 1995.
6. Jane's Unmanned Aerial Vehicles and Targets
7. חומרים מרוכבים – חומרים, שיטות ייצור ומוצרים, גדי מניקס
8. Hurwitz, A. (1964). "On The Conditions Under Which An Equation Has Only Roots With Negative Real Parts". Selected Papers on Mathematical Trends in Control Theory.
9. Routh, E.J. (1877). A Treatise on the Stability of a Given State of Motion, Particularly Steady Motion: Particularly Steady Motion. Macmillan and co..
10. Robert F. Stengel (1994). Optimal Control and Estimation. Dover Publications. ISBN 0-486-68200-5.
11. Nise, Norman S. (2004); Control Systems Engineering (4 ed.); Wiley & Sons; ISBN 0-471-44577-0
12. Minorsky, Nicolas (1922). "Directional stability of automatically steered bodies". J. Amer. Soc. Naval Eng. 34 (2): 280–309
13. Ang, K.H., Chong, G.C.Y., and Li, Y. (2005). PID control system analysis, design, and technology, IEEE Trans Control Systems Tech, 13(4), pp.559-576

14. <http://www.acrtucson.com/UAV/launcher/index.htm>
15. <http://www.controp.com/item/ESP-600C-payload>
16. http://www.barnardmicrosystems.com/L4E_propellers.htm
17. www.worldofkrauss.com
18. <http://www.wikipedia.com/>
19. <http://www.fas.org/>
20. <http://www.iai.co.il>

APPENDIX

Raymer Weight and Geometry Calculation:

%Chapter 3

```
close all; clear all; clc;

%Table 3.1
%flag: 1-Homebuilt Metal/Wood, 2-Homebuilt Composite, 3-General
Aviation
%Kvs: 1-Variable Sweep, 2-Fixed Sweep
flag=2;
Kvs=1;
Vmax=200/3.6;% Max Speed [m/s]
Vc=0.75*Vmax;% Cruise Speed [m/s]
Vl=sqrt(Vc^2/sqrt(3));% Loiter Speed [m/s]
Rmax=740.8e+3;%Max Range [km]
Emax=5;%Max Endurance [hr]
Wp=linspace(1,100,1000);% Payload Weight [lb]
%Wp=65;
eps=10^-5;

%Find Table 3.1 Values
[a,c] = WeW0_3 (flag,Kvs);
%Flight Segments: 1 -Climb, 2- Cruise, 3- Loiter, 4 - Land
mod=[1 2 3 4];
wiw0=zeros(1,length(mod));
R=[0 463e+3 Rmax-463e+3 0];%Range Segment Vector
E=[0 (R(2)/Vc) (Emax*3600-R(2)/Vc) 0];%Endurance Segment Vector

if sum(R)>Rmax
    disp('ERORR - Range is to big!')
end
if sum(E)>Emax*3600
    disp('ERORR - Endurance is to big!')
end

%Fuel Fraction segment w(i)/w(i-1) Estimation
for i=1:length(mod)
    wiw0 (i)=sigment (mod(i),R(i)/0.3048,Vl/0.3048,E(i));
end

%Fuel Fractions Product
wxw0=prod(wiw0);
%Fuel Fractions Estimation (Eq. 3.11)
wfw0=1.06*(1-wxw0);
%Find Suitable Wp for given Takeoff Gross Weight - w0
for i=1:length(Wp)
    eq=@(x)((Wp(i))/(1-wfw0-a*x^c)-x);
    %Bisection Method
    w0=root_find(eq,eps);
    if (w0>=220+eps)
        break;
    end
end
Wp220=Wp(i)
w0
wfw0
```

```

wf=wfw0*w0
we=w0-wf-Wp(i)

```

```

%the function get function and tolerance
%the function return the root of the function
function x_mid = root_find (equ,tol )
Tolerance = tol; %The accuracy of the f(x) to zero
Function = equ; %the given equation

x_min = 0;
x_max =500; %x_min and x_max is the ranged that the root will
searched in
x_mid = (x_min + x_max) / 2;%the midpoint between x_min and x_max

while abs(Function (x_mid)) > Tolerance

    if Function (x_mid) * Function(x_max) < 0
        x_min = x_mid;
    else
        x_max = x_mid;
    end

    x_mid= ( (x_min + x_max)/2);
end

```

```

function [wiw0] =sigment (flag,R,V,E)

Cbhp=0.4;%Table 3.4
eta=0.8;%Table 3.4
LD=10;%Fig. 3.6 (According to Wetted Area ratio Estimation - Fig.
3.5)

if flag==1
    wiw0=0.985;%Table 3.2
end
if flag==2
    wiw0=exp((-R*Cbhp)/(550*eta*LD*3600));%Eq. 3.6
end
if flag==3
    wiw0=exp((-E*Cbhp*V)/(550*eta*LD*0.866*3600));%Eq. 3.8
end
if flag==4
    wiw0=0.995;%Table 3.2
end

end

```

```

% Empty Weight to Gross Takeoff Weight ratio values
function [a,b] = WeW0_3 (Num,K)

switch Num
    case (1) % Homebuilt Metal/Wood
        a=1.19; b=-0.09;
    case (2) % Homebuilt Composite
        a=0.99; b=-0.09;
    case (3) % General Aviation
        a=2.36; b=-0.18;
end

```

```

if K==1
    a=1.04*a;
end

end

```

%Chapter 4

```
close all; clear all; clc;
```

```
% Wing General Geometry
```

```
AR=10;%Designer Selection (According to Table 4.1)
```

```
WS=65;%Average W/S Value of Similar Aircrafts
```

```
W0=220;%Value from Chapter 3 Solution [lb]
```

```
Croot=linspace(0.3,0.8,1000);%Designer Range of Chord Roots
```

```
Lambda=0.75;%According to Chapter 4 - Taper Ratio and Similar Aircrafts
```

```
bcanard=1.4;%Canard Wanted Breadth [m]
```

```
eps=1e-3;
```

```
%Wings Geometry According to Wanted Values
```

```
for i=1:length(Croot)
```

```
    Sref=W0*0.4536/WS;% [m^2]
```

```
    bwing=sqrt(AR*Sref);% [m]
```

```
    %Geometry Claculation
```

```
[Swing,Scanard,Crcanard,Ctcanard]=Crc_calc(Sref,Croot(i),bwing,Lambda,bcanard);
```

```
    ARwing=bwing^2/Swing;
```

```
    ARcanard=bcanard^2/Scanard;
```

```
    Ctwing=Lambda*Croot(i);
```

```
    MAC=(2/3)*Croot(i)*(1+Lambda+Lambda^2)/(1+Lambda);
```

```
        %Croot Canard wanted
```

```
        if (Crcanard<0.20+eps)
```

```
            break;
```

```
        end
```

```
    end
```

```
Crwing=Croot(i)
```

```
Ctwing
```

```
Swing
```

```
bwing
```

```
ARwing
```

```
Crcanard
```

```
Ctcanard
```

```
Scanard
```

```
bcanard
```

```
ARcanard
```

```
function [Sw,Sc,Crc,Ctc] = Crc_calc (Sr,Crw,b,L,bc)
```

```
Sw=(b/2)*(1+L)*Crw;%Swet
```

```
Sc=Sr-Sw;%Scanard
```

```
Crc=2*Sc/(bc*(1+L));%Croot Canard
```

```
Ctc=L*Crc;%Ctip Canard
```

end

%Chapter 5

close all; clear all; clc;

flag1=1;%Table 5.2: 1-Homebuilt, 2-General Aviation
flag2=2;%Table 5.4: 1-Homebuilt Metal/Wood, 2-Homebuilt Composite, 3-
General Aviation
flag3=1;%Table 5.5: 1-Homebuilt, 2-General Aviation

Vmax=200/3.6;%[m/s]
Vc=0.75*Vmax;%[m/s]
Vcf=3.28084*Vc;%Vcruise [ft/sec]
b=3.2317;%bwing from Chapter 4 [m]
AR=6.8;
t_c=0.17; %t/c for Eppler 1230 Airfoil
kwet=3.4;%Known Value - Flight Mechanics Lectures
fe=0.0055;%Known Value - Flight Mechanics Lectures
eta=0.8;%Table 3.4
n_sus=4;%Designer Selection - Sustained Turn

%HP/W Selection

hpw_cs=0.0848;% [hp/lb] - from Competitor Study
hpw_sel=sel(flag1);%[hp/lb] - First Statical Estimation
hpw_se2=se2(flag2,Vc);%[hp/lb] - Second Statical Estimation

LD_max=LD_calc(b,t_c,kwet,AR,fe);%L/Dmax Calculation
LD_cr=LD_max;%Because Driven by Propeller

hpw_cr=Vcf/(550*eta*LD_max);%in Level Unaccelerated Flight: L=W,D=T
Wcr_Wclimbe=0.9624;%from Chapter 3 Calculations
Wclimbe_Wto=0.985;%from Chapter 3 Calculations
Wcr_Wto=Wcr_Wclimbe*Wclimbe_Wto;
hpto_hpcr=1/0.75;%Desirable HPtakeoff/HPcruise Ratio
hpw_tmm=hpw_cr*Wcr_Wto*hpto_hpcr;%Eq. 5.4

hpw_sus=sus_Ratio(b,t_c,kwet,AR,fe,n_sus,Vcf,eta);
w0=220.0879;%from Chapter 3 Calculations [lb]
hpw_sus_to=hpw_sus*Wcr_Wto*hpto_hpcr;%Chapter 5 - Sustained Turn

%HP/W Selection - MAX to perform mission requirements

hpw_selected=max(max(max(max(hpw_cs,hpw_sel),hpw_se2),hpw_tmm),hpw_sus_to);
hp_needed=hpw_selected*w0; % [hp]

%W/S selection

ws_cs=14.38; % [lb/ft^2] - Competitor Study
ws_se=se3(flag3);%[lb/ft^2] - Statical Estimation

RAUs1=0.0023769; %Sea Level - [slug/ft^3]
Vstall=50; %Knots
Vstallf=1.6878*Vstall; % [ft/sec]
Cl=1.5; %for Eppler 1230 Airfoil
CLmax=0.9*Cl;%Known from Flight Mechanics Lectures
ws_stall=0.5*RAUs1*(Vstallf^2)*CLmax;%Eq. 5.6

```

RAUcr=0.00217; %Cruise in 3000ft - [slug/ft^3]
ws_cr=ws_cruise(b,t_c,kwet,AR,fe,Vcf,RAUcr);
ws_cr_to=ws_cr/Wcr_Wto;

RAUloit=RAUcr;%Chosen Same Altitude
ws_loit=ws_loiter(b,t_c,kwet,AR,fe,Vc,RAUloit);
Wloit_Wcr=0.9794;%Chapter 3 Calculations
Wloit_Wto=Wloit_Wcr*Wcr_Wto;
ws_loit_to=ws_loit/Wloit_Wto;

%W/S selection - MIN to ensure large enough wing for all flight
conditions
ws_selected=min(min(min(min(ws_cs,ws_se),ws_stall),ws_cr_to),ws_loit_
to);

%Analysis

%Vstall
Vstall_new=sqrt(2*ws_selected/(RAUsl*CLmax)); %[ft/sec]
Vstall_new_knots=0.59248*Vstall_new; %[knots]
CL_to=0.8*CLmax;
Vstall_to=sqrt(2*ws_selected/(RAUsl*CL_to));
Vstall_to_knots=0.59248*Vstall_to;
CL_cr=1.35;
Vstall_cr=sqrt(2*ws_selected/(RAUsl*CL_cr));
Vstall_cr_knots=0.59248*Vstall_cr;

%Best Range
ws_3kft=Wcr_Wto*ws_selected;
[Vbr_sl,Mbr_sl,Vbr_cr,Mbr_cr]=BRange
(b,t_c,kwet,AR,fe,ws_selected,RAUsl,RAUcr,ws_3kft);

%Best Endurance
Vbe=BEndurance(b,t_c,kwet,AR,fe,ws_selected,RAUsl);

```

```

function [LDmax] = LD_calc(b,t_c,kwet,AR,fe)

%Calculations from Chapter 4
Stop=1.42;
Sside=0.852;

Sref=b^2/AR;

Swetwing=Sref*(1.977+0.52*t_c);
Swetbody=(kwet/2)*(Stop+Sside);
Swet=Swetwing+Swetbody;

Swet_Sref=Swet/Sref;
Cd0=fe*Swet_Sref;

e=1.78*(1-0.045*AR^0.68)-0.64;
K=1/(pi*e*AR);

%L/Dmax in Best Range Performance
Clbr=sqrt(Cd0/K);
Cdbr=2*Cd0;

LDmax=Clbr/Cdbr;

```

end

```
function [hpw_sus] = sus_Ratio(b,t_c,kwet,AR,fe,n,Vc,eta)
```

```
%Chapter 4 Calculations
```

```
Stop=1.42;
```

```
Sside=0.852;
```

```
Sref=b^2/AR;
```

```
Swetwing=Sref*(1.977+0.52*t_c);
```

```
Swetbody=(kwet/2)*(Stop+Sside);
```

```
Swet=Swetwing+Swetbody;
```

```
Swet_Sref=Swet/Sref;
```

```
Cd0=fe*Swet_Sref;
```

```
e=1.78*(1-0.045*AR^0.68)-0.64;
```

```
%Chapter 5 - Sustained Turn
```

```
hpw_sus=2*n*sqrt(Cd0/(pi*e*AR))*Vc/(550*eta);
```

end

```
function [hpw] =se1 (Num)
```

```
switch Num
```

```
case (1) % Homebuilt
```

```
hpw=0.08;
```

```
case (2) % General Aviation
```

```
hpw=0.07;
```

```
end
```

end

```
function [hpw] =se2 (Num,Vc)
```

```
%Vcm - mph
```

```
Vcm=2.2369*Vc;
```

```
switch Num
```

```
case (1) % Homebuilt Metal/Wood
```

```
a=0.005; c=0.57;
```

```
case (2) % Homebuilt Composite
```

```
a=0.004; c=0.57;
```

```
case (3) % General Aviation
```

```
a=0.024; c=0.22;
```

```
end
```

```
hpw=a*(Vcm^c);
```

end

```
function [ws] =se3 (Num)
```

```
switch Num
```

```

        case (1) % Homebuilt
            ws=11;
        case (2) % General Aviation
            ws=17;
    end
end

```

end

```
function [ws_cr] = ws_cruise(b,t_c,kwet,AR,fe,Vc,RAUcr)
```

```
%Chapter 4 Calculations
```

```
Stop=1.42;
Sside=0.852;
```

```
Sref=b^2/AR;
```

```
Swetwing=Sref*(1.977+0.52*t_c);
Swetbody=(kwet/2)*(Stop+Sside);
Swet=Swetwing+Swetbody;
```

```
Swet_Sref=Swet/Sref;
Cd0=fe*Swet_Sref;
```

```
e=1.78*(1-0.045*AR^0.68)-0.64;
```

```
ws_cr=0.5*RAUcr*(Vc^2)*sqrt(pi*AR*e*Cd0); %Eq. 5.13
```

end

```
function [ws_loit] = ws_loiter(b,t_c,kwet,AR,fe,Vc,RAUloit)
```

```
Vl=sqrt(Vc^2/sqrt(3)); %[m/s]
Vlf=3.2808*Vl; %[ft/s]
```

```
%Chapter 4 Calculations
```

```
Stop=1.42;
Sside=0.852;
```

```
Sref=b^2/AR;
```

```
Swetwing=Sref*(1.977+0.52*t_c);
Swetbody=(kwet/2)*(Stop+Sside);
Swet=Swetwing+Swetbody;
```

```
Swet_Sref=Swet/Sref;
Cd0=fe*Swet_Sref;
```

```
e=1.78*(1-0.045*AR^0.68)-0.64;
```

```
ws_loit=0.5*RAUloit*(Vlf^2)*sqrt(3*pi*AR*e*Cd0); %Eq. 5.16
```

end

```
function [Vbrsl,Mbrsl,Vbrcr,Mbrcr] = BRange
(b,t_c,kwet,AR,fe,ws_selected,RAUsl,RAUcr,ws3kft)
```

```
Gamma=1.4; %Air
```

```

R=287.1;%Gas Constant
Tsl=288;%Sea Level Temrature [K]
hcr=3000; % Cruise Altitude [ft]
Tcr=Tsl-2e-3*hcr;% According toFlight Mechanics Lectures

```

```

%Chapter 4 Clculations

```

```

Stop=1.42;
Sside=0.852;

```

```

Sref=b^2/AR;

```

```

Swetwing=Sref*(1.977+0.52*t_c);
Swetbody=(kwet/2)*(Stop+Sside);
Swet=Swetwing+Swetbody;

```

```

Swet_Sref=Swet/Sref;
Cd0=fe*Swet_Sref;

```

```

e=1.78*(1-0.045*AR^0.68)-0.64;
K=1/(pi*e*AR);

```

```

Vbrsl=sqrt(2*ws_selected*(sqrt(K/Cd0))/RAUsl); %[ft/sec]
asl=sqrt(Gamma*R*Tsl);
aslf=asl/0.3048;
Mbrsl=Vbrsl/aslf;%Mach Number Calculation

```

```

Vbrcr=sqrt(2*ws3kft*(sqrt(K/Cd0))/RAUcr);
acr=sqrt(Gamma*R*Tcr);
acrf=acr/0.3048;
Mbrcr=Vbrcr/acrf;%Mach Number Calculation

```

```

end

```

```

function [Vbe] = BEndurance (b,t_c,kwet,AR,fe,ws_selected,RAUsl)

```

```

%Chapter 4 Calculations

```

```

Stop=1.42;
Sside=0.852;

```

```

Sref=b^2/AR;

```

```

Swetwing=Sref*(1.977+0.52*t_c);
Swetbody=(kwet/2)*(Stop+Sside);
Swet=Swetwing+Swetbody;

```

```

Swet_Sref=Swet/Sref;
Cd0=fe*Swet_Sref;

```

```

e=1.78*(1-0.045*AR^0.68)-0.64;
K=1/(pi*e*AR);

```

```

Vbe=sqrt(2*ws_selected*(sqrt(K/(3*Cd0)))/RAUsl); %[ft/sec]

```

```

end

```

```

%Chapter 6

```

```

%Engine Sizing
close all; clear all; clc;

flag=2;
Vmax=200/3.6;
Vc=0.75*Vmax;
Vcm=2.2369*Vc;%mph
Vl=sqrt(Vc^2/sqrt(3));
AR=6.8;
hpw_selected=0.0848;
ws_selected=11;
Wp=62.837;
%Wp=linspace(1,100,1000);
[a,b,c1,c2,c3,c4,c5] = WeW0_6(flag);
mod=[1 2 3 4];%
wiw0=zeros(1,length(mod));
wfw0=zeros(1,length(mod));
Rmax=740.8e+3;Emax=5;%hr
R=[0 463e+3 Rmax-463e+3 0];%
E=[0 (R(2)/Vc) (Emax*3600-R(2)/Vc) 0];%
%R=[0 Rmax 0 0];%
%E=[0 (R(2)/Vc) 0 0];%
eps=10^-5;

if sum(R)>Rmax
    disp('ERORR - Range is to big!')
end
if sum(E)>Emax*3600
    disp('ERORR - Endurance is to big!')
end

for i=1:length(mod)
    [wiw0(i),wfw0(i)]=sigment6
    (mod(i),R(i)/0.3048,Vc/0.3048,Vl/0.3048,E(i));
end

%wxw0=prod(wiw0);
%wfw0=1.06*(1-wxw0);
wf_w0=sum(wfw0);
%for i=1:length(Wp)
    eq=@(x)((Wp)/(1-wf_w0-
    (a+b*x^c1*AR^c2*hpw_selected^c3*ws_selected^c4*Vcm^c5))-x);
    w0=root_find(eq,eps);
    % if (w0>=220+eps)
        % break;
    %end
%end
%Wp220=Wp(i);
w0;
wf=sum(wfw0)*w0; %mission fuel
wf_tot=1.06*wf; %total fuel
we=w0-wf_tot-Wp;

%Engine Selection
HP=hpw_selected*w0;
HP_max=HP/0.8;

%Fixed Engine Sizing - Desert Aircraft: DA-200 (19hp)
hp_engine=19;

```

```

w0_FE=hp_engine/hpw_selected;
Wp_FE=Wp;
Range_FE=linspace(1e5,2e6,5000);

    for i=1:length(Range_FE)
        [wiw0_FE,wfw0_FE]=sigment_FE
(Range_FE(i)/0.3048,Vc/0.3048);
        Delta_wfw0=wfw0_FE-wfw0(3);
        wf_w0_FE=wf_w0+Delta_wfw0;
        eq=@(x)((Wp_FE)/(1-wf_w0_FE-
(a+b*x^c1*AR^c2*hpw_selected^c3*ws_selected^c4*Vcm^c5))-x);
        w0_new=root_find(eq,eps);
            if (w0_new>=w0_FE+eps)
                break;
            end
        end
    end

```

```

wf_w0_FE

```

```

function [wiw0,wfw0] =sigment6 (flag,R,Vc,Vl,E)
% 1 -climb, 2- cruse, 3- loiter, 4 - land
Cbhp=0.4;
eta=0.8;
%LD_6=13.4884;
LD_6=LDcr(Vc);

if flag==1
    wiw0=0.985;
end
if flag==2
    wiw0=exp((-R*Cbhp)/(550*eta*LD_6*3600));
end
if flag==3
    wiw0=exp((-E*Cbhp*Vl)/(550*eta*LD_6*0.866*3600));
end
if flag==4
    wiw0=0.992;
end

wfw0=(1-wiw0)*wiw0;

end

```

```

function [wiw0,wfw0] = sigment_FE (R,Vc)

Cbhp=0.4;
eta=0.8;
LD_6=LDcr(Vc);

wiw0=exp((-R*Cbhp)/(550*eta*LD_6*3600));

wfw0=(1-wiw0)*wiw0;

end

```

```

%the function get function and tolerance
%the function return the root of the function
function x_mid = root_find (equ,tol )

```

```

Tolerance = tol; %The accuracy of the f(x) to zero
Function = equ; %the given equation

x_min = 0;
x_max = 500; %x_min and x_max is the ranged that the root will
searched in
x_mid = (x_min + x_max) / 2; %the midpoint between x_min and x_max

while abs(Function (x_mid)) > Tolerance

    if Function (x_mid) * Function(x_max) < 0
        x_min = x_mid;
    else
        x_max = x_mid;
    end

    x_mid= ( (x_min + x_max)/2);
end

```

```

%Geometry Sizing
close all; clear all; clc;

flag=2;
w0_FE=224.0566;
FRR=4.5;
ws_selected=12.74;
Lambda=0.75;
AR=6.8;
Croot=linspace(0.3,0.8,1000);
bcanard=2.70;
eps=1e-5;

% Fuselage
% [a,c]=fuselage(flag);
% Length=a*w0_FE^c;%ft
%
% MAX_Diameter=Length/FRR;

%Wing
%Lcanard=0.5*Length;

for i=1:length(Croot)
    Sref_wing=w0_FE*0.0929/ws_selected;
    bwing=sqrt(AR*Sref_wing);

    [Swing,Scanard,Crcanard,Ctcanard]=Crc_calc(Sref_wing,Croot(i),bwing,L
ambda,bcanard);

    ARwing=bwing^2/Swing;
    ARcanard=bcanard^2/Scanard;
    Ctwing=Lambda*Croot(i);
    MAC=(2/3)*Croot(i)*(1+Lambda+Lambda^2)/(1+Lambda);

    if (Crcanard<0.275+eps)
        break;
    end
end
% Crcanard

```

```

% Croot(i)
% Scanard
% Swing
% bcanard
% bwing
% Scanard/(Scanard+Swing)

%New Main Wing Wingspan Calculations
bwing_new=3;
Swing_new=Swing
Scanard_new=Sref_wing-Swing_new
Croot_new=(2*Swing_new)/(1+Lambda)*bwing_new
Ctip_new=Lambda*Croot_new
ARwing_new=bwing_new^2/Swing_new

```

```

Svt=0.04*bwing_new*Swing_new/(0.30*2.1)

```

```

function [a,c] = fuselage(Num)

switch Num
    case (1) % Homebuilt Metal/Wood
        a=3.68; c=0.23;
    case (2) % Homebuilt Composite
        a=3.5; c=0.23;
    case (3) % General Aviation
        a=4.37; c=0.23;
end

end

```

```

function [LD] = LDcr (Vcr)

RAUcr=0.00217;
Cd0=0.0248;
ws_selected=11;
AR=6.8;
e=0.8451;

q=0.5*RAUcr*Vcr^2;
Part1=q*Cd0/ws_selected;
Part2=ws_selected/(q*pi*AR*e);

LD=1/(Part1+Part2);

end

```

```

function [Sw,Sc,Crc,Ctc] = Crc_calc (Sr,Crw,b,L,bc)

Sw=(b/2)*(1+L)*Crw;%Swet

Sc=Sr-Sw;%Scanard
Crc=2*Sc/(bc*(1+L));%Croot Canard
Ctc=L*Crc;%Ctip Canard

end

```

Rocket Booster Calculations:

```
clc
clear all

du=30.5;
ueq=2158.2;
g=9.81;
m2=103;
d_can=0.6;
l_can=3;
Af=(0.5^2)*pi;
Pa=1;
Pe=1;
Pc=68;
gama=1.2;
Ae_At=8.87;
Cf=1.597;
rho=1.225;
Isp=220;
C_st=Isp*g/Cf;
C_d=0.04;
eps=10^-3;
dt=3;

m1=150;
m1g=103;
u=ueq*log(m1/m2);
D=0.5*rho*u^2*C_d*Af;
m=(m1+m2)/2;
f=du-u+D/m*dt+g*dt;
while abs(f)>eps
    x=(m1+m1g)/2;
    ux=ueq*log(x/m2);
    Dx=0.5*rho*ux^2*C_d*Af;
    mx=(x+m2)/2;
    fx=du-ux+Dx/mx*dt+g*dt;
    u=ueq*log(m1/m2);
    D=0.5*rho*u^2*C_d*Af;
    m=(m1+m2)/2;
    f=du-u+D/m*dt+g*dt;
    if (fx*f)<0
        m1g=x;
    else
        m1=x;
    end
end
dt
mp=m1-m2
m_dot=mp/dt
At=C_st*m_dot/(Pc*101325)
d_t=sqrt(4*At/pi)
de=d_t*sqrt(Ae_At)
```